University of Leoben

Diploma Thesis:

Production and characterization of particle-stabilized nanocrystalline Cu for high temperature applications

Lisa Krämer

Leoben, March 2014

This work, supported by the European Communities under the Contract between EUROTOM and the Austrian Academy of Sciences, was carried out within the framework of the European Fusion Development Agreement. The views and opinions expressed herein do not necessarily reflect those of the European Commission.

University of Leoben
Franz Josef Straße 18
8700 Leoben
Austria

Erich Schmid Institute of Material Science
Austrian Academy of Sciences
Jahnstraße 12
8700 Leoben
Leoben

EIDESSTATTLICHE ERKLÄRUNG

Ich erkläre an Eides statt, dass ich diese Arbeit selbständig verfasst, andere als die angegebenen Quellen und Hilfsmittel nicht benutzt und mich auch sonst keiner unerlaubten Hilfsmittel bedient habe.

AFFIDAVIT

I declare in lieu of oath, that I wrote this thesis and performed the associated research myself, using only literature cited in this volume.

Datum	Unterschrift

i Danksagung

Mein besonderer Dank gilt Herrn Univ.Doz. Univ.-Prof. Dipl.-Ing. Dr.mont. Reinhard Pippan, der mir nicht nur ein interessantes Thema für meine Diplomarbeit vorgegeben hat, sondern auch durch weitere Anregungen und Ideen geholfen hat, diese umzusetzten.

Bei Dipl.-Ing. Dr.mont. Stefan Wurster möchte ich mich für die hilfreichen und konstruktiven Vorschläge bedanken und auch für die viele Zeit, die von ihm in abenteuerliche Versuche und Fehlersuche gesteckt wurde.

Mein Dank geht auch an Dipl.-Ing. Peter Kutleša für die Unterstützung bei meinen Experimenten, die durch seine große Erfahrung und Einfallsreichtum schneller gelangen und für die stets gute Laune, wenn auch einmal etwas schief ging.

Für die fachliche Unterstützung des Teams in der Werkstätte, Herrn Franz Hubner und Robin Neubauer, bedanke ich mich herzlich. Ebenso bei Frau Silke Modritsch (Metallographie), ohne die die Probenpräperation und –reinigung um vieles länger gedauert hätte. Mein Dank für die organisatorische Hilfe geht an Viktoria Schrutt und Maria Fließer.

Bedanken möchte ich mich auch bei der Firma Plansee SE, Austria, für das bereitgestellte Probenmaterial.

Weiters möchte ich mich bei meinen Kollegen am Institut für das freundliche Arbeitsklima und gute Ratschläge bedanken. Ebenso bei meinen Freunden und Studienkollegen, die mit gemeinsamen Lernen und Aktivitäten das Studium interessant und abwechslungsreich gestaltet haben.

Ein besonders großer Dank gilt meinen Eltern, die mich nicht nur finanziell unterstützt haben und meinen Großeltern, die immer stolz darauf sind, was ich mache. Auch meinem Freund und meinen Geschwistern danke ich dafür, dass sie immer bereit waren, mich zu unterstützen und anzutreiben.

ii Abstract

The goal of this master thesis is to stabilize nanocrystalline Cu for high temperatures applications. This is tried by stabilizing the Cu-grains with different particles. Eight different materials were deformed with high pressure torsion (HPT), their microstructure was investigated with scanning electron microscopy and their mechanical properties with hardness measurement and tensile tests. Four materials were produced by using powder as initial material (Cu-W, Cu-Y_2O_3, Cu-Fe and pure Cu) and for the other four materials industrial produced bulk materials were used (three W-Cu samples with different composition and pure Cu). For powders, a two-step HPT-process was used and the bulk materials were deformed in a single HPT-step. The obtained microstructure was in the range of hundreds of nm for higher applied strain and the influence of additional deformation steps at higher temperatures was investigated.
To compare the microstructural stability of different materials at higher temperatures, samples were annealed in a vacuum furnace and in air by inductive heating. Materials produced by powder compaction showed after heat treatment, additional to grain growth, a generation of porosity. Emerging of pores was especially strong for pure Cu, Cu-Y_2O_3 and Cu-W specimens on which little deformation were applied. If the applied strain was high enough, Cu-W samples showed a good stability at higher temperatures and up to 810 °C the microstructure did not change. Industrial produced W-Cu samples also got a good temperature stability after little applied strain.
In tensile tests, additions of W and Y_2O_3 decreased the ductility and the particles agglomerate in the samples, which were produced with powders. This caused an early fracture. The surface of W-Cu tensile samples influenced the fracture behavior as a poor surface quality caused an early fracture. Fe was the only element which influenced positively the behavior in tensile testing and after the proper heat treatment fracture strains in the same range as for Cu-bulk samples could be obtained.

iii Kurzfassung

Das Ziel dieser Diplomarbeit ist es nanokristallines Cu für Hochtemperaturanwendungen zu erzeugen indem Cu-Körner durch Partikel stabilisiert werden. Es wurden acht verschieden Materialien mittles High Pressure Torsion (HPT) verformt, ihre Mikrostruktur anhand Rasterelektronenmikroskopie und ihre mechanischen Eigenschaften mittels Härtemessung und Zugversuchen untersucht. Vier dieser Materialien wurden aus Pulver hergestellt (Cu-W, Cu-Y_2O_3, Cu-Fe und eine reine Cu-Probe), die anderen vier aus industriell hergestelltem Festmaterial (drei W-Cu Proben mit unterschiedlicher Zusammensetzung und ein rein Cu). Durch einen zweistufigen HPT-Prozess bei Pulvern, bzw. eine einfache HPT-Verformung bei Festmaterial, wurde ein sehr feine Mikrostruktur eingestellt, die sich bei höheren Verformungen im Bereich hundert bis einige hundert Nanometer befindet. Zusätzlich wurde bei erhöhten Temperaturen HPT-verformt und die Auswirkungen auf Mikrostruktur und mechanische Eigenschaften untersucht.
Um die Temperaturstabilität der Materialien vergleichen zu können, wurden Glühversuche im Vakuumofen und mittels induktiver Heizung durchgeführt. Dabei kam es bei den aus Pulver hergestellten Materialien nicht nur zu Kornwachstum der Cu-Matrix, sondern auch zu Porenbildung. Diese war besonders stark bei rein Cu, Cu-Y_2O_3 und niedrig verformten Cu-W. Ansonsten konnte höher verformtes Cu-W durch seine Temperaturestabilität bis zu 810 °C überzeugen, genauso wie die Proben aus industriell erzeugten W-Cu, für die bereits wenig Verformung ausreichend war.
Allerdings verringerte bei Zugversuchen die Beimengung von W und Y_2O_3 die Duktilität und Agglomerate, bei den aus Pulver erzeugten Proben, führten bereits früh zum Bruch. Bei den W-Cu Proben war außerdem die Oberflächenqualität der Zugproben von großer Bedeutung, da Oberflächenfehler einen frühzeitigen Bruch hervorriefen. Nur Fe beeinflusste das Zugverhalten positiv und mit der richtigen Wärmebehandlung konnten sogar ähnliche Bruchdehungen bei höherer Festigkeit wie beim Cu-Festmaterial erreicht werden.

Contents

1 Motivation

Nanocrystalline materials have an interesting combination of properties like high strength and acceptable ductility, but at high temperatures the grain size increases and the properties change. However, many applications at higher temperatures require a challenging mix of properties and most importantly that they do not change over a wide temperature range. Hence, in this work, it was tried to produce copper-based materials with a nanocrystalline matrix which is stabilized by fine particles to slow down the motion of grain boundaries and to allow high temperature applications.
Microelectronics and certain components in fusion technology have both in common that the used materials must have a high thermal conductivity and an acceptable ductility and strength both at room and higher temperatures. Additionally, it is also important in fusion technology that the materials do not become radioactive because of neutron bombardment. Cu fulfills this conditions as it is one of the metals with the highest thermal conductivity and is also eligible for application in fusion reactors [1].
Another requirement for applicability is the possibility to produce nanocrystalline materials cost-effectively at a larger scale. Nanocrystalline materials produced by high pressure torsion (HPT) are free of pores and the output is in the range of cm^3. Furthermore, with this process it is also possible to mix immiscible components as Cu-W and Cu-Y_2O_3 or elements with poor solubility as Cu-Fe. Therefore, the elements in powder form were mixed and compacted and deformed by HPT. The simplicity and speed of this process allows to produce a relatively high amount of particle-stabilized nanocrystalline material in a short time which cannot be produced easily otherwise. The immiscibility of the elements is important for stabilizing the material at higher temperatures as the particles cannot dissolve in the matrix and thereby they are capable to hinder the movement of grain boundaries and oppress grain growth.
This thesis shows how nanocrystalline Cu can be stabilized with different particles and how this effects the mechanical properties. To check the thermal stability of the microstructure a large number of thermal treatments were performed. In addition, challenges of the production of bulk samples starting with powders are described and for comparison bulk W-Cu composites were deformed by HPT, annealed and investigated.

2 Literature overview

2.1 Production of nanocrystalline materials

Nanostructured materials (NsM) can be produced by one of the following four methods: Firstly, bulk NsM can be achieved by producing separated crystals in the range of nanometers and an additional consolidation step. Another method is to strongly deform a single- or coarse grained polycrystal until, due to a large increase of crystal defects, a nanostructure is generated. The third approach starts with an unstable material such as metallic glasses or supersaturated solid solutions. In a second step crystallization in glasses or precipitation in supersaturated solid solutions takes place and NsM are obtained. Furthermore, NsM can be obtained by depositing atoms or molecules by using Chemical Vapor Deposition (CVD), Physical Vapor Deposition (PVD), precipitation of dilute solutions or electrochemical methods [2].
The disadvantages of the first and last method are the porosity which cannot be fully prevented and the little amount of out-coming material, respectively. In contrast to these two approaches the second method starts already with bulk material and only refines the microstructure by applying high plastic deformation. This can be achieved by ball milling, extrusion, shear, wear or can result from high energy irradiation. In the 1980s, Russian research groups developed methods to deform bulk materials strongly enough to achieve a NsM [3].
Those methods are summarized as Severe Plasctic Deformation (SPD) and are defined [4]: *"as a metal forming method under an extensive hydrostatic pressure that may be used to impose a very high strain on a bulk solid without the introduction of any significant change in the overall dimension of the sample and having the ability to produce exceptional grain refinement."*
The importance of this route is shown by the great variety of processes which were developed in the last years such as the equal channel angular press process (ECAP), the accumulative roll-bonding (ARB) process, the cycle extrusion compression (CEC) process, the cyclic closed-die forging (CCDF) process, the repetitive corrugated straightening (RCS) process, the high pressure torsion (HPT) process and many more. The advantages are the low porosity and the high output, so that samples for mechanical testing can be produced quickly and the superior properties can be shown [5].

2.2 HPT - High pressure torsion

In the HPT-process, the cylindrical specimen is deformed between two anvils under high hydrostatic pressure while one of the anvils rotates and applies shear strain causing grain refinement and an increase in hardness. An advantage is the easily changed pressure and temperature (cooling by liquid nitrogen or inductive heating) under which the process is conducted [6]. Furthermore, the initial condition of the material to be deformed can vary as not only bulk material but also powders can be easily consolidated and plastically deformed. The time intensive step of mechanical alloying of immiscible elements can be omitted and a source of errors as impurities introduced during a long mixing procedure is avoided [7]. Additionally, even high-strength and brittle materials can be deformed because of the high hydrostatic pressure [8].
By deformation, dislocations are generated, but they are not randomly distributed. In the beginning, they are mainly at the grain boundaries. Later on, when the concentration of dislocations at the boundaries becomes too high, they divide grains into cells with more or less misorientations. With increasing strain, the original grains cannot be seen any longer and the microstructure becomes finer until a saturation grain size is obtained which does not change even after further deformation. This grain size depends on the deformed materials (alloying elements, purity), the deformation temperature and eventually on the pressure [8], but not on the original microstruc-

ture; so by deforming single- and polycrystalline material, the saturation grain size is the same. A steady state where the grain size reaches a saturation can be described with a process that eliminates dislocations as dynamic recrystallization and recovery and so, new dislocations evolving due to a continuous deformation are counterbalanced (the dislocation density stays the same) [7, 9].
The equivalent strain (ϵ_v) in the sample can be calculated with:

$$\epsilon_v = \frac{2\pi nr}{t\sqrt{3}} \tag{1}$$

where r is the radius, n the number of turns and t the thickness of the sample [10].
In Equation 1 can be seen that at radius zero the deformation should also be zero but the applied pressure also affects the center region and as soon as the rotation axis of the anvils shifts a little, deformation occurs at radius zero [8, 11].
The form of the anvil influences the deformation behavior: In Figure 1 schematic pictures of three different types of HPT can be seen. The cavities in Figure 1c reduce the height loss which occurs in planar anvils (see Figure 1a and Figure 1b) and additionally enables to apply a hydrostatic pressure. Only a small amount of material flows into the gap between the anvils until the friction force balances the pressure which leads to the material flow. This is the cause for the hydrostatic pressure which enables to deform brittle materials and also prevent the touching of the anvils which would result in a strong increase of friction [8]. The friction between anvil and material

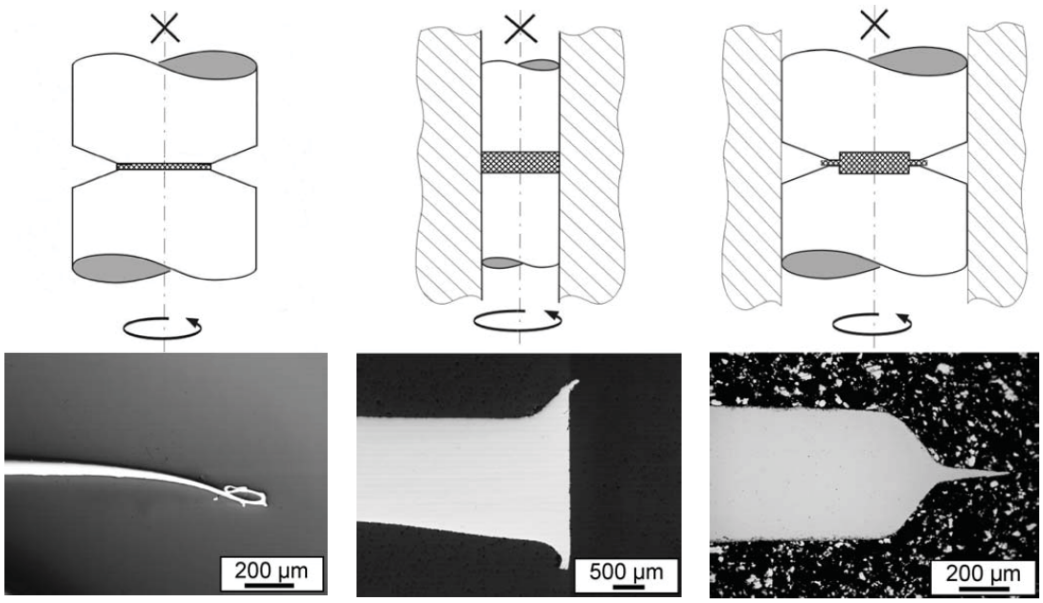

(a) idealized and unconstrained HPT **(b)** idealized and constrained HPT **(c)** practical solution, quasi-constrained

Figure 1: Schematic pictures of three different HPT-types and the corresponding bisected samples underneath taken out of [8].

also causes that a small region (<20 µm) on the surface is not as strongly deformed and shows coarser grains than the majority of the material [8, 12].

2.3 Hall-Petch Effect

Not only strain-hardening induced by the increasing amount of dislocations occurs, but also a hardening effect due to the decreasing grain size can be observed. This is called Hall-Petch effect and bases on the fact that grain boundaries are invincible for dislocations which begin to build up. That causes an increasing force on following dislocation in the same slip plane and impedes further deformation which equals an increase in hardness. This is described in Equation 2:

$$\sigma = \sigma_0 + \frac{\kappa_y}{\sqrt{D}} \tag{2}$$

where σ is the flow stress, σ_0 is the lattice friction stress in a poly crystal with infit grain size, D the grain size and κ_y the Hall-Petch constant which depends on the material [13]. However, this equation is only valid down to a grain size of approximately 20 nm. Conrad et al.[14] suggests three grain size regimes (see also Figure 2):

(a) Regime I, d $\approx 10^{-6}$ m to 10^{-3} m: in the material cell structures are developed until the grain size is smaller than the cell size and the Hall-Petch law is fulfilled.

(b) Regime II, d $\approx 10^{-8}$ m to 10^{-6} m: The grain size is smaller than the typical cell size of the used material and the deformation is only realized by intergranular dislocations until the separation of them becomes larger than the grain size because of elastic interaction. The flow stress in regime II is only weakly dependable on the grain size.

(c) Regime III, d $< 10^{-8}$ m: The spacing between the dislocations becomes larger than the grain size and so no intergranular dislocation activities occur and the Hall-Petch law ceases to be valid.

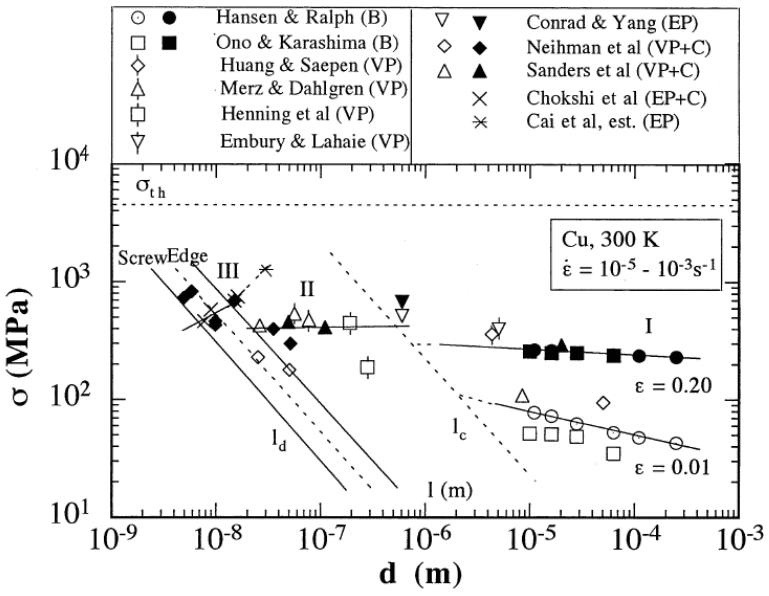

Figure 2: The flow stress σ as a function of grain size d with results from different research groups. The flow stress can be grouped in 3 regimes. [14]

In contrary to Conrad et al., Chen et al. [15] postulates that the Hall-Petch law is also valid for grain sizes smaller than 10 nm and explains the discrepancy with process induced flaws or porosity in the tested specimens.

2.4 Deformation of pure Cu

As the grain boundaries are not pinned by another phase, the recovery and recrystallization in pure Cu is more pronounced than in multiphase materials and the saturation grain size larger. In literature, different saturation grain sizes after severe plastic deformation are obtained (80 nm to 90 nm [16], 200 nm [17], 250 nm [18]) depending on the purity of the used Cu, the temperature at which the material was deformed and even on deformation parameters such as pressure or geometry of the anvils.
Kilmametov et al. [7] showed with in-situ XRD that as soon as the deformation stops, recovery starts and even at room temperature the needed recovery time is in the range of 100 s. In Figure 3, the recovery at room temperatures can be seen. The relative change of the full width at half maximum (FWHM) implies a broadening or narrowing of a diffraction peak. FWHM depends on the grain size and in highly deformed material also on the density of dislocations and internal stresses caused by dislocations. Thus, the decrease of FWHM after the deformation process stopped is related to an increase of the structural size and recovery.

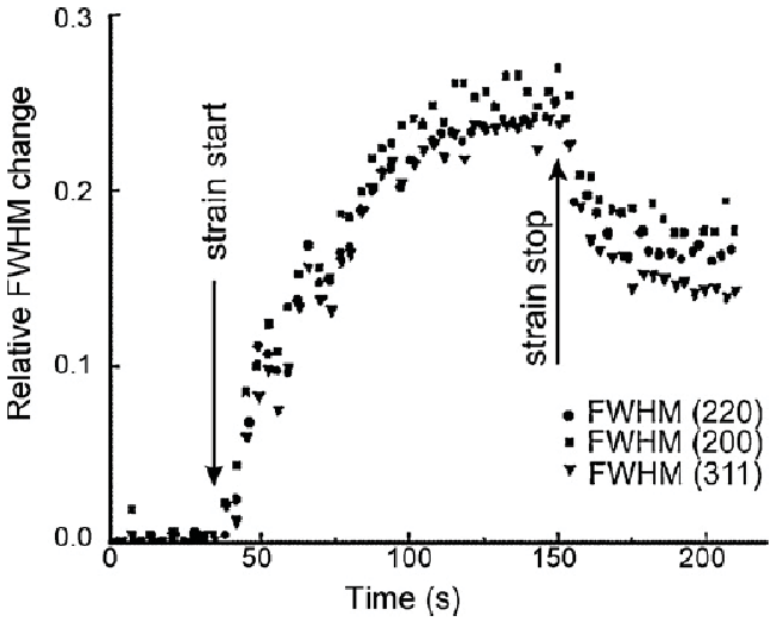

Figure 3: Time-dependent FWHM for 2 0 0 (squares), 2 2 0 (circles) and 3 1 1 (triangles) Bragg peaks of Cu. [7]

2.5 Deformation of Cu-W

In Figure 4a, the phase diagram of Cu-W can be seen which shows that even up to the melting point of Cu the miscibility is zero. So, with classical metallurgical methods no Cu-W alloy can be produced.
Pintsuk et al.[1] solved this problem by using laser sintering or plasma spraying and with both methods, a microstructure in the range of µm has been achieved. However, there is the danger

of vaporization of Cu or delamination. In case of plasma spraying, no fully dense material can be produced. Additionally, plasma sprayed samples show a poor thermal conductivity because of residual porosity. Another method is to use HPT to refine the microstructure by deformation of consolidated Cu-W powder or a coarse bulk material which is produced by liquid phase sintering. In [19–21] it has been shown for W-Cu bulk material, that after an equivalent strain of $\epsilon_v = 256$ at room temperature the particle size of W is 10 nm to 20 nm and it does not change after applying more strain. Until then, the fragmentation of W-particles follows a fractal distribution [20].
The refinement of the harder W in the softer Cu can be explained by a localized region with high plastic deformation where also the W-particles are deformed until the plastic deformation spreads throughout the whole sample because of the strong strain-hardening in the localized region [22].

2.6 Deformation of Cu-Fe

The Cu-Fe phase diagram shows a spinodal decomposition and at room temperature the miscibility of Cu in Fe and Fe in Cu is almost zero but near the melting temperature T_m of Cu the solubility of Fe goes up to about 5 wt% (Figure 4b).
In recent years it was tried to generate a supersaturated solid solution by HPT-process. As soon as the Fe- or Cu-fragments go below a certain size they become unstable because of capillary pressure [23]. This can be used to produce nanocrystalline materials with a grain size of about 15 nm being smaller than the grain size achievable with HPT deformation of the pure materials (300 nm for Cu and 400 nm for Fe). During heating, the supersaturated solid solution becomes unstable and pure nm-scaled Cu- and Fe-crystals begin to evolve. The obtained structures are stable up to annealing temperatures of 620 °C for 1 h before grain growth occurs. Interesting is the fact that the hardness of the supersaturated solid solution increases with increasing annealing temperature until the material decomposes and the hardness decreases [10].

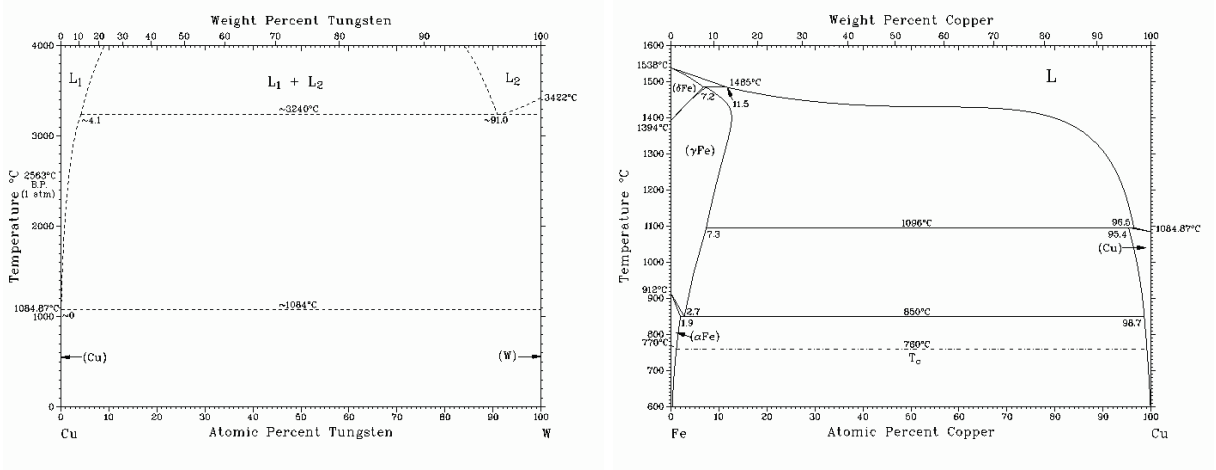

(a) Phase diagram Cu-W [24]

(b) Phase diagram Cu-Fe [25]

Figure 4: The phase diagrams of Cu-W and Cu-Fe show both a spinodal decomposition but contrary to Cu and W, Cu and Fe show a very low solubility near the melting points (≈ 5 wt%).

2.7 Deformation of Cu-yttria

Stobrawa et al. [26] produced Cu-yttria microcomposites with different compositions by milling Cu and Y_2O_3 powders in a planetary ball mill in an argon-methanol atmosphere for 30 h. This was

done until the particle size was below 200 nm with a majority share of 20 nm to 40 nm particles. After milling, low temperature sintering at 550 °C to 570 °C was conducted. The grain size did not increase during sintering, but the danger of agglomeration of the nanocrystalline powder or increasing porosity of the sintered material exists.
The compression test shows that a higher amount of Y_2O_3 increases the yield strength and up to 1 wt% the plasticity of the material is not reduced. But samples containing more than 2 wt% Y_2O_3 can be brittle.

2.8 Reinforcing the matrix for applications at higher temperature

One of the drawbacks of nanocrystalline materials is the poor microstructural stability at higher temperature as the large amount of grain boundaries not only encourages creeping but also grain growth and so worsens the ratio between hardness and ductility. Pure Cu was deformed by HPT to a resulting strain of $\epsilon_v = 100$ at a radius of 3 mm and subsequently annealed. In Figure 5a, the development of micro-hardness and grain size over annealing temperature can be seen. With increasing annealing temperature the grain size increases and so the hardness decreases. To take advantage of the superior properties of nanomaterials also at higher temperatures, it is important to stabilize their microstructure. In the last years, a stabilization was achieved by addition of dispersed particles, mostly oxides (e.g. Y_2O_3) or carbides (e.g. WC) [26–30]. The idea is to place fine particles at the grain boundaries to hinder their movement and oppress grain growth, but the efficiency depends on the content of particles and their size. Additionally, the fine dispersoids in the grain hinder dislocation movement by forcing them to by-pass the particles or to leave behind a dislocation loop around the dispersoids (Orowan bowing), leading thus to strain hardening stronger than in pure materials [13].
One obstacle when producing dispersion strengthened nanocrystalline materials is how to insert the particles in the matrix as most of the time immiscible elements are used (e.g.: Y_2O_3 in Cu). Stobrawa et al. [26–30] obtain the desired structure by using powder metallurgic technology namely milling the primary powders, compacting and finally sintering. In contrast to the Cu-WC samples, the pure Cu softens after annealing at 550 °C for 8 hour and after annealing at 600 °C the hardness is nearly reduced by half (see Figure 5b). Similar results for pure Cu can be found in [18], where after annealing at 0.5 T_m (T $\approx$ 400 °C) for 1 hour the values of undeformed Cu are reached again.
A result of milling is that the powder which is in the µm-range is refined to below 50 nm and homogeneously distributed throughout the whole material. However, the properties as hardness, yield strength and conductivity are not maximal because of a remaining porosity, which cannot be fully removed by compacting and sintering, and furthermore, because of the brittleness of the dispersoids [27] .

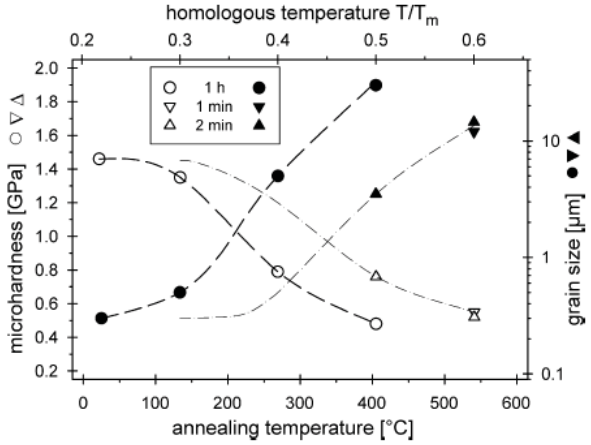

(a) Evolution of microhardness (open symbols) and grain size of pure Cu: The hardness decreases with increasing annealing temperature, but the grain size increases. Annealing time also influences the hardness and grain growth [18].

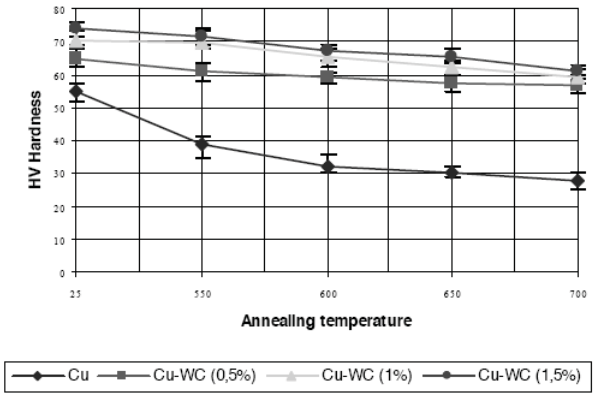

(b) The hardness decreases not as strong if the Cu was stabilized with WC [30]. For lower annealing temperatures the influence of the compositions is stronger and after annealing at 700 °C the difference between different compositions is small.

Figure 5: Hardness and grain size depend on the annealing temperature, but also on the annealed material.

3 Experimental

3.1 Starting material

As initial material for the majority of the produced specimen powders were used. Additionally, three bulk materials produced by Plansee SE, Austria (W – 10 wt% Cu, W – 20 wt% Cu and W – 25 wt% Cu) and one pure Cu-bulk material (Cu: 99,9% purity) were used as reference materials. In Figure 6 W – 20 wt% Cu as it was received can be seen with gray-blue W-particles in a reddish Cu-matrix. Comparison of results from HPT-specimen produced via the powder route or from bulk materials allows the depiction of the influence of the powder route on the microstructure and the mechanical properties of the final bulk material. Due to the large specific surface of powders and the decrease of purity, the properties of the produced materials might be changed in comparison to initial bulk specimens.
Powders were measured (Cu – 25 wt% W, Cu – 12 wt% Fe - equals the vol% of W - and Cu – 4 wt% Y_2O_3) and mixed by a circular mixing tool. In Figure 7, SEM-micrographs of powder particles used for this thesis can be seen. The Cu-powder consists of dendritically grown particles which are approximately 2 µm in width and 20 µm in length. It can be seen that the powder is agglomerated. Larger particles in the Fe and W-powder have a diameter of 2 µm but a large amount of the particles is smaller than 0.5 µm. The shape of the Fe-particles (99,9% purity) is globular but W.particles are more polyhedral. The particle size of the Y_2O_3-powder (99,90% purity) is not homogeneous and is difficult to determine (approximately 5 µm) because it is also agglomerated. Furthermore, the yttria-particles are full of cracks.

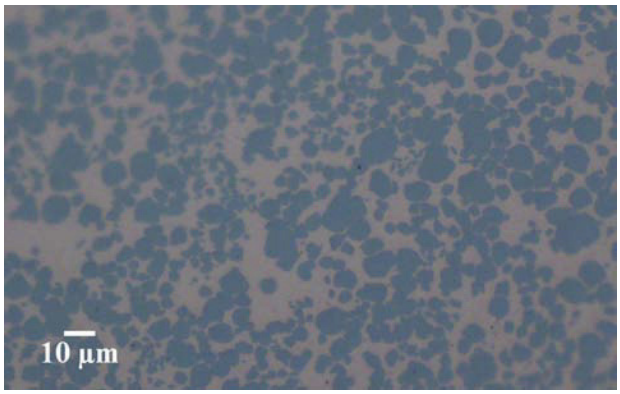

Figure 6: Light microscopic image of industrial produced W – 25 wt% Cu as it was received fron Plansee SE, Austria. The W-phase is gray-blue and Cu gray-red.

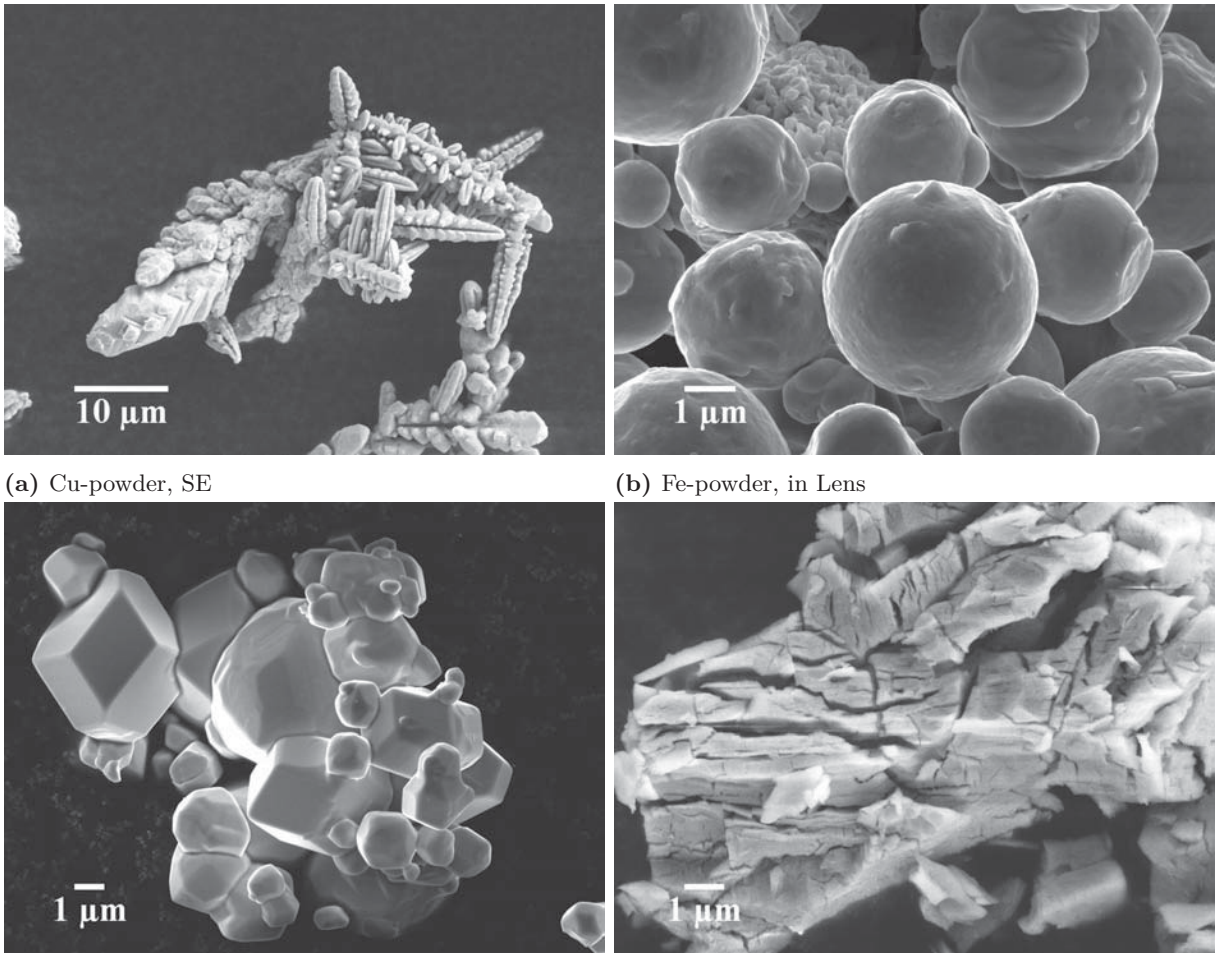

(a) Cu-powder, SE

(b) Fe-powder, in Lens

(c) W-powder, in Lens

(d) yttria-powder, SE

Figure 7: SEM-micrographs of the powders which were used for the consolidation of various HPT-deformed specimen. They consist of dentritically (a), globular (b) and polyhaedrical (c) shaped particles but the yttria-powder (d) consists of fragments full of cracks.

3.2 Two-step HPT-process

For this thesis two different HPT-devices were used in a two-step process (Figure 8). First, larger samples were produced with an HPT-devices with a maximal force of 4000 kN, but due to the used high force and amount of material, the deformation causes heating of the material. To minimize this effect, only a low velocity (≈0.07 rpm) can be used. The second HPT-engine can deform smaller specimen with a maximal force of 400 kN and a velocity of ≈0.7 rpm. One big advantage of the smaller HPT-engine is the possibility of deforming not only at room temperature, but in a temperature range from −196 °C to 720 °C.
After mixing the powders, they are filled into a Cu-ring with an outer diameter being larger than the cavity of the anvils. The ring is glued on the lower anvil of the larger HPT. The inner diameter of the Cu-ring is as large as the cavity and thereby the amount of material that can be processed, is maximized. The anvils are closed, force of approximately 210 kN applied and one anvil is rotated for 2° to 3° against the other. The compact disc has to be removed so that the flattened Cu-ring can be cut off. That is important in order to prevent cracks from growing from the edge to the center on the one side and on the other, to prohibit the mixing of Cu of the ring with the powder and so changing the percentages of Cu in the specimen.
The disc is placed again in the anvil and is deformed for 10 turns at room temperature. The final measurements are 4 cm in diameter and 7 mm in height. Afterward, it is cut into half with a cutting disc (Struers Secotom) and a slice with a thickness of 2 mm is produced that can be used for hardness measurement. For the second HPT-step, two pieces (8 mm thick) are cut parallel to the first cuts and are turned round to a cylinder with a diameter of 7 mm to 8 mm (see Figure 8). These two cylinders are not fully circular as the height of the first large HPT-disc is smaller than the radius of the cylinders, but due to the compression deformation in the second HPT-step this is compensated. For the second HPT-step, pieces are cut off the cylinders at different radii (0 mm to 8.5 mm) which are approximately 0.8 mm thick. Figure 8 shows schematically the two-step HPT-process [31] and Figure 9 shows the cutting for a real Cu - 4 wt% Y_2O_3 sample.

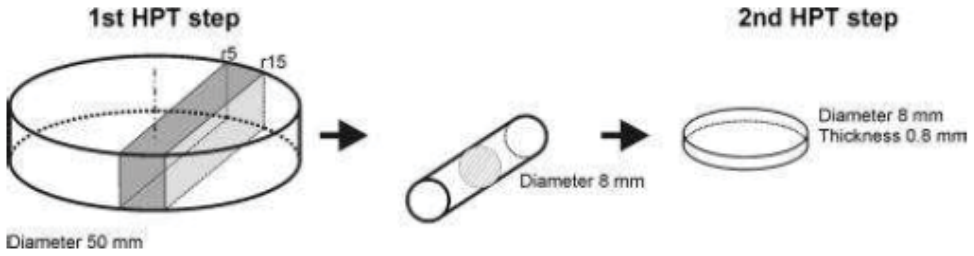

Figure 8: Schematic illustration of the two-step HPT-process for compacting and deforming powders given by Bachmaier et al. [31].

The exact outline of the second HPT-step on the smaller HPT varies from sample to sample. Not only is the number of turns (hence, the strain) and velocity of the rotation (hence, the strain rate) changeable but also the applied pressure and temperature. Even the diameter of the final specimen can be altered by using anvils with different cavities. For all but one sample, anvils with cavities of 8 mm are used and the pressure varies from 5 GPa to 7 GPa, so that the specimens are comparable. After the HPT-process, the height is reduced to approximately 0.5 mm because material was pressed between the anvils. This thickness was used for determined the equivalen v. Mises strain depending on the radius (subsection 2.2: HPT - High pressure torsion). For deforming the samples at higher temperatures, a water-cooled coil is placed around the anvils.

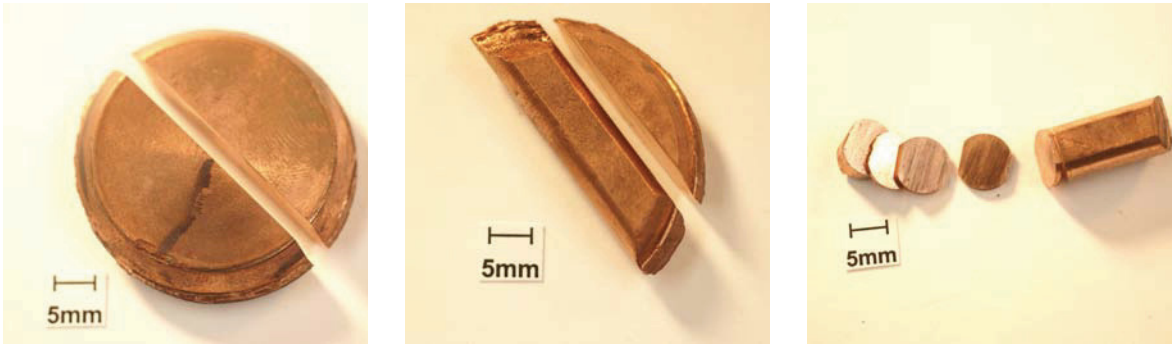

(a) large HPT-sample, cut in half **(b)** after cutting and turning round **(c)** finished for second HPT-step

Figure 9: Preparation for the second HPT-step: (a) Large HPT-sample was cut in half and a 2 mm slice was removed for hardness measurements and (b) A 8 mm piece was turned round. (c) The cylinder is cut into pieces with a height of 0.8 mm.

The anvils are heated inductively and which then heat the sample. The temperature is measured with a pyrometer on the anvil surface.
For further investigations the samples were cut into half which shows a fully tangential view and at a radius of 3 mm which shows a fully radial view in the center and towards the edge the tangential part increases. Those pieces were embedded (EpoFix from Struers with coal), grinded (SiC) and polished (OPS). In the beginning the samples were only cleaned with 2-Propanol in an ultrasonic cleaner, but doing so not all of the OPS-particles were removed. An additional cleaning step with soapy water in an ultrasonic cleaner and manual cleaning is needed to achieve clean specimens.

3.3 Thermal treatment of HPT-processed materials

The thermal treatment were either conducted in a vacuum furnace and inductively in vacuum as well as in air. The samples were placed on Al_2O_3 to reduce the heat conduction to the quartz glass tube for annealing in vacuum and on a steel anvil for the heat treatment in air (see Figure 10). Temperatures within the vacuum furnace were 720 °C, 800 °C, 810 °C and 900 °C and inductively achieved temperatures were 580 °C, 850 °C, 900 °C and 1000 °C. In the vacuum furnace, the heating rate was 10 °C min^{-1} and the holding time 1 h. The furnace cooling occurred under vacuum and was due to that fact slow. With inductive heating the end temperature was reached after approximately 1 min and the temperature was kept constant for 30 s to 60 s. In the furnace, the pressure was approximately 10^{-4} Pa at room temperature and 10^{-3} Pa at higher temperatures and during inductive heating, the minimal pressure was 10^{2} Pa.

3.4 Characterization of the processed material

The microstructure was characterized in a light-microscope and scanning electron microscope (SEM) type LEO 1525 using secondary electrons (SE) or backscattered electrons (BSE). For determination of the chemical composition of the produced materials, energy dispersive X-ray analyzes (EDX) were also performed at the SEM LEO 1525. Typical settings used were a voltage of 15 kV to 20 kV and a working distance between 0.5 cm to 1 cm, but for EDX scans larger distances were used. For this thesis, contrast and brightness of SEM micrographs were adjusted to improve the distinguishability.
The grain size of Cu in selected materials was determined with linear intercept method by using

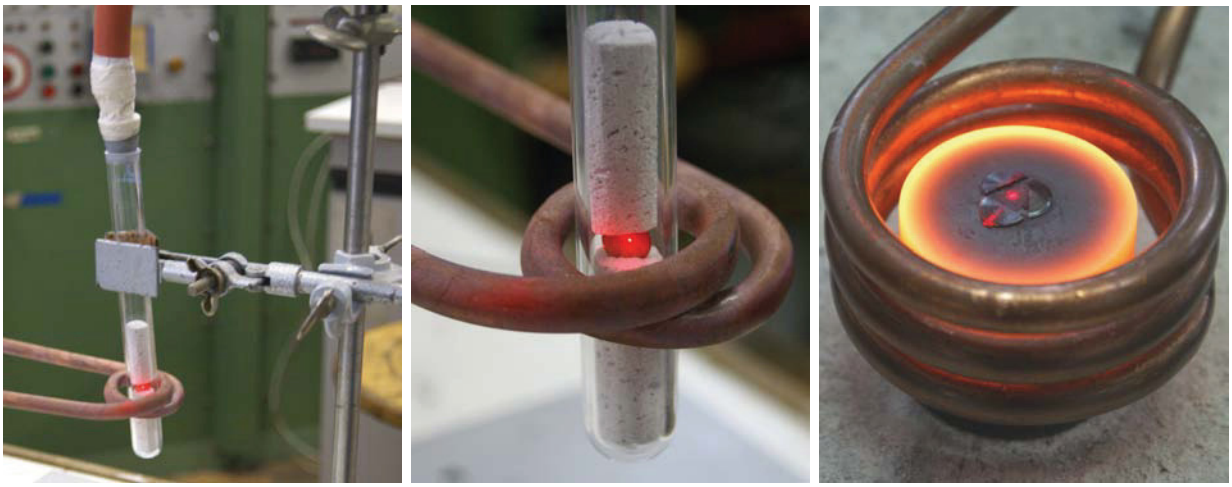

(a) annealing in vacuum **(b)** annealing in vacuum **(c)** annealing in air

Figure 10: Samples were annealed in vacuum and air to investigate the influence of higher temperature on structural stability. (a) and (b) show annealing in vacuum and in (c) the heat treatment in air of three HPT-samples can be seen.

SEM-micrographs (which are included in section 4). Six lines (two in shear direction, two perpendicular to the shear direction and two under 45°) were used.
To characterize the particle size of W, SEM-images were used. For the evaluation with ImageJ, ellipsoidal particles were assumed.

The Vickers hardness was measured with BUEHLER Microsmet using 500 g or 1000 g along the radii of the specimen divided in half. Hence, the correlation between hardness and strain can be seen. The distance between the measured points were 250 µm for small indentations and 500 µm for larger ones.

Tensile tests were conducted at room temperature to determine mechanical properties in dependance of the resulting microstructure as a consequence of the chemical composition, the applied strain and the thermal treatment. The fact that after the second HPT-step the sample thickness is only about 450 µm complicates the testing as the maximal diameter of the tensile specimen must be smaller. The average diameter was approximately 300 µm and even so not all samples could be produced fully circular, nevertheless, the correct cross-section area was taken into account for evaluation of stress. The HPT-discs were cut into halves after the second HPT-step, so that material at the edge (at radius 1.5 mm to 2 mm) which has experienced more strain could be tested.
To reduce geometrical mistakes as shoulder offset and the thermal influence the circular grinding tool (see Figure 11) developed by G. Rathmayr was used [32]. This tool consists of a grinding disc, an adjustable specimen holder, a liquid cooling system and a dial gauge. There are two shafts with a fixation for the samples in the specimen holder, which are synchronically driven by a motor. Due to this fact, the twisting moment on the sample is almost zero, because no side can slow down or accelerate individually. To measure the position of the specimen holder on the linear bearing, a dial gauge is used. The linear bearing is perpendicular to the axes of the grinding disc, so that the rotation axis of the specimen is perpendicular to the shoulder. For the liquid cooling system, water with some additive (Corrozip from Struers) is used.

As the specimen and the grinding disc rotate, the diameter is adjusted by moving the specimen holder along the linear bearing. After the grinding, an additional polishing step can be conducted. This was omitted because of the danger of breaking the very thin specimens (diameter $\sim 300\,\mu m$). Before testing, the diameter was measured with transmitted light on an optical microscope and it was controlled if the samples were completely circular.
The testing was performed at a Kammrath&Weiss (K&W) miniature tensile testing device and the exact procedure for tensile testing and evaluation is described by Rathmayr et al. [32]. Two different load cells were used: 200 N and 10 kN. A diode provided the light from underneath the specimen, so that the recorded pictures show a high contrast between the sample (dark) and the background (light).
The specimens were lying on the holder to avoid bending and only plasticine was used to absorb the released energy upon fracture and prevent the specimen from flying away. The speed of testing was $2.5\,\mu m\,s^{-1}$. During testing, pictures of the sample were taken with a single lens flex camera. They are used to determine the changing specimen geometry such as the thickness reduction and the increase in length. With this information available, it is possible to calculate true stress-strain values by using a Matlab package written by G. Rathmayr [32]. It was not controlled in this thesis if all requirements for a correct determination of true stress and true strain are fulfilled. Thus, only strain-stress curves are obtained.

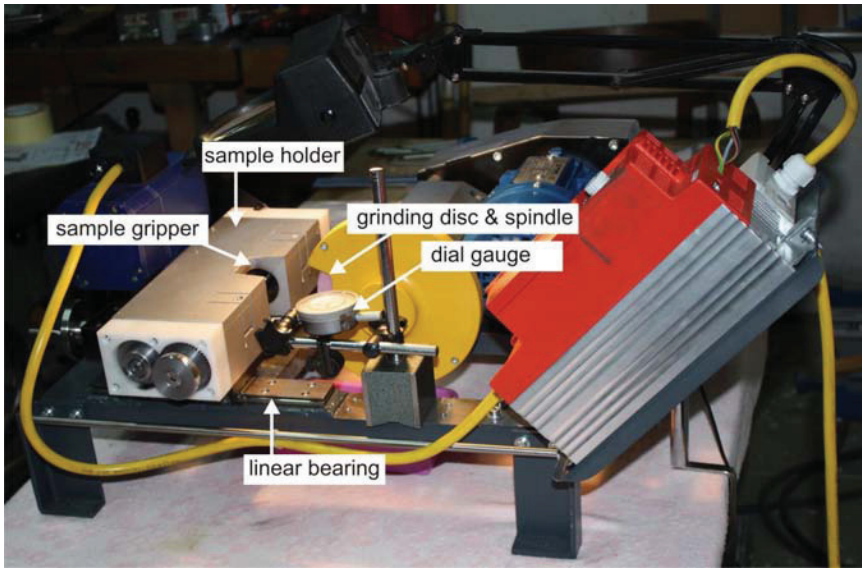

Figure 11: Picture of circular grinding tool which allows producing tensile samples with gauge length in the mm-regime and a diameter below 1 mm.

4 Results

In this thesis, the deformation behavior of several materials composed of one or two phases are described. The deformation was applied by HPT-process using different parameters (applied deformation, deformation temperature). An important aspect of this work is the investigation of the high temperature stability of the microstructure. Hardness measurements and tensile test were performed to characterize mechanical properties. For structural characterization SEM-images were taken and EDX-scans were performed. SEM-micrographs were used to investigate the grain size, the fraction size distribution of particles and the fracture surface. In Table 1 an overview of the used materials, HPT-parameters and results are shown.

Table 1: Overview of samples used in this thesis

material	1st HPT-step	number of turns in the 2nd HPT-step	annealing	shown results: hardness	EDX	tensile test	grain size	fraction size distribution of particles
Cu - 25 wt% W	10 turns at RT	30 at RT	-	yes	yes	yes	yes	yes
		30 at RT	1 h at 720 °C	yes	-	-	-	-
		30 at RT	1 min at 850 °C	yes	-	-	-	-
		30 at RT	1 h at 900 °C	yes	-	-	-	-
		30 at RT	1 min at 1000 °C	yes	-	-	-	-
		200 at RT	1 h at 900 °C	yes	-	-	-	-
		400 at RT	-	yes	yes	-	yes	yes
		400 at RT	1 h at 720 °C	yes	-	-	-	-
		400 at RT	1 h at 810 °C	yes	-	-	-	-
		0 at 500 °C	-	yes	-	yes	yes	-
		5 at 500 °C	-	yes	-	yes	yes	-
		30 at 500 °C	-	yes	-	yes	yes	-
		30 at 500 °C + 5 at RT	-	yes	-	-	yes	-
		30 at RT + 5 at 500 °C	-	yes	-	yes	yes	-
Cu - 12 wt% Fe	10 turns at RT	30 at RT	-	yes	yes	yes	yes	-
		30 at RT	1 min at 850 °C	yes	-	-	-	-
		30 at RT	1 h at 900 °C	yes	-	-	-	-
		200 at RT	-	yes	-	-	-	-
		400 at RT	-	yes	yes	-	yes	-
		30 at 500 °C	-	-	-	yes	-	-
		30 at 500 °C + 5 at RT	-	-	-	yes	-	-
		30 at RT + 5 at 500 °C	-	-	-	yes	-	-
Cu - 4 wt% Y_2O_3	10 turns at RT	30 at RT	-	yes	yes	yes	yes	-
		30 at RT	1 min at 580 °C	yes	-	-	-	-
		30 at RT	1 min at 680 °C	yes	-	-	-	-
		30 at RT	1 h at 810 °C	yes	-	-	-	-
		30 at RT	1 min at 850 °C	-	-	-	-	-
		30 at RT	1 min at 1000 °C	yes	-	-	-	-
		121 at RT	-	yes	-	-	-	-
		200 at RT	-	yes	-	yes	-	-
		400 at RT	-	yes	yes	-	-	-
		30 at 500 °C + 5 at RT	-	-	-	yes	-	-
Cu-powder	-	30 at RT	-	yes	-	yes	yes	-
	-		1 h at 720 °C	-	-	-	-	-
Cu-bulk	-	30 at RT	-	yes	-	yes	yes	-
W - X wt% Cu, X=10, 20, 25	-	30 at RT	-	yes	-	yes	-	-
	-	30 at RT	5 h at 800 °C	yes	-	-	-	-
	-	30 at RT	5 min at 900 °C	yes	-	-	-	-
	-	30 at RT	5 min at 1000 °C	yes	-	-	-	-
W - 25 wt% Cu	-	100 at RT	-	yes	-	-	-	-

4.1 Deformation at room temperature

4.1.1 Hardness

In Figure 12 it can be seen that the hardness of 13 different HPT-deformed samples depends on the chemical composition and the applied strain. In general, it can be said that the hardness increases with increasing strain: For higher strain all three materials, Cu – 25 wt% W, Cu – 4 wt% Y_2O_3 and Cu – 12 wt% Fe, approach about the same value (right side of Figure 12). Cu – 12 wt% Fe reaches that hardness very quickly, but in the region $\epsilon_v = 1000 - 8000$ the hardness abates for 20 HV to 30 HV before it increases again. Cu – 25 wt% W and Cu – 4 wt% Y_2O_3 show a very similar distribution of hardness. At low strains, the hardness increases slightly before it stays stable for $\epsilon_v \approx 1000$. Then the hardness increases more strongly and even after $\epsilon_v = 10000$ the curve does not level. Interesting is that even the pure Cu-specimen produced out of powder shows the same hardness as W- and yttria-reinforced Cu, while the Cu-sample produced with bulk material is softer (only 180 HV instead of 215 HV).

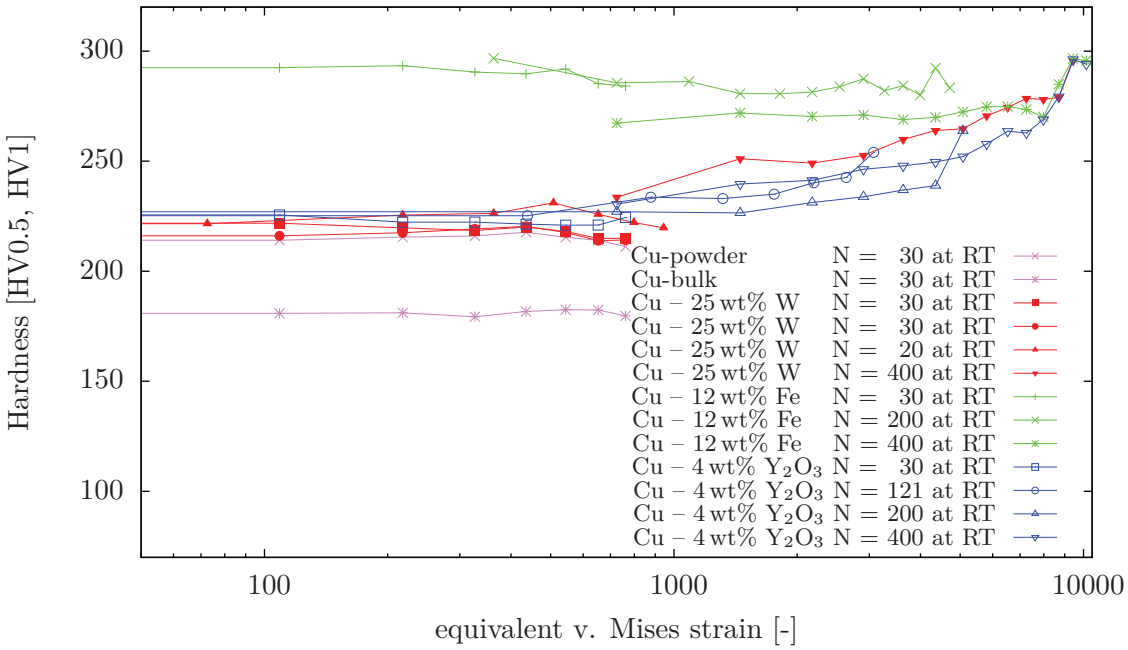

Figure 12: Vickers hardness as function of equivalent v. Mises strain. Notice the logarithmic scale for equilvalent strain. The hardness depends on chemical composition: Fe-particles influences it even at low strains, whereas W and yttria only distribute and increase hardness after higher deformations.

4.1.2 Scanning electron microscopy

The micrographs in Figures 13 to 15 and 17 to 23 show the samples in the same position. The samples were bisected in the middle or at a radius of 3 mm and in the SEM-images the radius changes from the left to the right (compare subsection 3.2). The images are never taken at the very edge of the sample, because of possible edge effects influencing the structure.
In Figure 13 the different behavior of bulk and powder as initial material can be seen. The microstructure is homogenous in both specimens and the grain size decreases only slightly with higher deformation (at larger radii). Compared to the deformed bulk material, the grain size in

the powder specimen is half the size. The grain size is even smaller if the Cu-powder is mixed with additional powders as Fe, W or yttria. Additionally, the decrease of grain size from the center to the edge is in these specimens more pronounced than in the Cu-bulk sample. Table 2 summarizes the grain size of all investigated powder-processed materials and the size decreases compared to bulk processed Cu due to three different aspects:

- using powder instead of bulk material
- addition of elements (W, Fe) or particles (yttria)
- applying higher strains

In the following images (especially in Figure 14 and 19 at higher resolution), there are some bright circular particles with a diameter of $\approx 100\,\text{nm}$. These are OPS-particles which are in the beginning not fully removed by cleaning after the polishing step (see subsection 3.2).
The gray particles in Figure 14 and Figure 15 are W-particles, while the Cu-matrix is darker. In Figure 17 and Figure 18 Fe-particles are darker than the surrounding Cu-matrix. Similar to the Fe, the yttria-particles are also dark-gray.
The portion of the larger particles decreases with higher applied deformation. This can be observed by comparing specimens with different amount of applied strain (compare specimen with 30 turns and specimens with 400 turns) and comparing the center with the edge of the same sample. In Figure 16, the fraction size of W-particles can be seen and with higher strain the portion of larger particles nearly vanishes. After higher applied strain, a large amount of the particles become too small to be measured by SEM and so the absolute number of particles decreases.
The co-deformation of Fe in the Cu-matrix works well and only some circular particles do not change their shape or size after deformation. In Figure 17a and Figure 18e such dispersoids can be seen and compared to the initial powder (Figure 7b) they do not change their shape. The microstructure of these particles is in the range of 200 nm and so the grains are more coarsen than the surrounding matrix (Figure 17c and Table 2).
Y_2O_3-particles (Figure 19) only break up at higher strains and they are not plastically deformed. So, their form is more angular in the center as well as at the edge and only the particle size changes.
W-particles are strongly agglomerated and it needs a very high strain to break them up (Figure 14 and Figure 15). Even after higher applied strain large agglomerates and particles remain in the samples. Because of some breaking of the particles, the fractions of small particles increase. Furthermore, the shape of the larger dispersoids changes to a more elongated form. This can be observed by comparing Figure 14a and Figure 14d, where the form changes for two large W-particles from circular in the center of the specimen to elongated at larger radii. Small particles have a circular shape. Interesting is how the Cu-matrix flows around larger particles as it happens in Figure 14a and Figure 15b as well as in Figure 18e. At higher resolution, it can be seen that small W-particles flow with the Cu-matrix around the agglomerates.

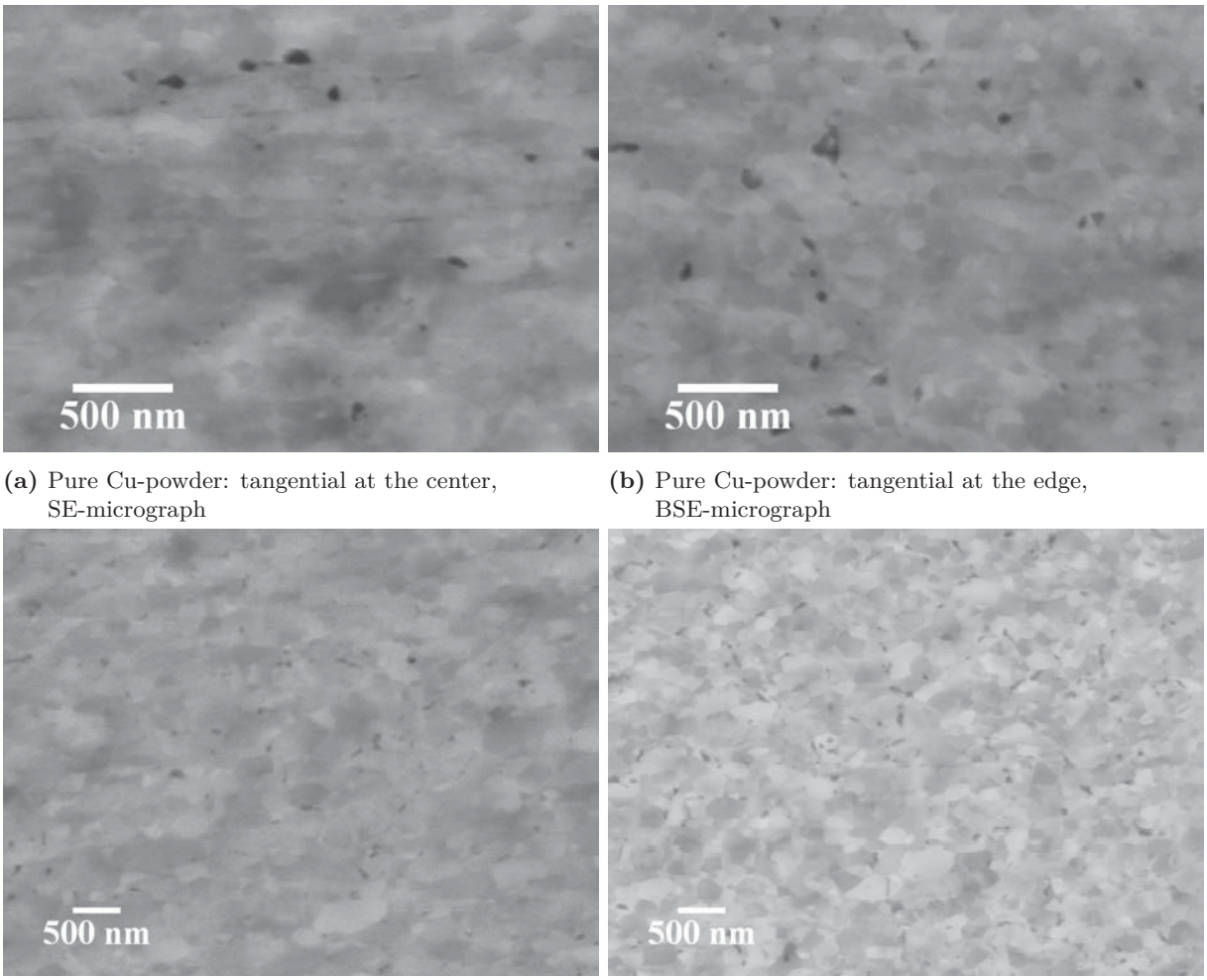

(a) Pure Cu-powder: tangential at the center, SE-micrograph

(b) Pure Cu-powder: tangential at the edge, BSE-micrograph

(c) Pure Cu-bulk: tangential at the center, SE-micrograph

(d) Pure Cu-bulk: tangential at the edge, BSE-micrograph

Figure 13: SEM-micrographs of two pure Cu-samples (one produced with powder and one with bulk as initial starting material) were deformed for 30 turns at room temperature.

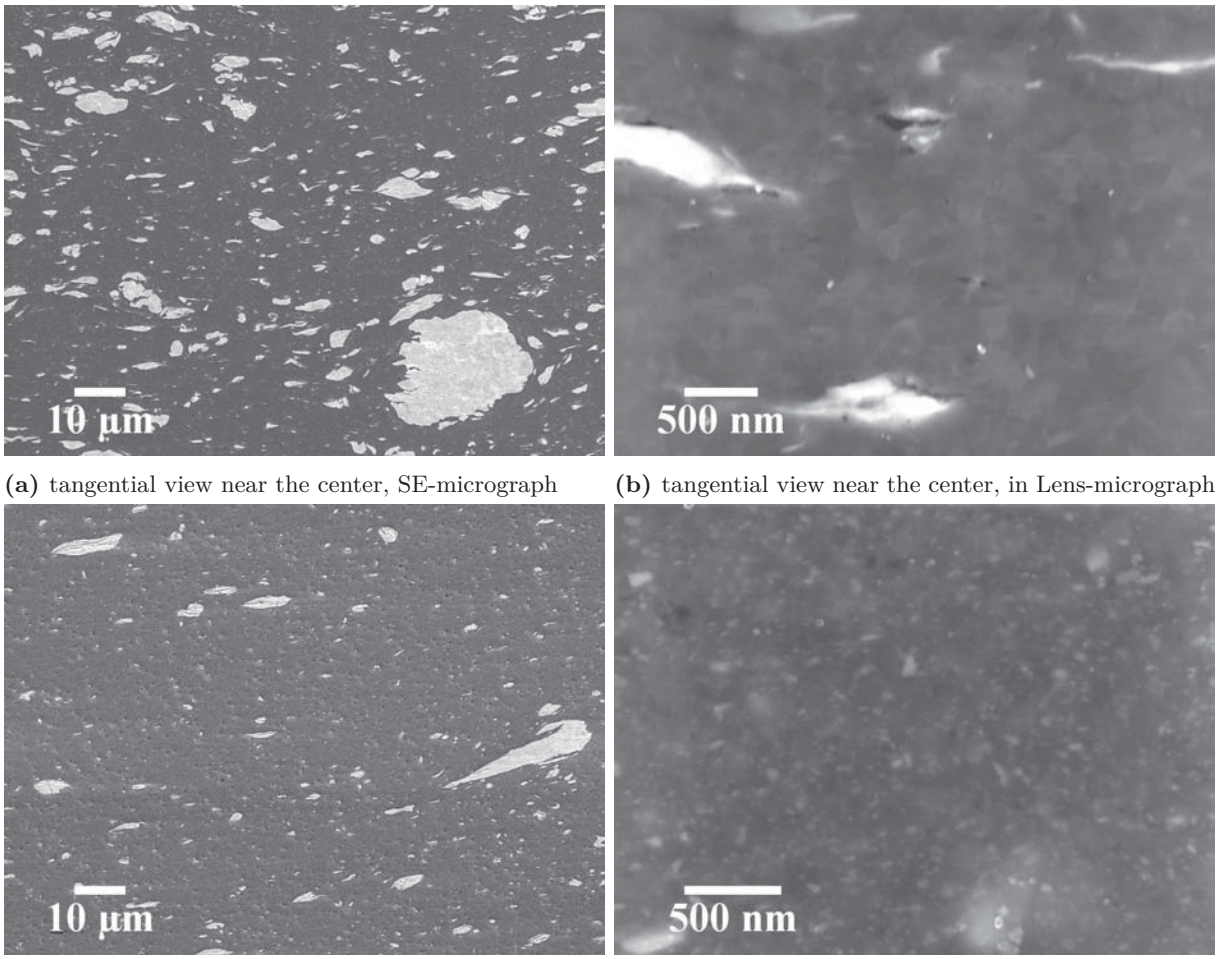

(a) tangential view near the center, SE-micrograph

(b) tangential view near the center, in Lens-micrograph

(c) radial view near the edge, SE-micrograph

(d) radial view near the edge, in Lens-micrograph

Figure 14: SEM-micrographs of Cu – 25 wt% W after 30 turns at room temperature: The grain size of Cu refines with higher strain, i.e. from the center to the edge of the specimen.

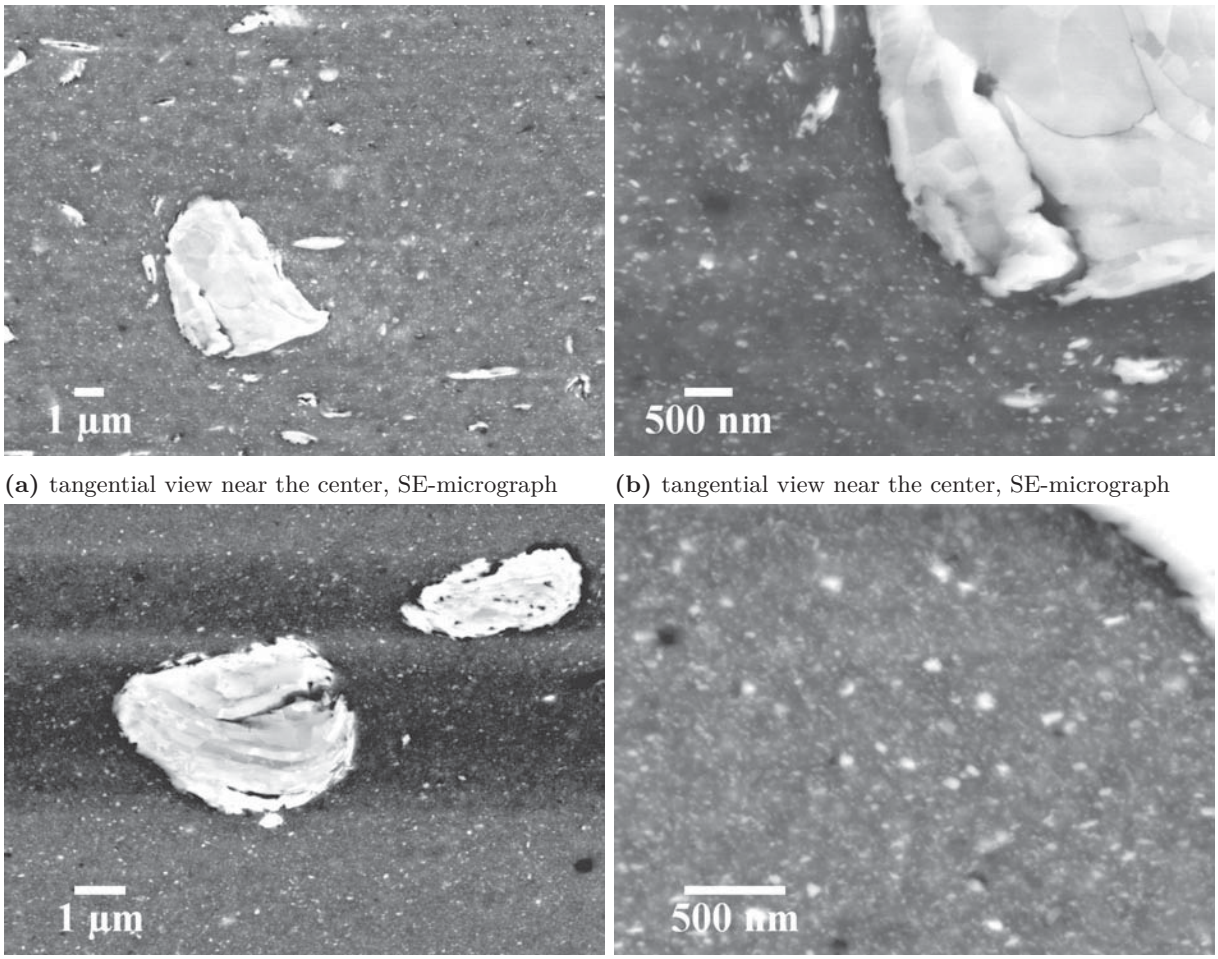

(a) tangential view near the center, SE-micrograph

(b) tangential view near the center, SE-micrograph

(c) tangential view near the edge, SE-micrograph

(d) tangential view near the edge, BSE-micrograph

Figure 15: SEM-micrographs of Cu – 25 wt% W after 400 turns at room temperature: The W-particles become smaller at the edge, but even after such high applied strain large particles still remain.

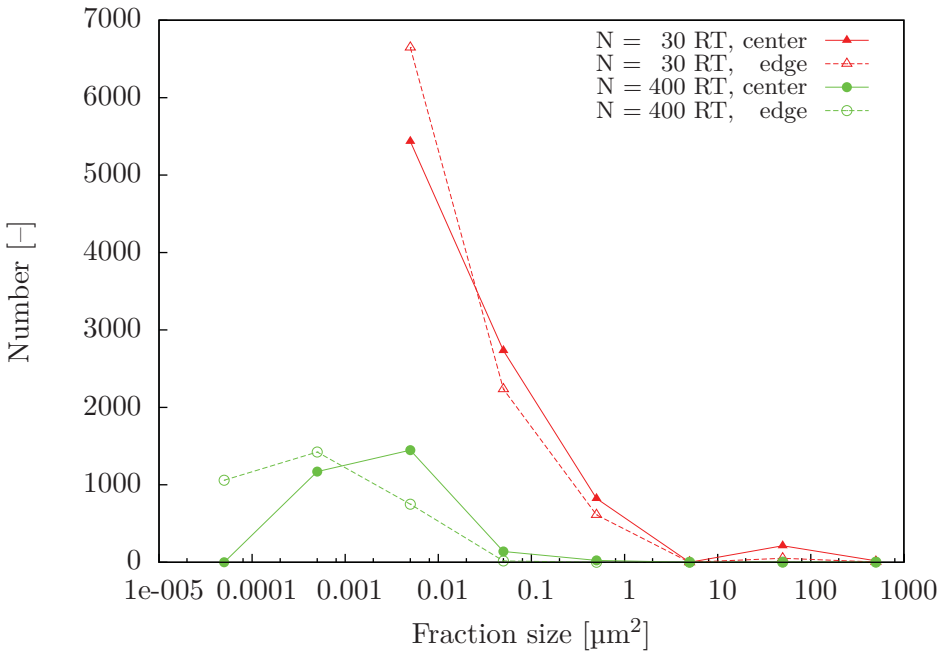

Figure 16: Fraction size distribution of W-particles after 30 and 400 turns near the center and the edge. The low number after 400 turns is due to the limited SEM resolution.

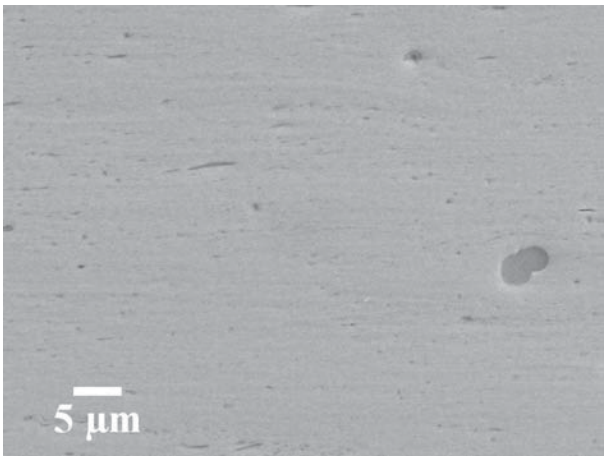

(a) tangential view near the center, SE-micrograph

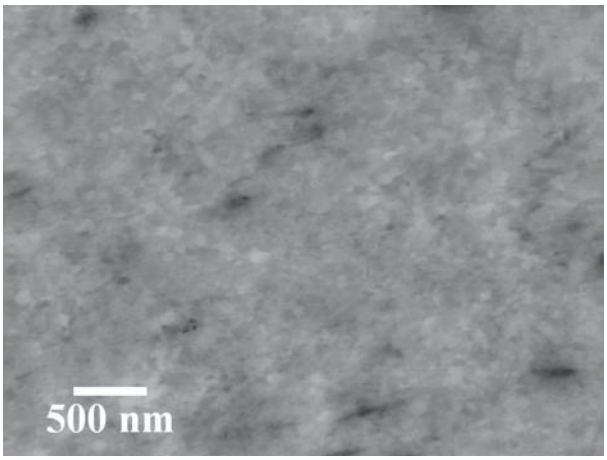

(b) tangential view near the center, SE-micrograph

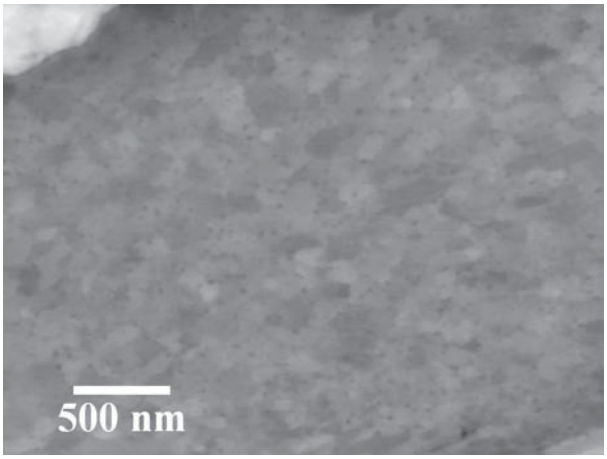

(c) tangential view at a undeformed Fe-particle near the center of the HPT-disc, SE-micrograph

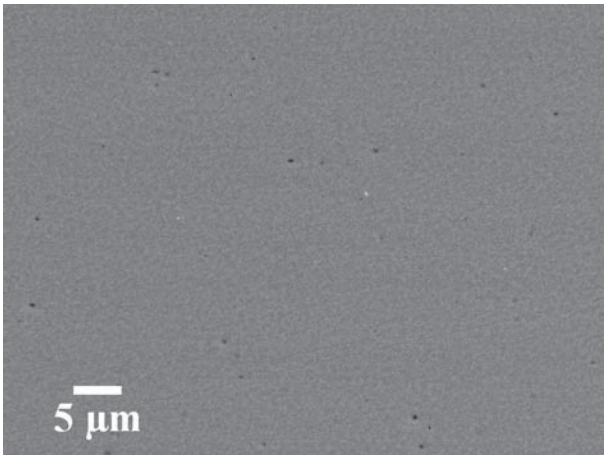

(d) tangential view near the edge, SE-micrograph

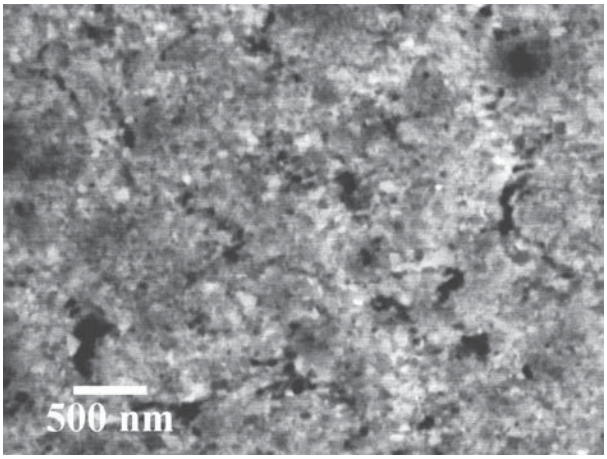

(e) tangential view near the edge, BSE-micrograph

Figure 17: Microstructure of Cu – 12 wt% Fe after 30 turns at room temperature. The Cu-grain size decreases slightly from the center to the edge and grain size of the Fe-grains is approximately two times as large.

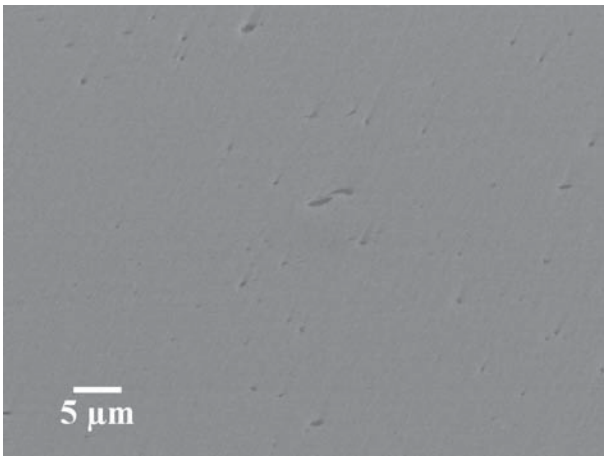

(a) tangential view near the center, SE-micrograph

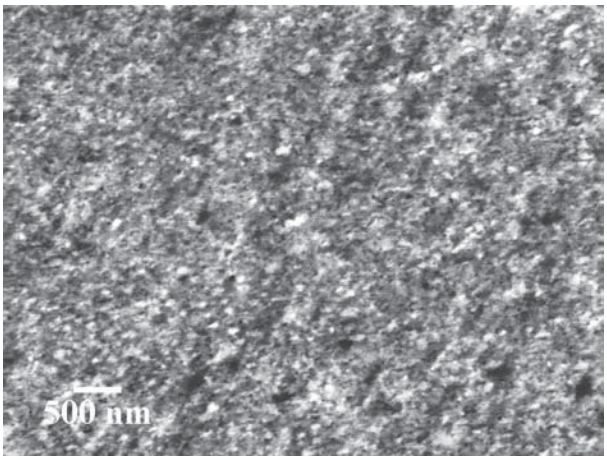

(b) tangential view near the center, BSE-micrograph

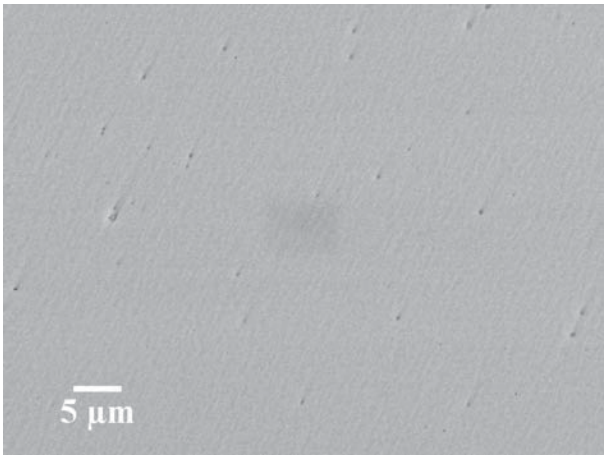

(c) tangential view near the edge, SE-micrograph

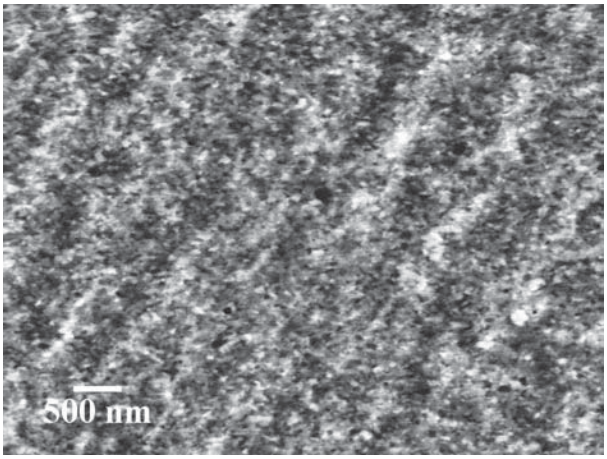

(d) tangential view near the edge, BSE-micrograph

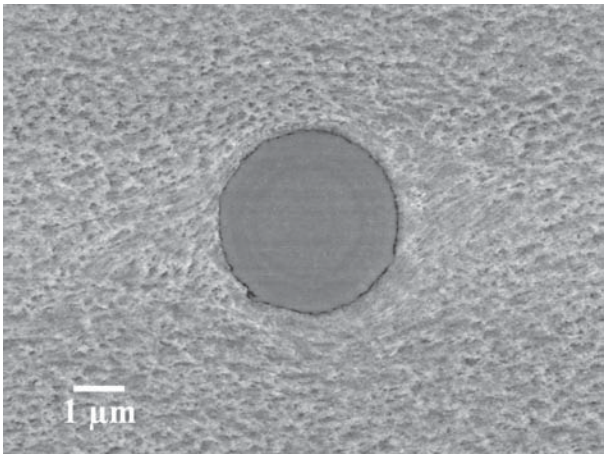

(e) Fe-particle in Cu, SE-micrograph

Figure 18: Microstructure of Cu – 12 wt% Fe after 400 turns at room temperature. The Cu-grain size decreases slightly from the center to the edge and in Figure 18e the flow of the Cu-matrix around an almost perfectly circular Fe-particle can be seen.

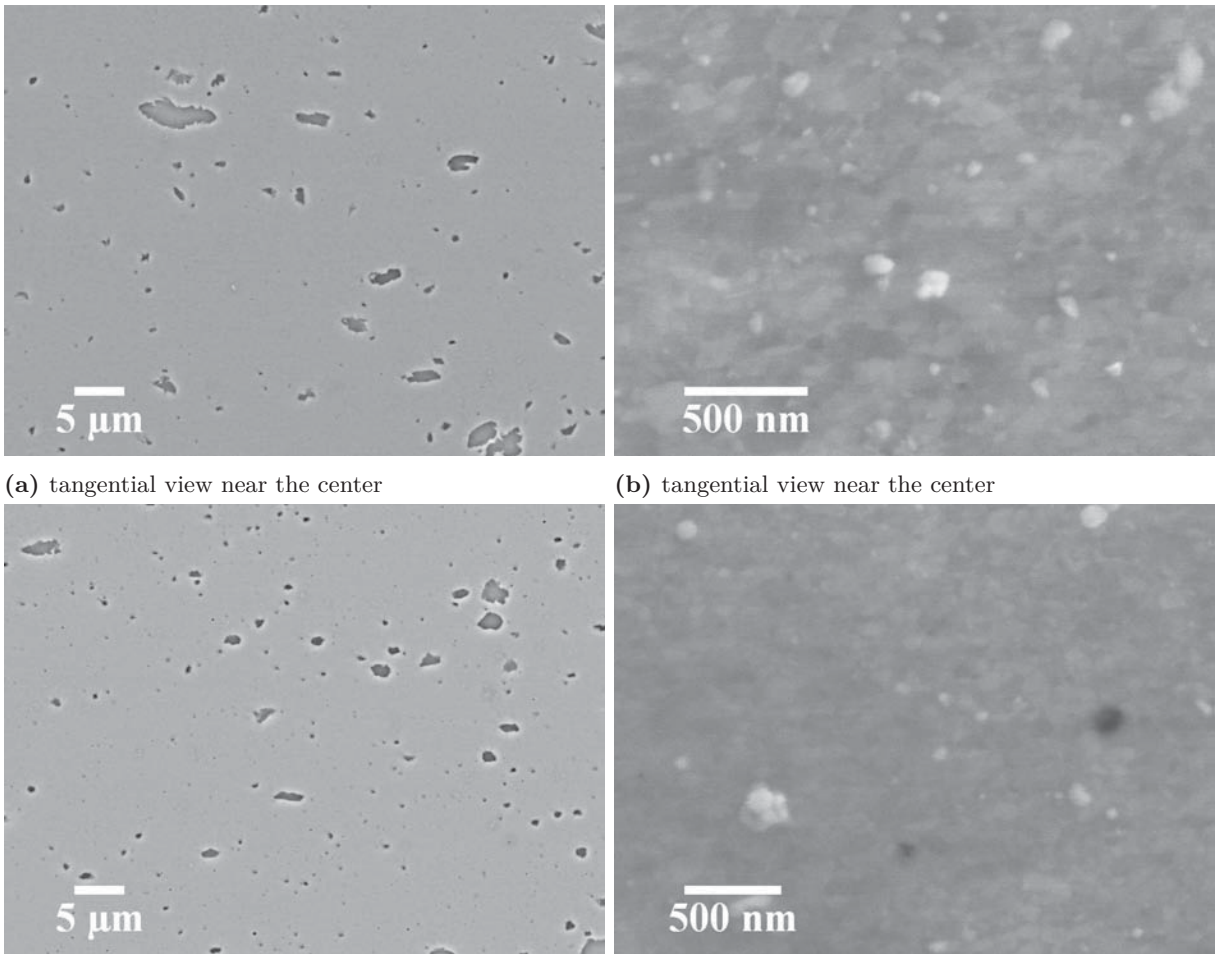

(a) tangential view near the center

(b) tangential view near the center

(c) radial view near the center

(d) radial view near the center

Figure 19: SEM-micrographs (SE) of Cu – 4 wt% Y_2O_3 after 30 turns at RT. The yttria-particles do not change their form, but with higher strain their size decreases by fracture of the particles or clasters of particles.

Table 2: Grain size of the Cu-matrix after HPT-deformation near the center and the edge

		Number of turns [–]	Grain size near the center [nm]	Grain size near the edge [nm]
1	Cu–powder	30	300	240
2	Cu-bulk	30	520	470
3	Cu – 25 wt% W	30	250	120
4	Cu – 25 wt% W	400	120	100
5	Cu – 12 wt% Fe	30	120	100
6	Cu – 12 wt% Fe	400	100	<70
7	Cu – 4 wt% Y_2O_3	30	230	150

For comparison W-bulk material produced by Plansee SE, Austria with different Cu percentages were deformed by HPT. The appearance of W in BSE micrographs is light gray and Cu is again darker (dark gray to black). In Figure 20, a W – 10 wt% Cu sample deformed up to 30 turns can be seen. W-lamellas are in the center parallel to direction of strain, but with higher strain, at the edge of the sample, the lamellas are more distorted and finer. With a higher amount of Cu, the W-lamellas become finer and the microstructure becomes more homogeneous. The structure of W – 20 wt% Cu with 30 turns at room temperature (Figure 21) is more uniform than with only 10 wt% Cu, but W – 25 wt% Cu (e.g Figure 22) is even more homogeneously. Hence, at the edge of this sample and at higher resolutions (Figure 22c) areas with a homogenous mix of Cu and W can be seen. For further investigations, the applied strain was increased and after 100 turns at room temperature, separated Cu and W areas remain only at the center (Figure 23a). But even in this area (Figure 23a: up to a radius of 500 µm or at an equivalent v. Mises strain of approximatly 450) the microstructure is very fine and the largest W-lamellas are in the range of 1 µm (Figure 23b). At the edge of the same sample, the structure is so fine and homogeneously that W- and Cu-grains smaller than 50 nm are only vaguely perceptible (Figure 23d).

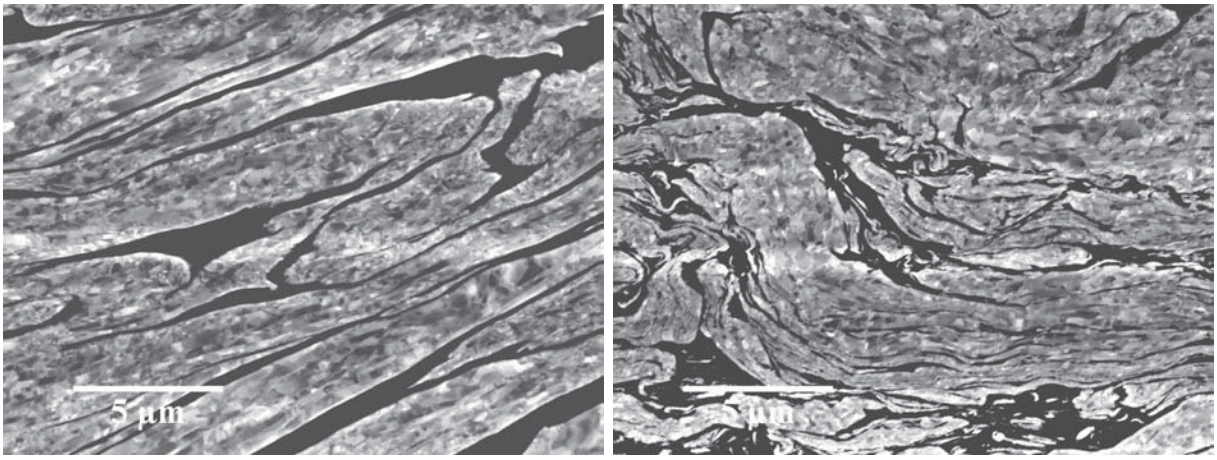

(a) tangential view near the center **(b)** tangential view near the edge

Figure 20: SEM-micrographs (BSE) of W – 10 wt% Cu after 30 turns at room temperature. W- and Cu-lamellas oriented in direction of strain can be seen, which become more distorted near the edge.

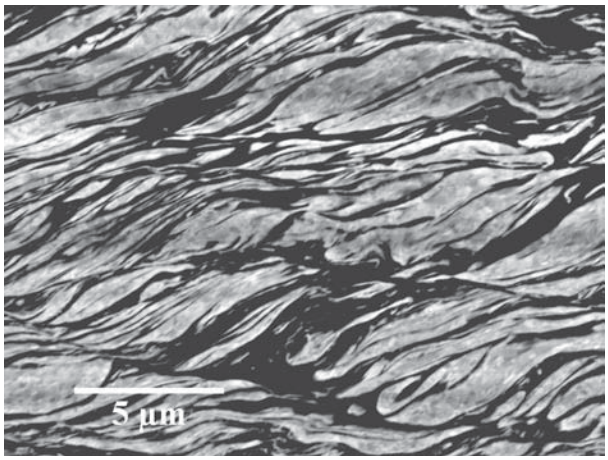

(a) tangential view near the center, BSE-micrograph

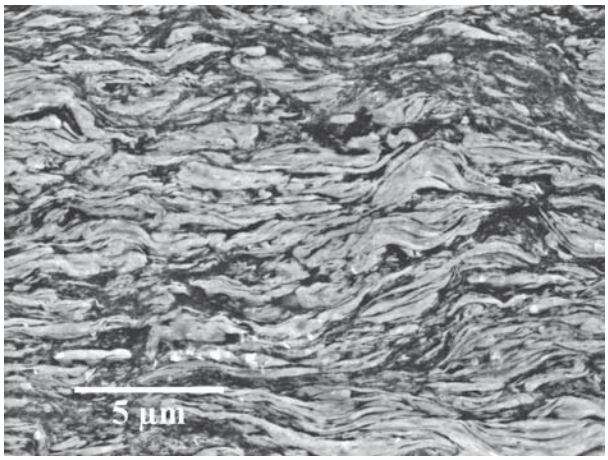

(b) tangential view near the edge, SE-micrograph

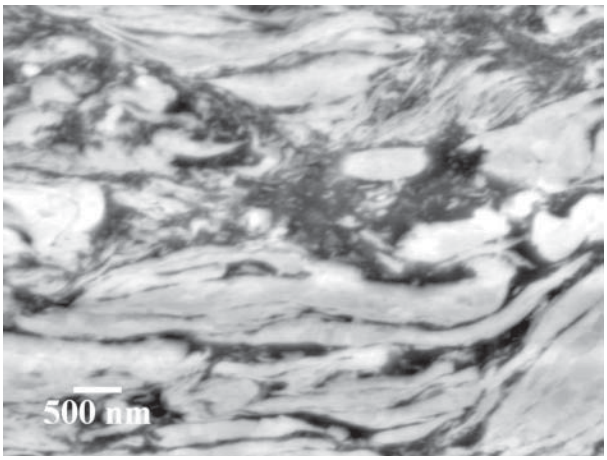

(c) tangential view near the edge, BSE-micrograph

Figure 21: SEM-micrographs of W – 20 wt% Cu after 30 turns at room temperature: The lamellas refine and the structure becomes more homogenous.

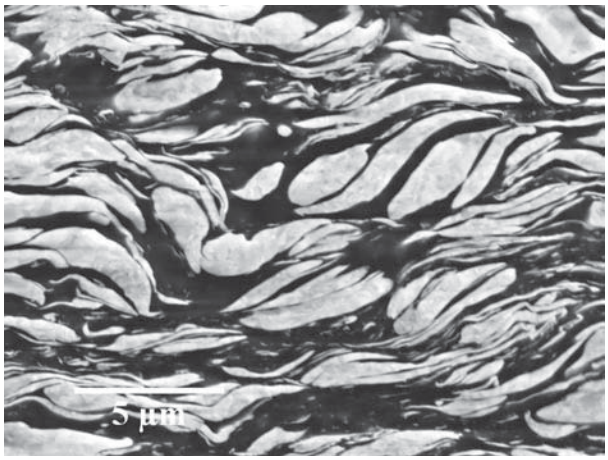

(a) tangential view near the center, SE-micrograph

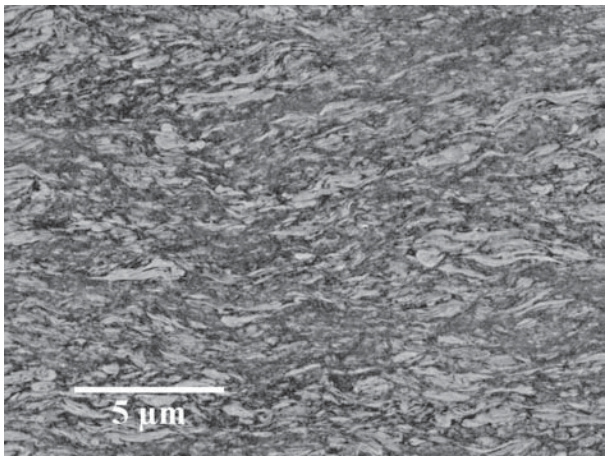

(b) tangential view near the edge, BSE-micrograph

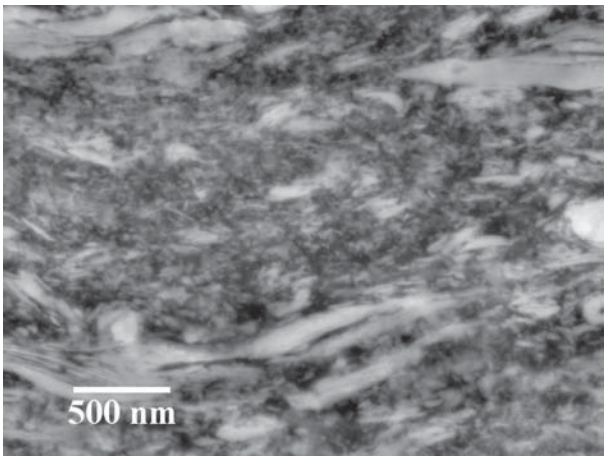

(c) tangential view near the edge, BSE-micrograph

Figure 22: SEM-micrographs of W – 25 wt% Cu after 30 turns at room temperature: The microstructure refines and shows no longer a lamellar structure near the edge.

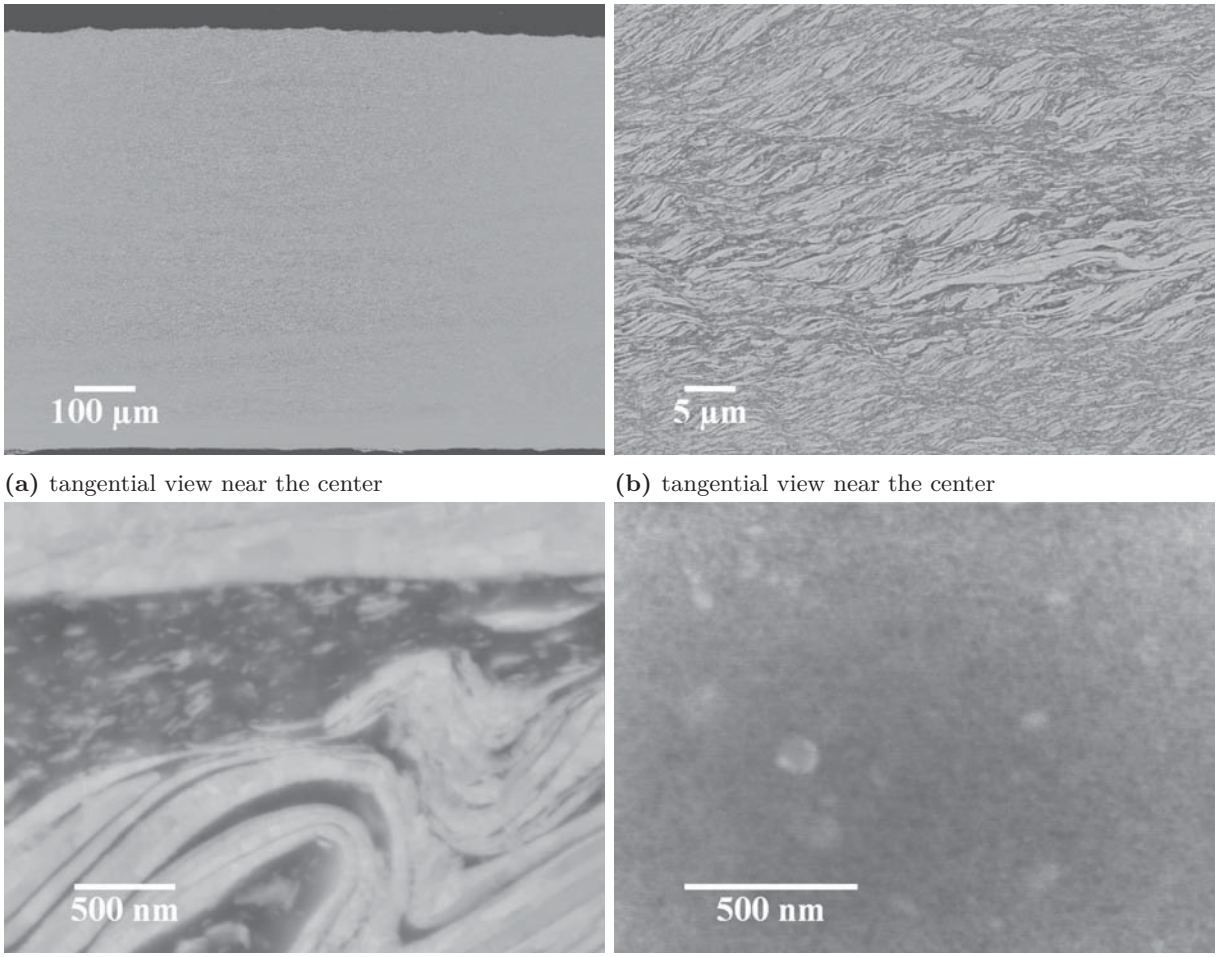

(a) tangential view near the center

(b) tangential view near the center

(c) tangential view near the center

(d) tangential view near the edge

Figure 23: SEM-micrographs (BSE) of W – 25 wt% Cu after 100 turns at room temperature: At the edge it is no longer possible to distinguish W from Cu and only in a small region in the center a pronounced lamellar structure exists.

4.1.3 Energy dispersive X-ray analysis

To investigate the distribution of the added particles, energie dispersive X-ray anlalysis (EDX) has been used. In Figure 24 a scan across a Fe-particle in a Cu-matrix and in (a) the content of Cu and Fe along a line scan across this particle can be seen. The other two images show the distribution of the same elements in the same investigated area and it can be seen that the dark-gray particle in (a) coincide with the red area in (c) and the dark areas with the Cu-matrix (b). The diagram in Figure 25 shows an EDX-line scan along the radius of a bisected Cu – 12 wt% Fe sample. The red line shows the content of Fe and the green one the content of Cu. Due to the low solubility of Fe in Cu the percentage of Fe is nearly 100 wt% and 0 wt% in the particle and the matrix, respectively. Only the average percentage of Fe is 12 wt% in the sample.

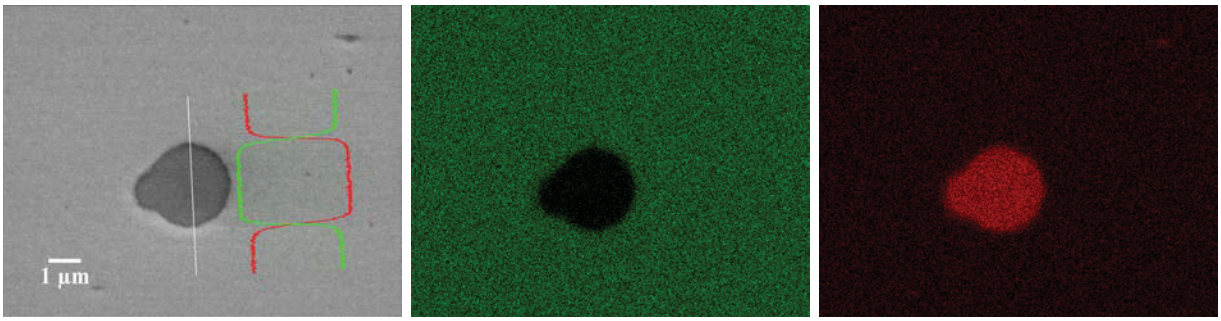

(a) SEM-micrograph (SE) **(b)** Cu-distribution **(c)** Fe-distribution

Figure 24: EDX-line and area scan over an Fe-particle (red) in Cu-matrix (green).

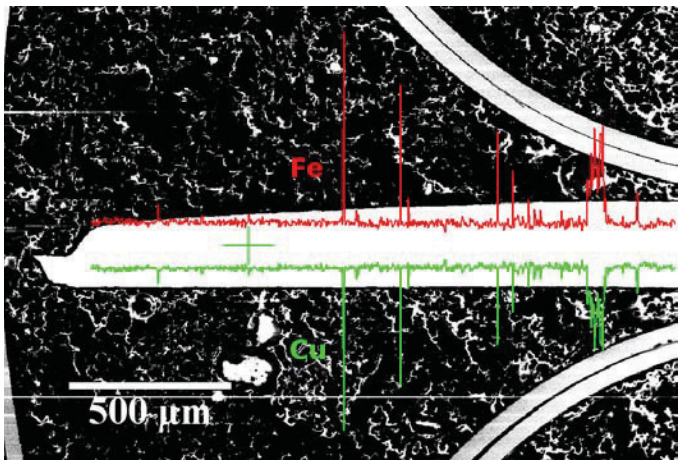

Figure 25: SEM-micrograph with an EDX-line scan over a biseced Cu – 12 wt% Fe sample deformed for 30 turns at room temperature.

The diagrams in Figure 26 show again EDX-line scans along the radius of bisected HPT-discs with three different compositions (Cu – 25 wt% W, Cu – 12 wt% Fe and Cu – 4 wt% Y_2O_3) with 30 and 400 turns at room temperature. The red lines are the moving average of the investigated elements Fe, W and Y and the green lines show the trend of the percentage. So while the trend line for Cu – 12 wt% Fe with 30 turns at room temperatures decreases with the radius, it is the other way around for the sample with 400 turns, where the amount of Fe increases slightly along the radius. In the diagrams of Cu – 25 wt% W both trend lines decrease along the radius, but the slope of the sample with 400 turns is steeper and the percentage of W in specimen with 30 turns at room temperatures varies stronger. On the other hand, the percentage of Y does not show a linear course, but there are several plateaus for one sample (400 turns at RT) and varies along the radius for the other one (30 turns at RT) without showing a defined trend.

4.2 Deformation at higher temperatures

4.2.1 Hardness

To improve the properties of some of investigated W-containing materials, the temperature of the second HPT-step is increased from room temperature to 500 °C, which is above the brittle to ductile transition temperature of W. In Figure 27 the line with squares represents the sample, which was deformed for 30 turns at room temperature and it is included for reference. The specimens marked with circles, which were both deformed for 5 turns at 500 °C, show a decreased hardness - especially at the center - compared to the sample represented by squares. In contrast to the magenta lines, the blue marked in samples are only annealed at 500 °C under pressure, but not deformed and have got a higher hardness than the deformed ones. Even though they were cut of at the same radius in the large disc after the first HPT-step, they show a different behavior along the radius. This might come from a still inhomogeneous distribution of - in this case - W-particles after the first HPT-step. Interesting is that the sample with 30 turns at 500 °C (orange line) has the same hardness as the ones after 5 turns at 500 °C. The two pronounced peaks in hardness are caused by W-agglomerates and should be ignored for comparing with other samples. After 30 turns at 500 °C and 5 turns at room temperature (red line) the hardness increases and at higher radii approaches the hardness of the sample only deformed at room temperature. Contrary to this, the hardness for the sample represented by the green line (30 turns at temperature and 5 turns at 500 °C) is lower, though the sum of the applied strain is the same.
In summary, it can be pointed out that there is a very pronounced influence coming from an increased deformation in the last step. The hardness and thus the microstructure is strongly influenced by deformation temperature, the number of turns and most important, the sequence of deformation steps. Thus, deformation steps at different temperatures are not commutative.

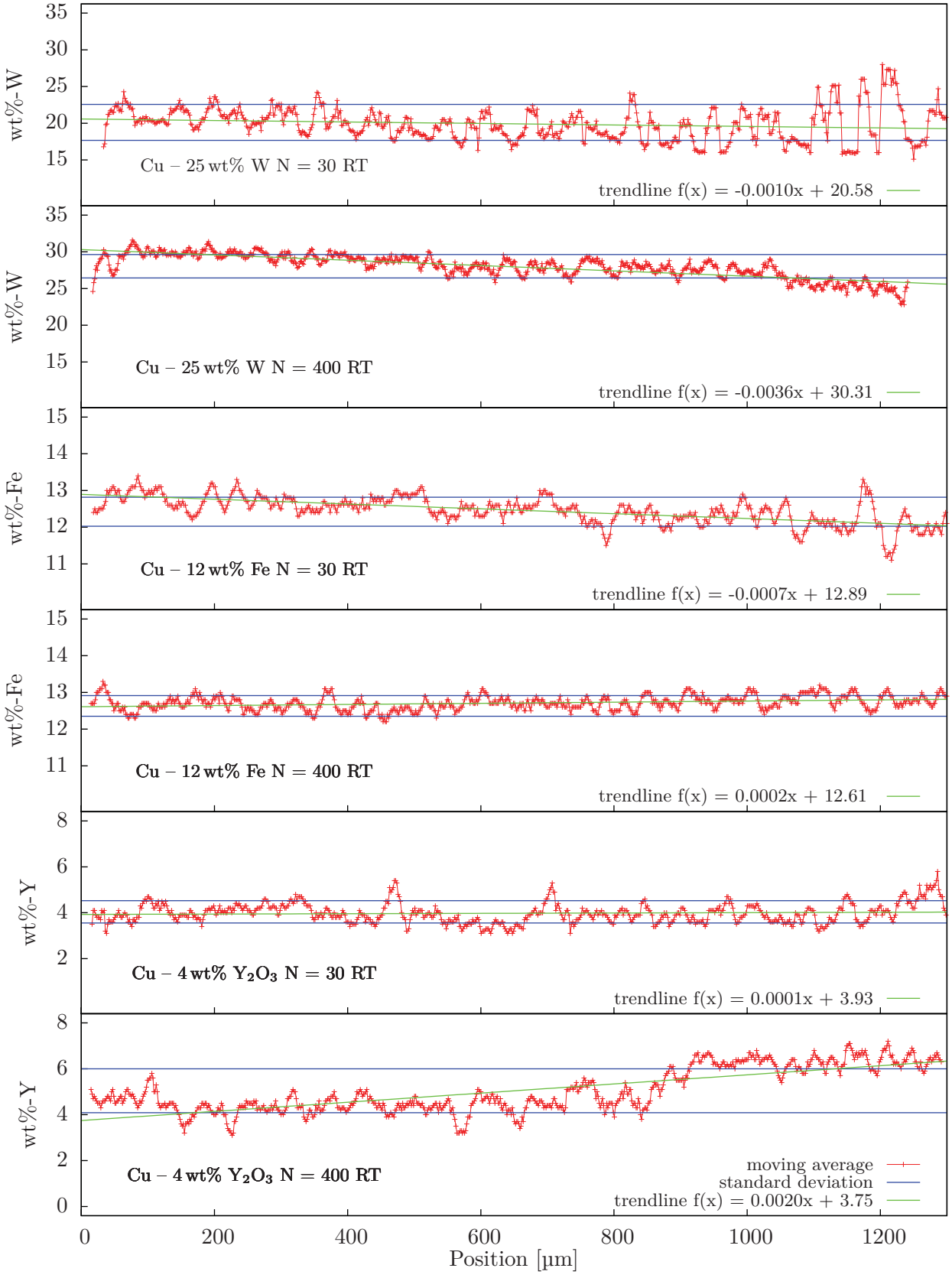

Figure 26: Energy dispersive line scans of HPT-samples with 30 and 400 turns at room temperature. The scans show no radius dependence of the content of W, Y or Fe.

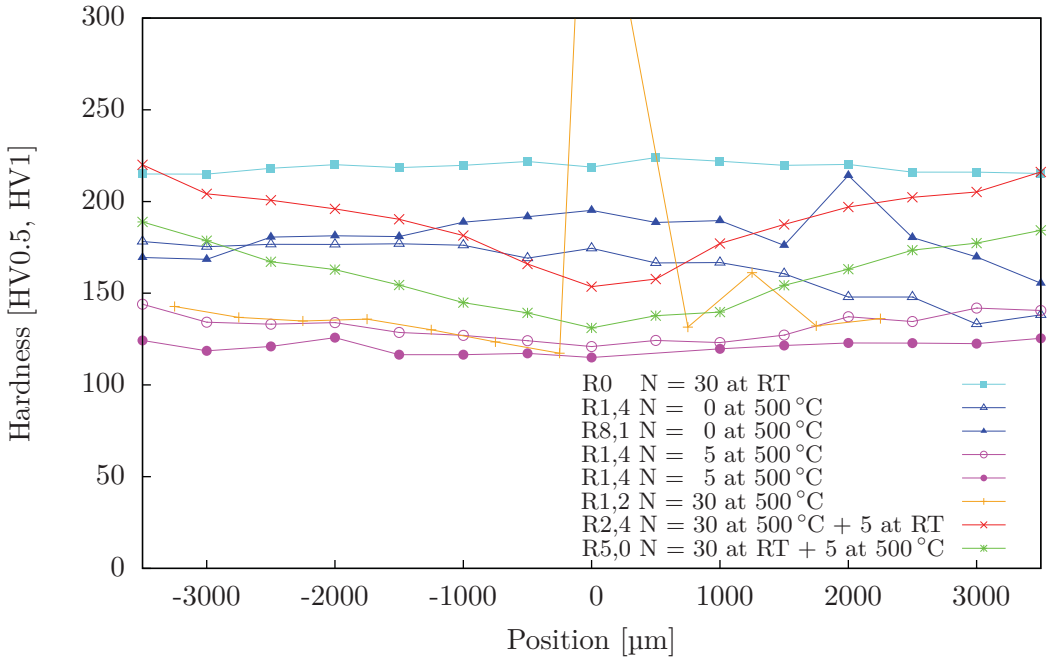

Figure 27: Vickers hardness as function of radius for W-stabilized Cu, which is deformed at room temperature, 500 °C and at both temperatures.

4.2.2 SEM-images

The following SEM-images show a radial view of the microstructure near the edge of the specimens deformed at 500 °C and the determined grain sizes in Table 3. The sample with the largest grain size is deformed for 30 turns at 500 °C (Figure 28) and is followed by the specimen with 5 turns at 500 °C (Figure 30). In Figure 28a in the left lower corner only larger W-particles can be seen and the Cu-matrix is more coarse in this area, too. This is caused by a very large W-agglomerate, which is located at the left side of the investigated area.
Compared to the other specimens, the sample which was first deformed for 30 turns at room temperature and then for 5 turns at 500 °C (Figure 29) has got more homogeneously distributed W-particles and also the lowest Cu-grain size. Even though only large W-agglomerates can be seen in the sample which was annealed under pressure - for the same amount of time which is needed for 5 turns - without additional deformation to the first HPT-step, the Cu-matrix does not grow as strong as in other samples (compare Table 3).

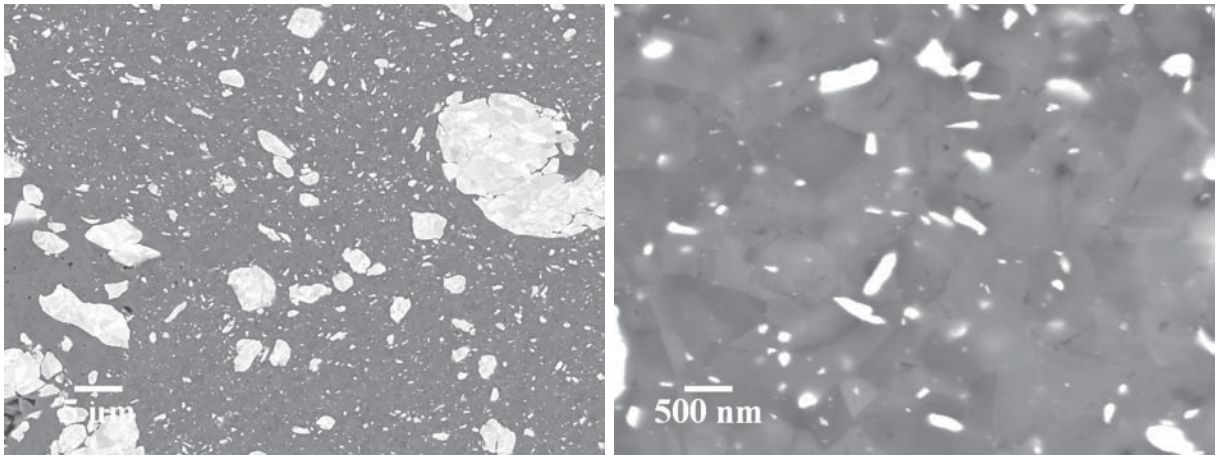

(a) radial view near the edge, SE-micrograph **(b)** radial view near the edge, BSE-micrograph

Figure 28: SEM-images of Cu – 25 wt% W after 30 turns at 500 °C: The Cu-matrix shows a strong recrystallized structure especially at (a) at the left side, where only large W-particles can be found.

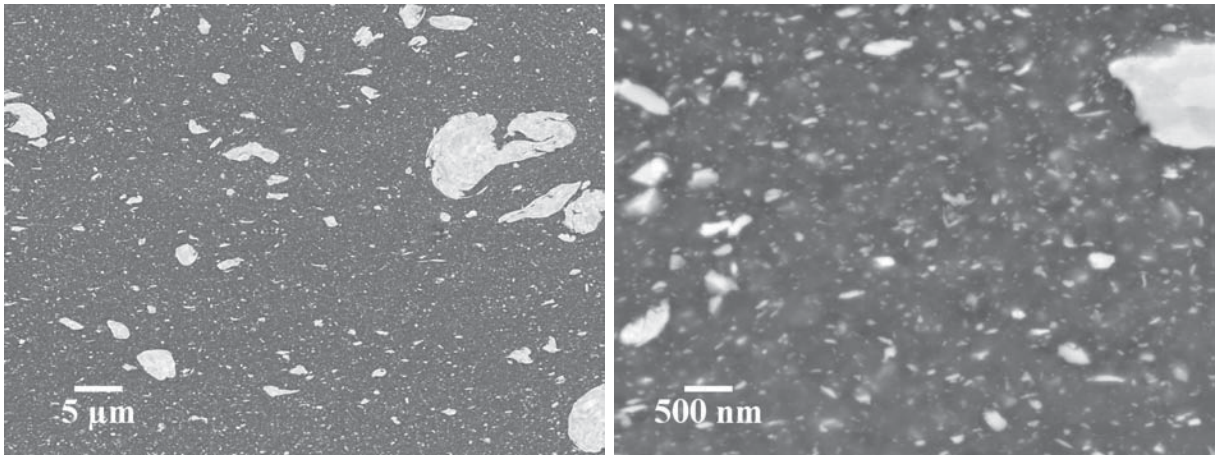

(a) radial view near the edge, BSE-micrograph **(b)** radial view near the edge, BSE-micrograph

Figure 29: SEM-images of Cu – 25 wt% W after 30 turns at room temperature and 5 turns at 500 °C: The W-particles are refined and stabilize the grain size of the Cu-matrix. The Cu-grains are not strongly coarsened.

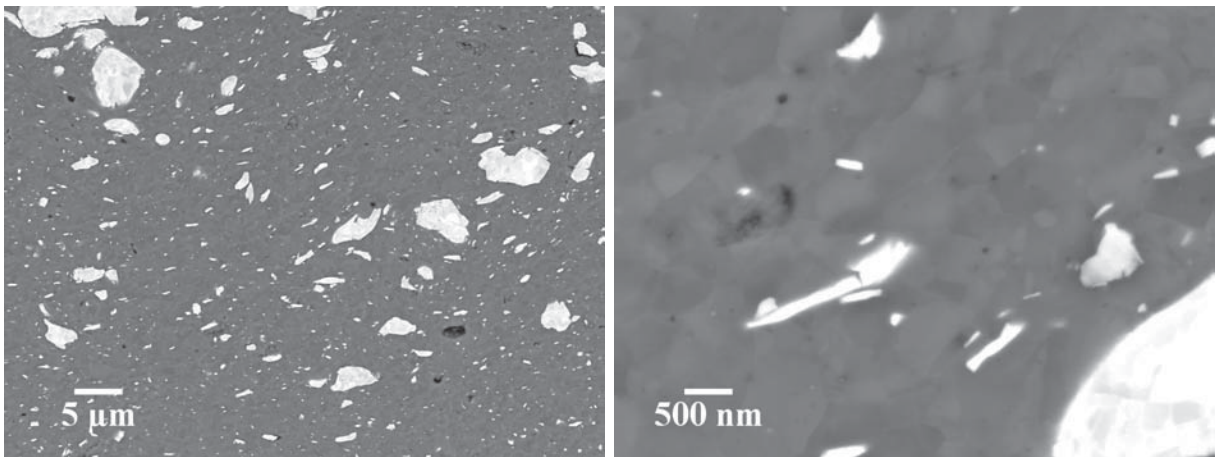

(a) radial view near the edge, BSE-micrograph **(b)** radial view near the edge, BSE-micrograph

Figure 30: SEM-images of Cu – 25 wt% W after 5 turns at 500 °C: Strong grain growth of the Cu-matrix occurs.

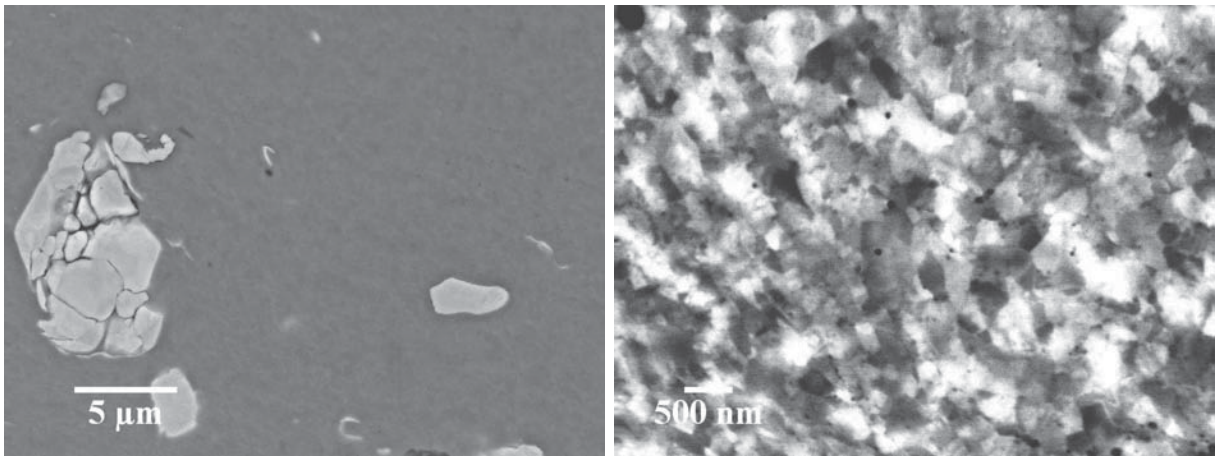

(a) tangential view at the Cu-matrix and W-agglomerate near the edge, SE-micrograph

(b) tangential view at the Cu-matrix near the edge, BSE-micrograph

Figure 31: SEM-images of Cu – 25 wt% W after 0 turns at 500 °C: As expected, no refinement of W-particles takes place. However, the Cu-matrix does not coarsen as strong as in other samples.

Table 3: Cu-grain size near the edge of the Cu-matrix after HPT-deformation

		Number of turns [–]	grain size near the edge [nm]
1	Cu – 25 wt% W	30 at 500 °C	670
2	Cu – 25 wt% W	30 at 500 °C + 5 at RT	370
3	Cu – 25 wt% W	30 at RT + 5 at 500 °C	200
4	Cu – 25 wt% W	5 at 500 °C	560
5	Cu – 25 wt% W	0 at 500 °C	300

4.3 Tensile testing

4.3.1 Tensile testing of pure Cu deformed with HPT

Both pure Cu samples (powder and bulk as starting material) are deformed by HPT and tensile tests are performed at room temperature (Figure 32). The virgin material of the stress-strain curve with the purple line was bulk Cu and for the blue stress-strain curve a powder was used. The yield strength of the powder processed material is higher, which was expected by the hardness measurement. In contrary, the bulk material shows significant strain hardening and obtains a higher tensile stress additionally to the higher fracture strain.
SEM-micrographs (Figure 33) show the fracture surface of both samples. For Cu-bulk it evident that a fully ductile, intergranular fracture has occurred, but at the same resolution the dimples in the tensile specimen produced of initial Cu-powder are smaller and not distributed as evenly.

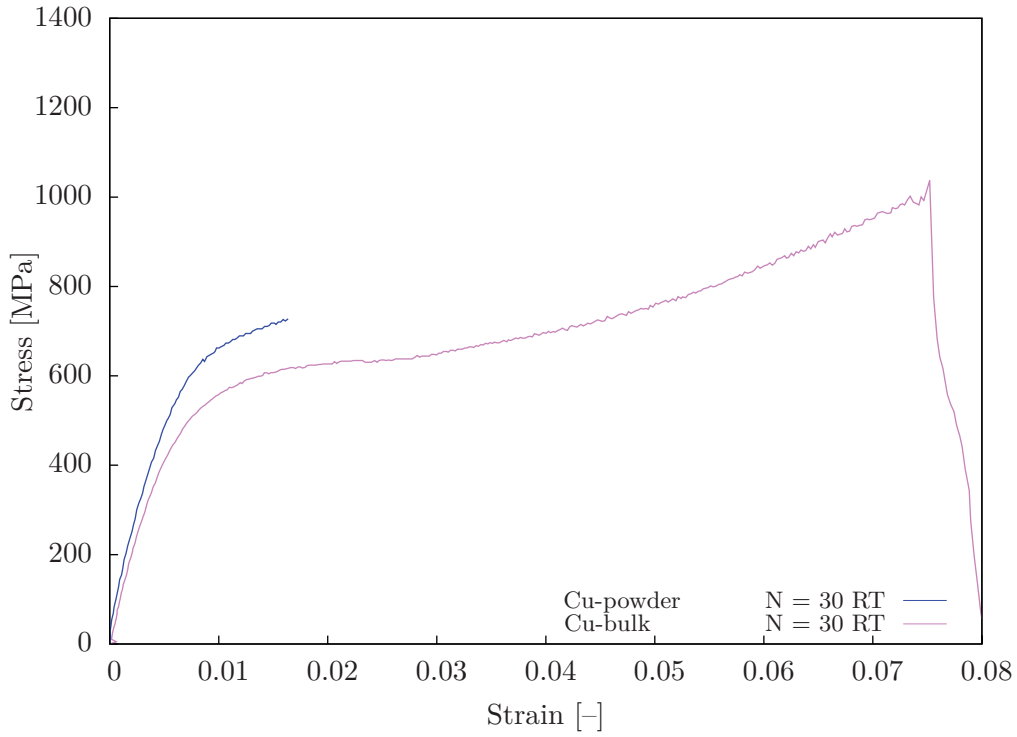

Figure 32: Tensile tests of two pure Cu-samples can be seen. For one bulk was used as initial material (purple) and for the second powder was used (blue). Even though nothing was added to the Cu-powder, the properties of this material change strongly compared to the bulk processed material.

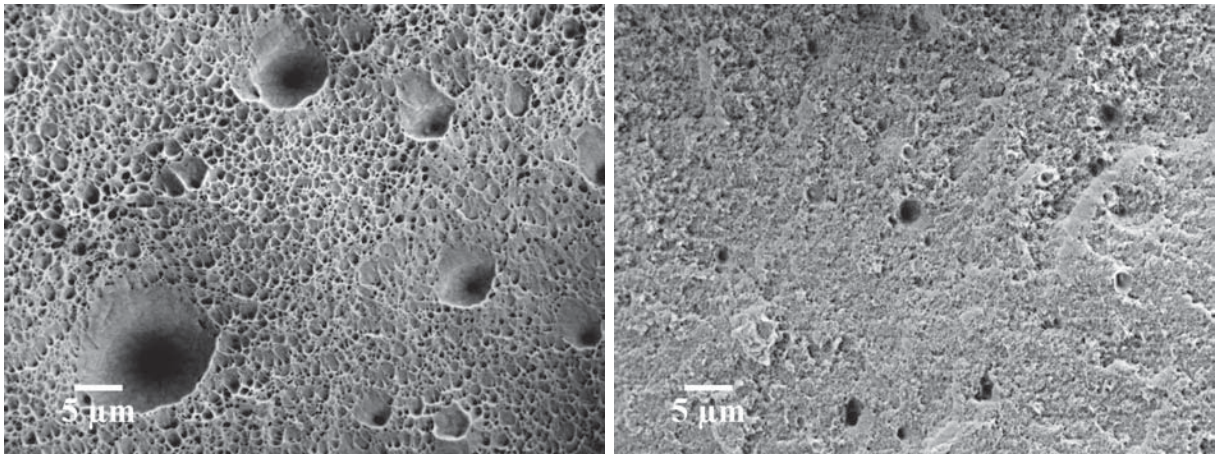

(a) View at the ductile fracture surface of HPT-deformed Cu-bulk, SE-micrograph

(b) View at the fracture surface of HPT-deformed Cu-powder, SE-micrograph

Figure 33: SEM-micrographs of the fracture surfaces of HPT-deformed pure Cu tensile specimens showing larger dimples for the more ductile bulk material and a less pronounced ductile fracture surface of the HPT-deformed Cu-powder.

4.3.2 Tensile testing of W-reinforced Cu

In Figure 34 the stress in dependence of strain of W-reinforced Cu can be seen. The two red lines are obtained on samples which are deformed for 30 turns at room temperature and show the highest yield stress. Compared to pure Cu, this two samples have similar properties as HPT-deformed Cu-powders. The differences can be explained by fluctuation in the production and testing. The other five samples are deformed at 500 °C in the last HPT-step and the purple (5 turns at 500 °C) and green (30 turns at 500 °C) lines show a significant plastic deformation and even a rudimentary strain hardening, but the tensile strength is only a third of the strength of the samples deformed for 30 turns at room temperature.
The SEM-micrographs (Figure 35) of a sample which was deformed for 30 turns at room temperature show the elongated form of W-particles due to the HPT-process and again a ductile, intergranular fracture of the Cu-matrix, while the W-particles are teared out or fracture brittle. Large agglomerates of W, as they can be seen in Figure 36, break along the particles boundaries or intergranular.

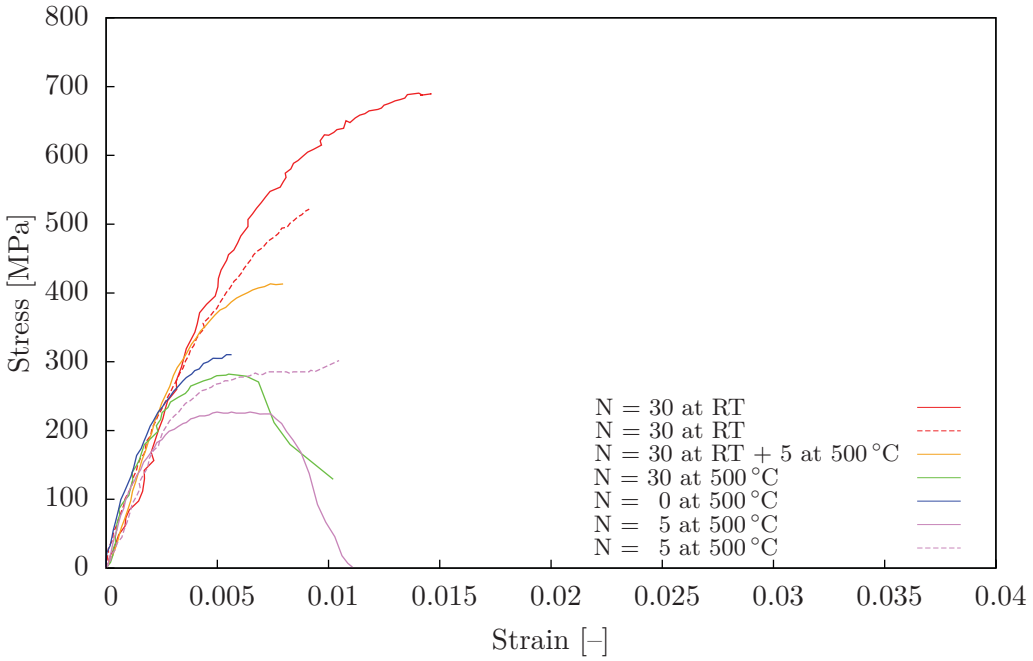

Figure 34: This stress-strain diagram shows the results of Cu – 25 wt% W samples which were deformed differently by HPT. The highest tensile strengths are obtained by defoming only at room temperature, but additional turns at 500 °C at the small HPT-device increase the plastical deformability.

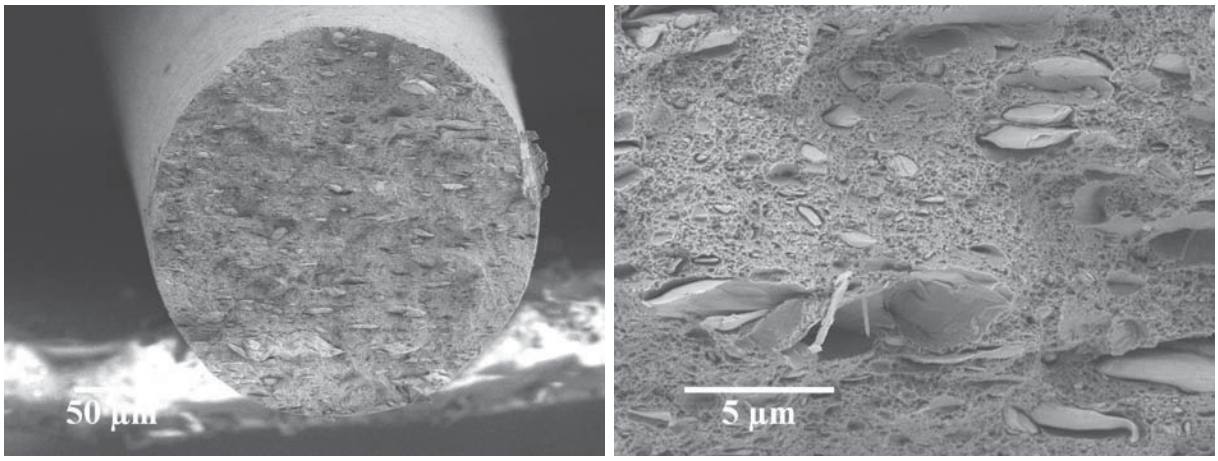

(a) overview of the fracture area **(b)** detail of fracture matrix and W-particles

Figure 35: SEM-micrographs (SE) of the fracture surface of a Cu – 25 wt% W sample deformed by HPT for 30 turns at room temperature. In (a) the elongation of the W-particles can be seen and in (b) the different behavior of Cu and W in a tensile test can be compared.

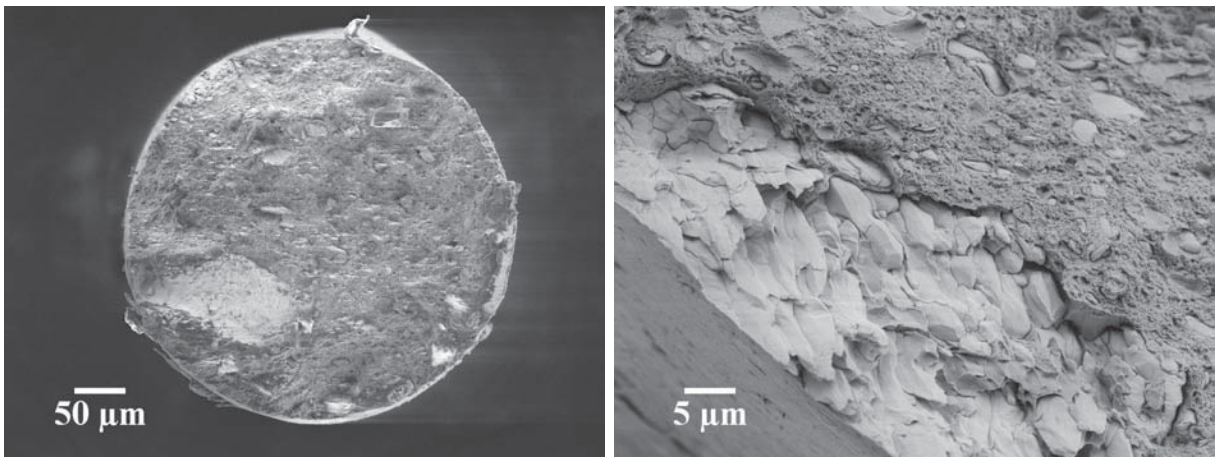

(a) overview of the fracture area **(b)** detail of fracture matrix and W-particles

Figure 36: SEM-micrographs (SE) of the fracture surface of Cu – 25 wt% W sample with 30 turns at room temperature and 5 turns at 500 °C. A W-agglomerate with a diameter in the range of 100 µm can be seen. While the fracture of the Cu-matrix is ductile, the W-agglomerate breaks along the particle boundaries or along the W-grain boundaries.

4.3.3 Tensile testing of Fe-reinforced Cu

In contrary to brittle W, Fe does not decrease the ductility in tensile testing so strong. The curves also show an increased amount of plastic deformation and strain hardening even after being deformed only at room temperature during the HPT-process. Additionally, the tensile strength for samples which are deformed for 30 turns at room temperature is approximately two time as high as for W-reinforced specimens with the same HPT strain path. This can be explained by the Hall-Petch effect due to the smaller grain size (see Table 2). A similar behavior has been observed for the Vickers hardness (see Figure 12). The orange line (30 turns at room temperature and 5 turns at 500 °C) obtains a lower yield strength, but due to a high strain hardening the tensile stress at fracture is approximately as high as for the other Cu – 12 wt%Fe specimens and most importantly the fracture strain is nearly two time higher.
SEM-micrographs show the fracture surface and in Figure 38 two samples - (a) deformed at room temperature and (b) additional turns at 500 °C - can be seen and both show necking due to the tensile test. In Figure 39, the overview (a) shows significantly less necking.

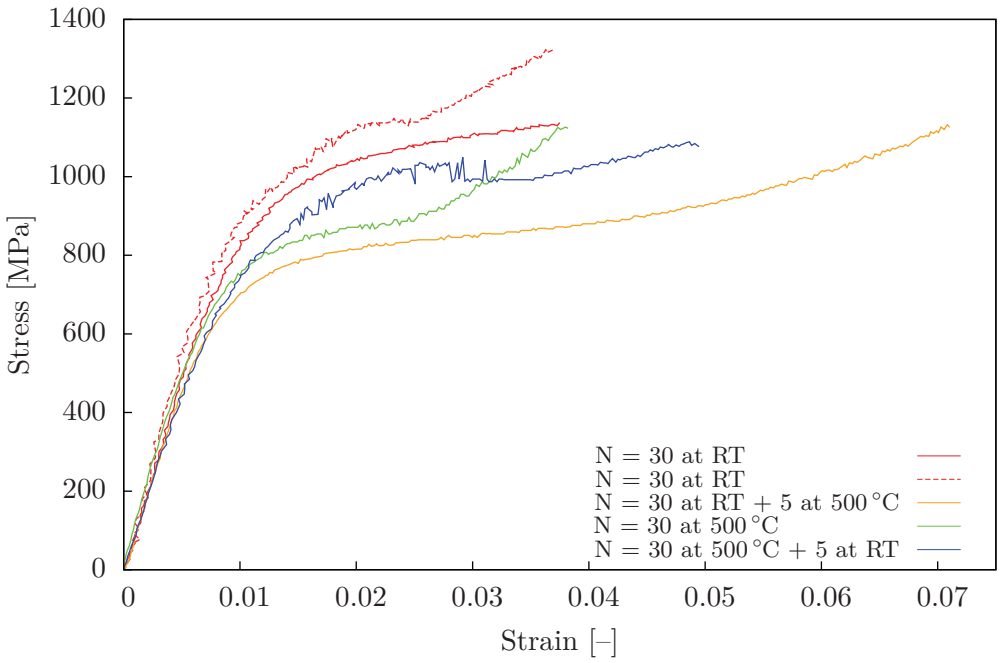

Figure 37: Fe-reinforced samples show depending on the HPT-deformation different behaviors in tensile testing. Not only variies the tensile strength, but also the strain hardening and the fracture strain.

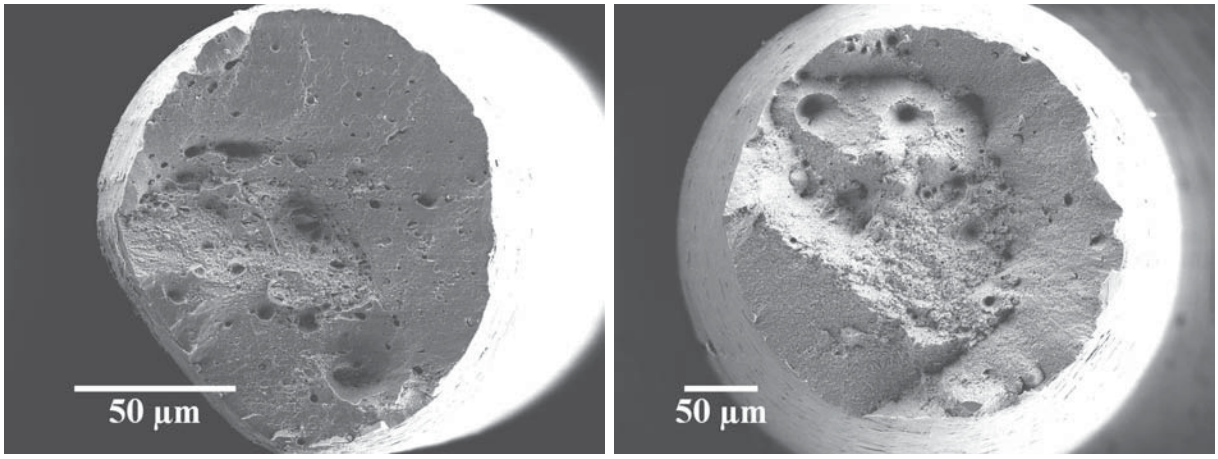

(a) overview of a Cu – 12 wt% Fe specimen deformed for 30 turns at room temperature in the second HPT-step

(b) overview of Cu – 12 wt% Fe deformed for 30 turns at room temperature and additional 5 turns at 500 °C

Figure 38: SEM-images (SE) of the fracture surface of two Cu – 12 wt% Fe with HPT-deformation at different temperatures. Both show a pronounced necking.

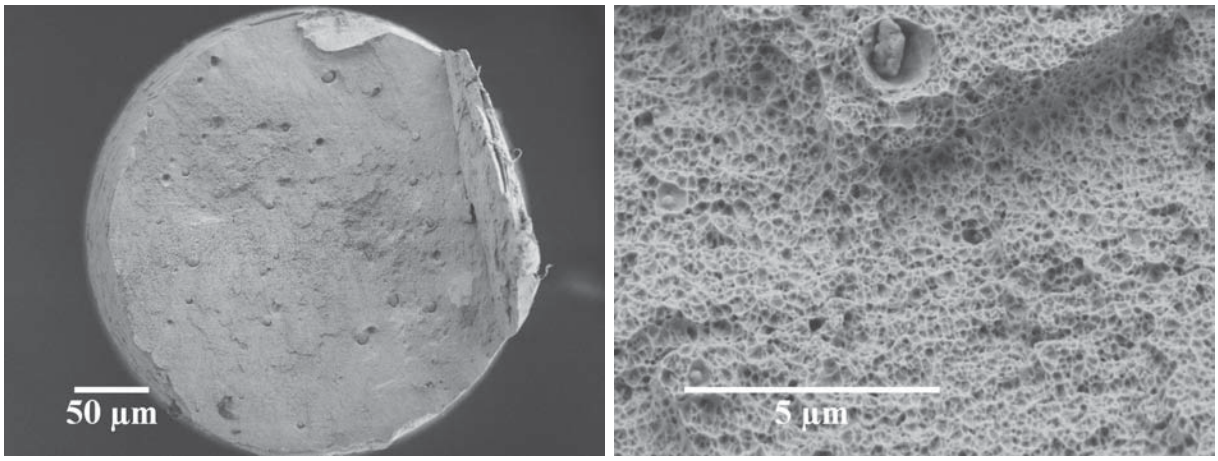

(a) overview of the fracture area

(b) detail of matrix and Fe-particles

Figure 39: SEM-micrograph (SE) of the fracture surface: After 30 turns at 500 °C and 5 turns at room temperature the Cu-matrix fractures ductile, while the remaining larger Fe-particles are pulled out.

4.3.4 Tensile testing of yttria-reinforced Cu

In Figure 40 it can be seen that the behavior in tensile testing of yttria-reinforced Cu is similar to HPT-deformed Cu-powder and W-reinforced Cu. A higher applied deformation, as 200 turns compared to 30 turns, increases the tensile strength, but fracture strain remains the same. On the other hand, deformation at 500 °C seems to reduce strength and ductility. SEM-images (Figure 41 and Figure 42) show that the oxide-particles are very brittle and even cracks and crumbeled dispersoids can be detected. In both specimen, ductile fracture behavior of the matrix can be observed but the existence of large and brittle oxides do not improve the results of these materials in a tensile test.

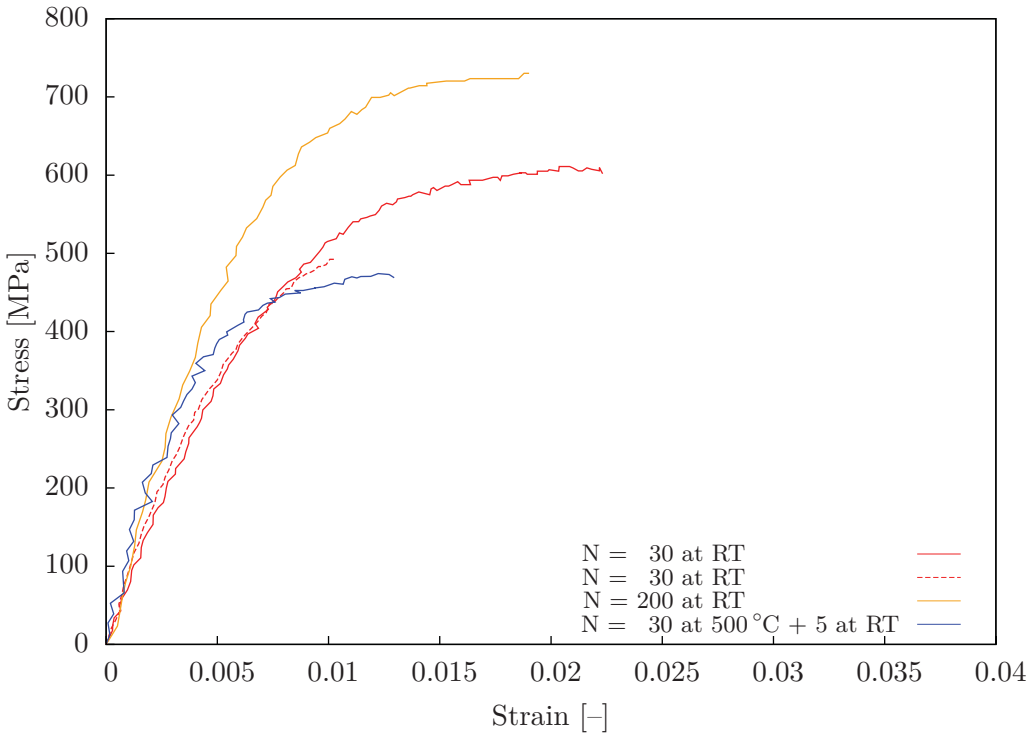

Figure 40: Stress-strain diagram of yttria-reinforced Cu samples. Due to changing of the amount of applied strain and the deforming temperature the results of tensile stress vary.

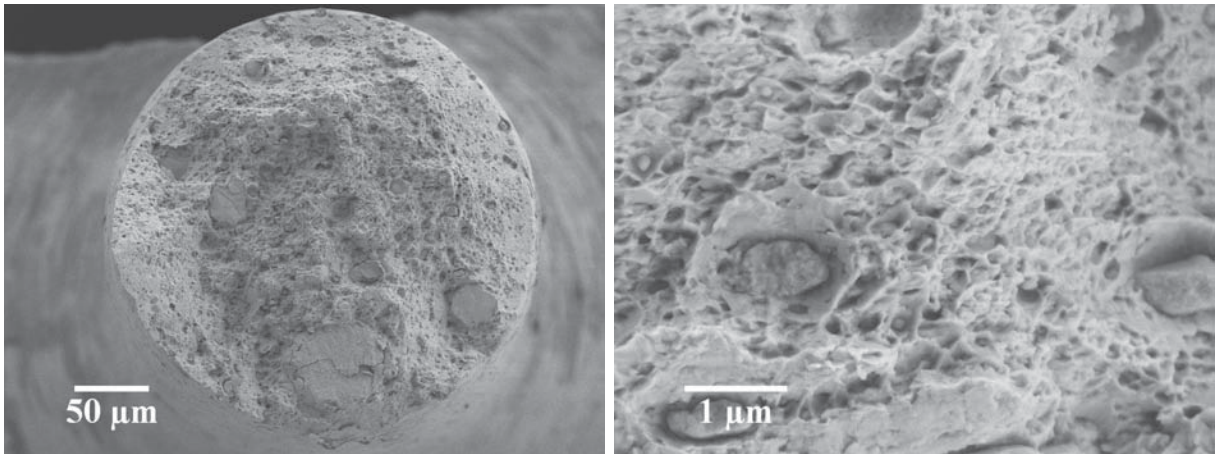

(a) overview of the fracture area **(b)** detail of matrix and yttria-particles

Figure 41: The SEM-images (SE) of the fracture area of an yttria-reinforced Cu sample with 30 HPT-turns at room temperature shows a ductile fracture of the Cu-matrix and a brittle failure of the Y_2O_3-particles. Additionally, large Y_2O_3-agglomerates can be seen.

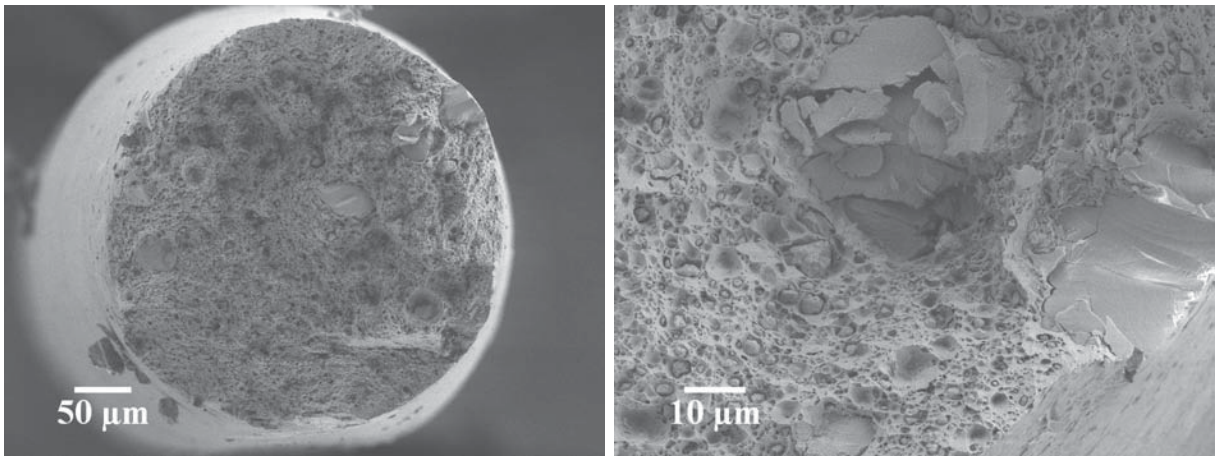

(a) overview of the fracture area **(b)** detail of matrix and yttria-particles

Figure 42: SEM-images (SE) of the fracture surface: Even though the matrix shows a ductile fracture, the yttria-particles fail brittle and even after deforming for 30 turns at 500 °C and 5 turns at room temperature cracks in the large oxide-particles are detectable.

4.3.5 Tensile testing of nanocomposites from industrially produced W-Cu

Due to the high amount of W, the samples in Figure 43 show high Youngs moduli and tensile strength, but also a low ductility. Depending on the composition, the Youngs modulus decreases with increasing Cu-content but even higher Cu-amount does not markedly increase the ductility. The sample W – 20 wt% Cu even fails at 200 MPa which is only one seventh of the tensile test of the other two specimens. The corresponding SEM-image (Figure 44b) shows that the initiation of fracture is at the edge of the sample which indicates a defect indroduced during the sample preparation.
In Figure 44 the fracture surfaces of these three samples are compared. The fracture surface of W – 10 wt% Cu looks rough and the lamellas from the HPT-deformed microstructure can be detected (see Figure 21). Compared to this sample, the other two have a more homogenous fracture surface and the origin of fracture can be found at the surface of the samples. Due to the appearance of the fracture surface, it can be concluded that the microstrucure becomes finer if the volumes of Cu and W are more equal and the obtained surface quality during sample preparation becomes more important for tensile testing.

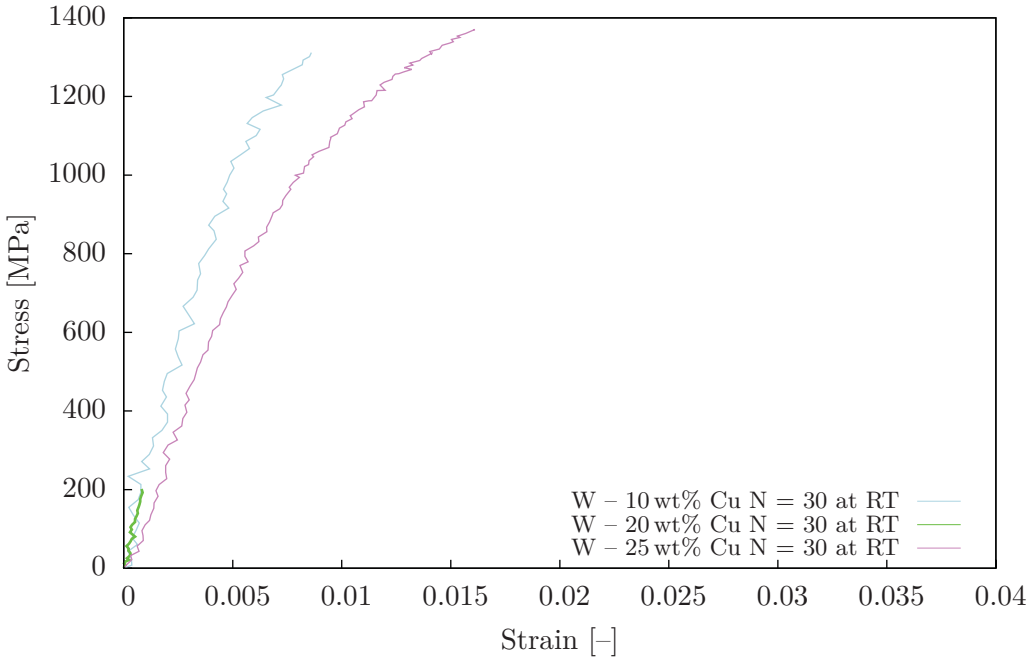

Figure 43: Due to the high percentage of W, these industrial produced virgin samples show low ductility in tensile testing. One specimen - W – 20 wt% Cu - even breaks at one seventh of the fracture stress of the other two samples (due to a defect).

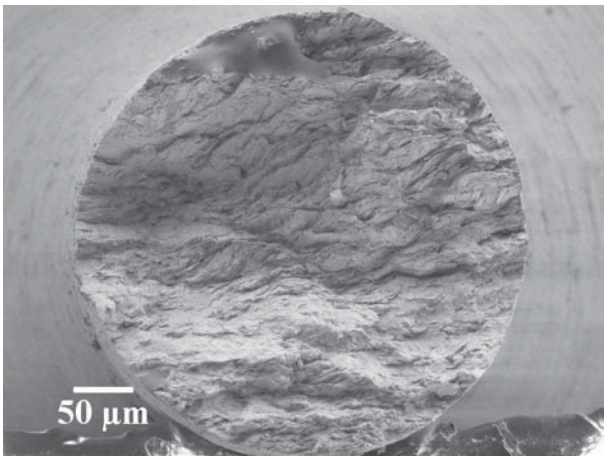

(a) SEM-images (SE) of the fracture area of W – 10 wt% Cu (30 turns at RT)

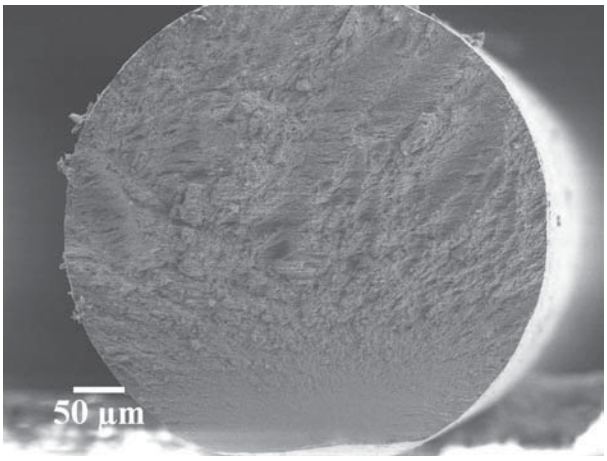

(b) SEM-images (SE) of the fracture area ofW – 20 wt% Cu (30 turns at RT)

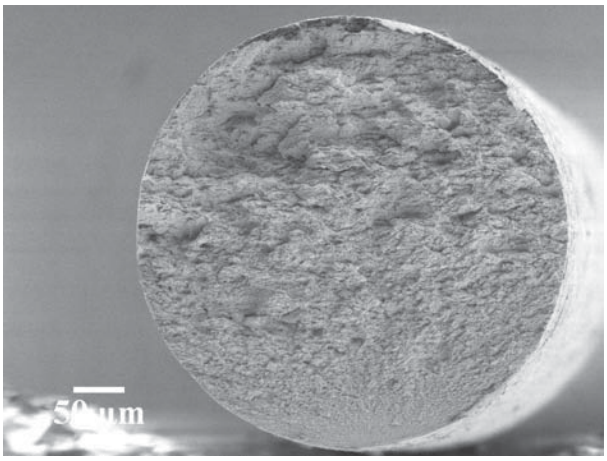

(c) SEM-images (SE) of the fracture area ofW – 25 wt% Cu (30 turns at RT)

Figure 44: The appearance of the fracture surface changes with the composition of the sample. With only 10 wt% Cu the area looks rough and no origin of fracture can be detected, but for the other two samples - 20 wt% and 25 wt% Cu - the critical area for starting the fracture lies at or near the surface. In both cases, the region of crack initiation is at the bottom of the fractographs.

4.4 Annealing of HPT-deformed specimens

4.4.1 Annealing of W-reinforced Cu

After annealing the HPT-deformed samples, the hardness depending on the applied strain is measured. In Figure 45, Cu – 25 wt% W in different deformation and annealing states can be compared to samples without applied temperature treatment (green lines): To the right side, the strain increases and so does the hardness. Specimen, which are deformed for 400 turns at room temperature, show no decrease in hardness after annealing, whereas all samples, which are only deformed for 30 turns at room temperature and are annealed, become softer. Also, the sample with 200 turns at room temperature and annealed at 900 °C experiences a decrease of hardness, but it can be clearly seen that to the right, i.e. at higher applied strains, the sample is significantly harder.

SEM-micrographs of annealed Cu – 25 wt% W can be seen in Figure 46 and Figure 47. The

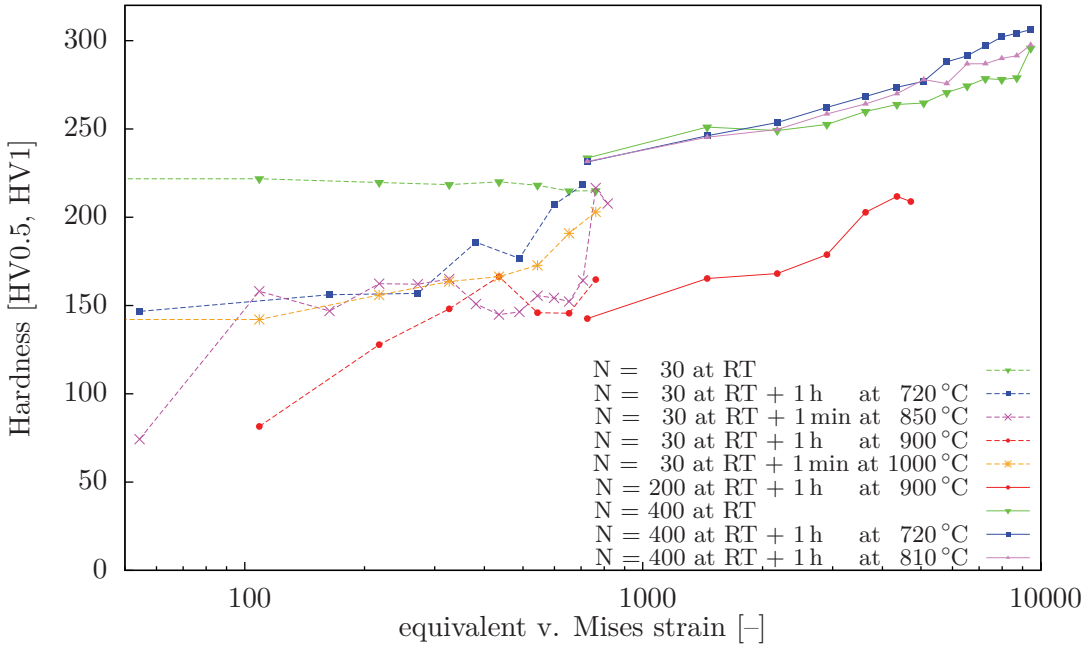

Figure 45: Hardness of Cu – 25 wt% W depending on applied strain and annealing treatment. Please notice the single logarithmic scale for the applied strain.

microstructure of the sample with 400 turns at room temperature and annealing for 1 h at 720 °C does not change the microstructure compared to the same sample without heat treatment, but the SEM-image of the sample with 200 turns shows coarser W-particles which are all circular. Samples with less applied strain show also pores additionally to the recrystallized, coarsen matrix. Those are positioned next to W-particles most of the time and they are in the same size range as the grain size of Cu.

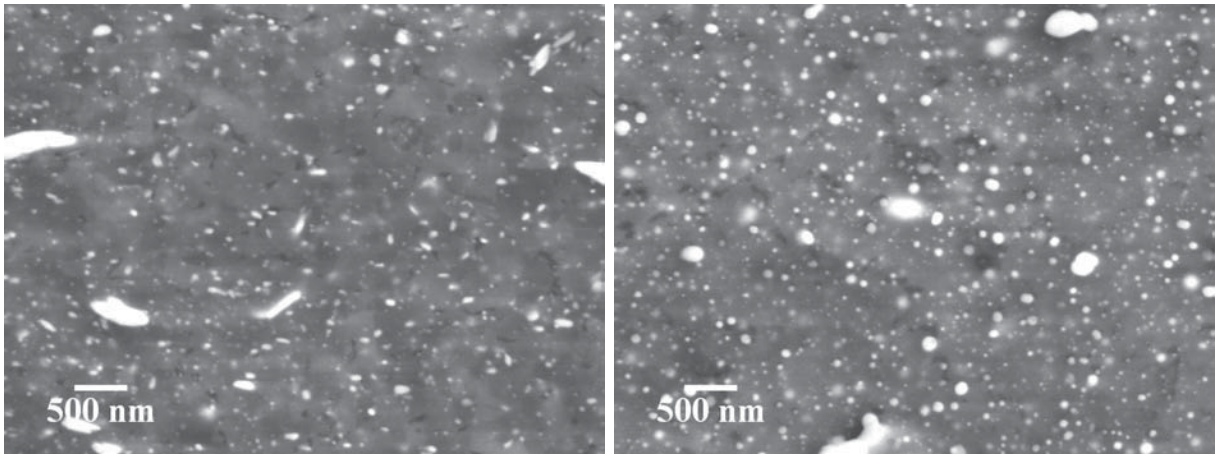

(a) Sample with 400 turns deformed at room temperature, which has been annealed for 1 h at 720 °C.

(b) Sample with 200 turns deformed at room temperature, which has been annealed for 1 h at 900 °C

Figure 46: SEM-micrographs of Cu – 25 wt% W with 400 and 200 turns at room temperature, which have been annealed. Both show no strong grain growth of the Cu-matrix or appearance of pores.

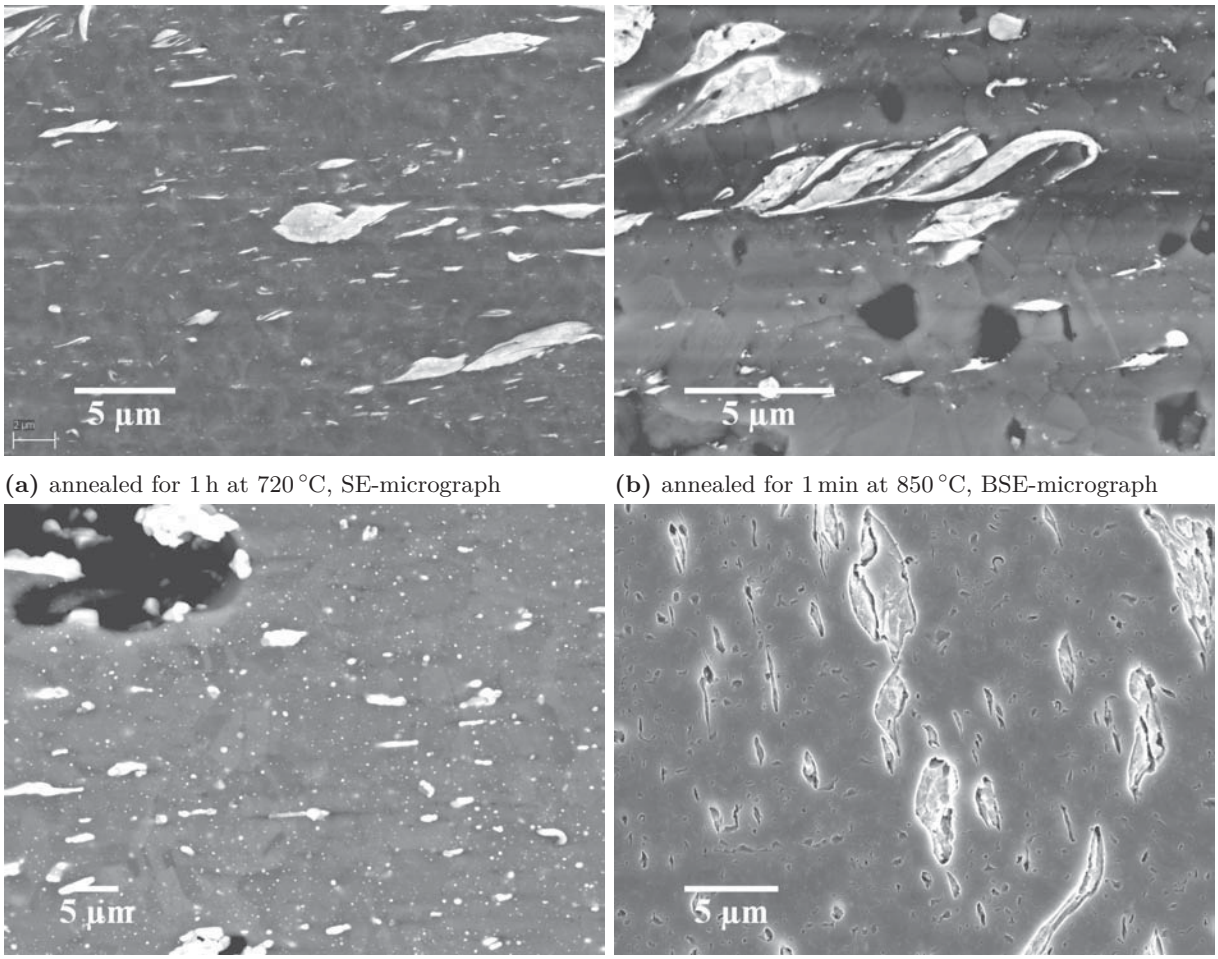

(a) annealed for 1 h at 720 °C, SE-micrograph

(b) annealed for 1 min at 850 °C, BSE-micrograph

(c) annealed for 1 h at 900 °C, SE-micrograph

(d) annealed for 1 min at 1000 °C, SE-micrograph

Figure 47: SEM-micrographs near the center of Cu – 25 wt% W with 30 turns at room temperature, which show the influence of the heat treatments: Coarsening of the microstructure and appearance of pores occurs.

4.4.2 Annealing Fe- and yttria-reinforced Cu as well as pure Cu

In Figure 48 the hardness of Cu – 12 wt% Fe and Cu – 4 wt% Y_2O_3 after deforming at room temperature and different heat treatments can be seen. Fe-reinforced Cu softens with increased annealing time and temperature (left diagram: compare the two annealed samples to the green line of the specimen without heat treatment). On the contrary, material reinforced with yttria obtains always the same hardness after different heat treatments.

Fe-reinforced Cu recrystallizes stronger if annealing time and temperature are increased. The

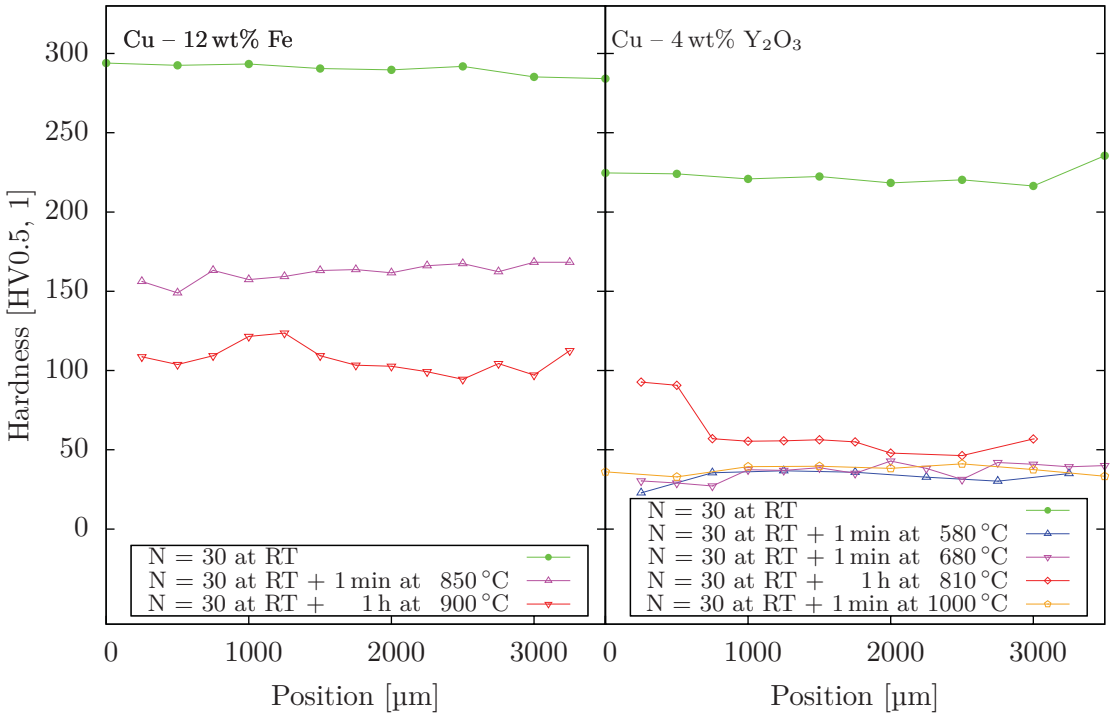

Figure 48: Hardness of Fe- and Y_2O_3-reinforced Cu after various heat treatments.

SEM-images (Figure 49) show that the specimen annealed inductively for 1 min at 850 °C obtains Cu-grains in the range of 500 nm and Fe-particles with a diameter of 100 nm. After 1 h at 810 °C the Fe-particles and Cu-grain size are both in the range of µm. The larger Fe-particle in the left image is not due to segregation from supersaturated solid solutions or coarsening at higher temperature, but it has not been refined during HPT-process.

During annealing, Cu – 4 wt% Y_2O_3 shows strong grain growth of the Cu-matrix and pores emerge. This is clearly visible in the SEM-images of two samples with different applied annealing temperature (Figure 50). The sample, which has been annealed at 580 °C, was compacted under vacuum to reduce the inclosed air, but the SEM-image in Figure 50a show no reduction of pores after annealing.

Pure Cu-powder was deformed for 30 turns and annealed for 1 h at 720 °C. Because of the lack of stabilizing particles, the grain growth is only hindered by emerging pores. But the volumes of these pores is large enough to change of the annealed sample. In Figure 51 the Cu-grain growth, emerging of pores, and the deforming of the sample can be seen.

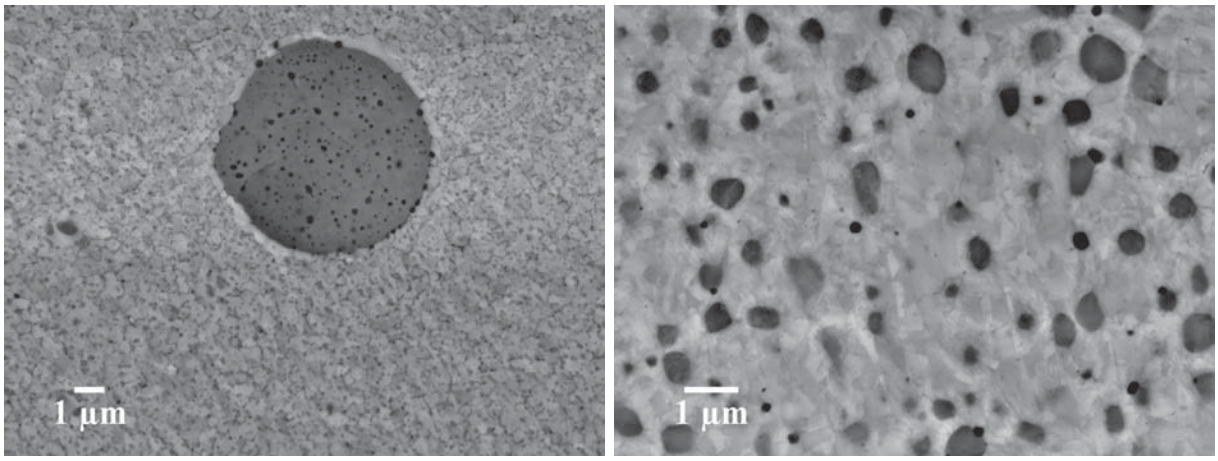

(a) annealed for 1 min at 850 °C, radial view near the center (BSE-micrograph)

(b) annealed for 1 h at 900 °C, tangential view near the center (SE-micrograph)

Figure 49: SEM-micrographs of Cu – 12 wt% Fe with 30 turns at room temperature, which have been annealed at two different temperatures for two different times. Coarsening of the Fe-particles and the Cu-grains can be seen.

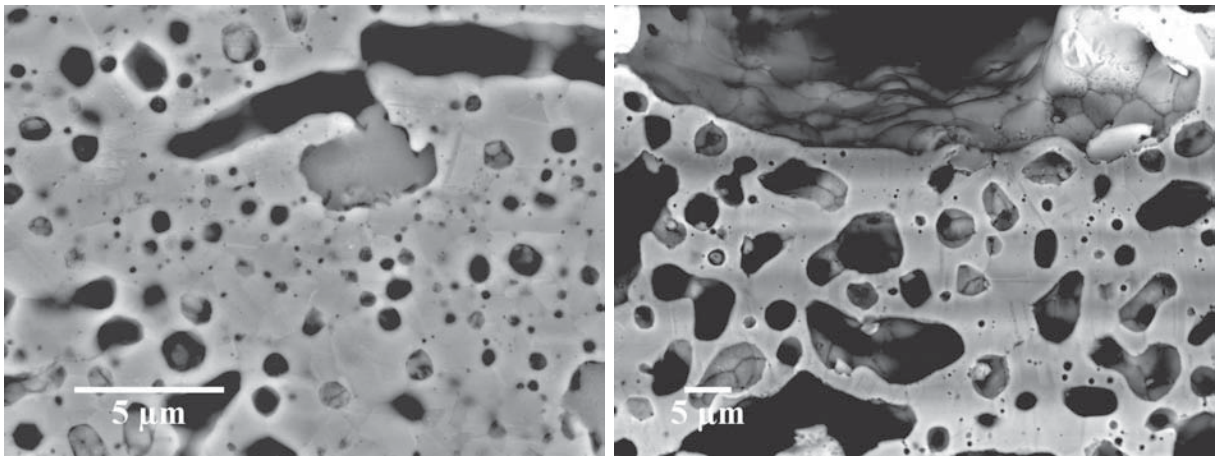

(a) annealed for 1 min at 580 °C

(b) annealed for 1 min at 850 °C

Figure 50: SEM-micrographs (BSE) of HPT-deformed Cu – 4 wt% Y_2O_3 with 30 turns at room temperature, which has been annealed inductively. It can be observed that the Cu-matrix coarsens strongly and a large amount of pores emerges most probably due to the expansion of the enclosed gas.

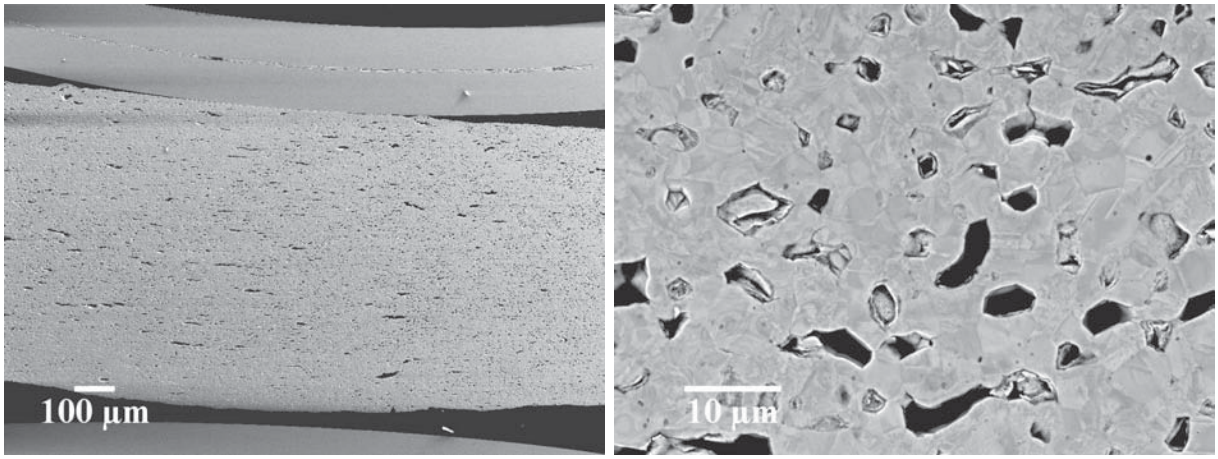

(a) annealed for 1 h at 720 °C, SE-micrograph

(b) annealed for 1 h at 720 °C, BSE-micrograph

Figure 51: SEM-micrographs of HPT-deformed Cu powder with 30 turns at room temperature, which has been annealed for 1 h at 720 °C. It can be observed that the Cu coarsens strongly and a large amount of pores emerges. The sample even changes its shape due to the heat treatment.

4.4.3 Annealing of industrial produced W-Cu specimens

Three different materials from Plansee SE, Austria are deformed by HPT and annealed. In Figure 52, the hardness as a function of position and annealing treatment is presented. The temperature treatment hardly influences the hardness of the material with the lowest amount of Cu (W – 10 wt% Cu). Even the fluctuations due to the inhomogeneous structure are larger than the absolute reduction. In contrary to W – 10 wt% Cu, W – 20 wt% Cu becomes harder with annealing. Especially pronounced is this hardening for both samples annealed at 900° (red lines) - for the short inductive heating treatment as well as for the long furnace annealing. But also the specimen annealed at 1000° (orange line) shows an increase in hardness. Only the violet line (annealing at 800° for 5 h) is lower than the reference sample without any heat treatment. For W – 25 wt% Cu, the difference in hardness is not larger than the range of the errors in hardness measurement.

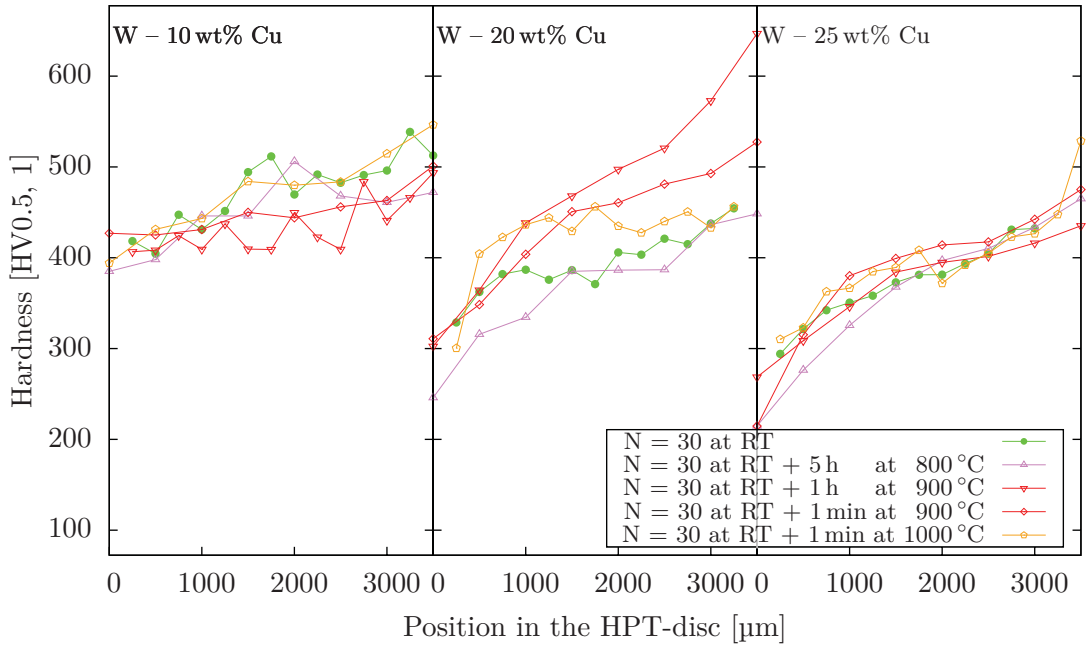

Figure 52: Vickers hardness of three different industrial produced materials. The hardness various due to the four different applied heat treatments.

Additionally to the hardness, the microstructure is investigated. For W – 10 wt% Cu no difference can be detected (Figure 53) between the annealed samples. Compared to the structure without annealing (Figure 20), the W-lamellas are rounded. In contrary, differences between the heat treatments can be observed (Figure 54) for W – 20 wt% Cu : All three micrographs show coarser W-lamellas compared to the sample without annealing (Figure 21), but this is less pronounced for the sample annealed at 900°. It is the same for W – 25 wt% Cu (Figure 22 and 55) as all samples coarsen due to annealing.

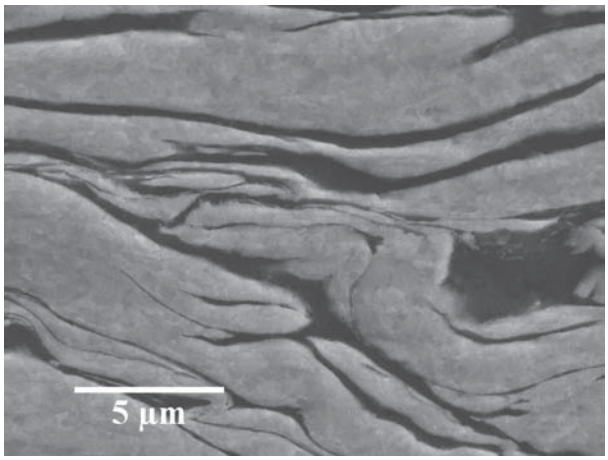

(a) tangential view near the center: 5 h at 800 °C

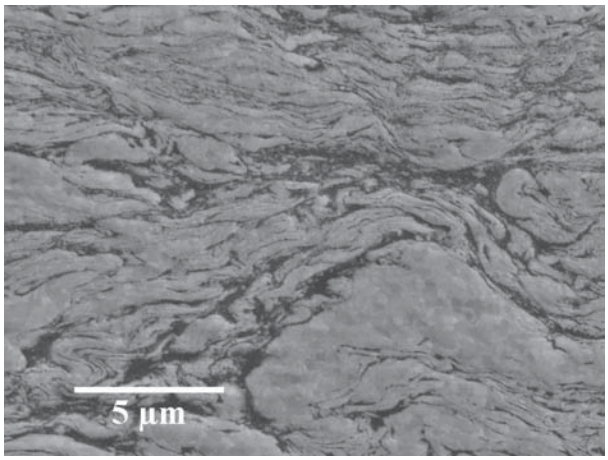

(b) tangential view near the edge: 5 h at 800 °C

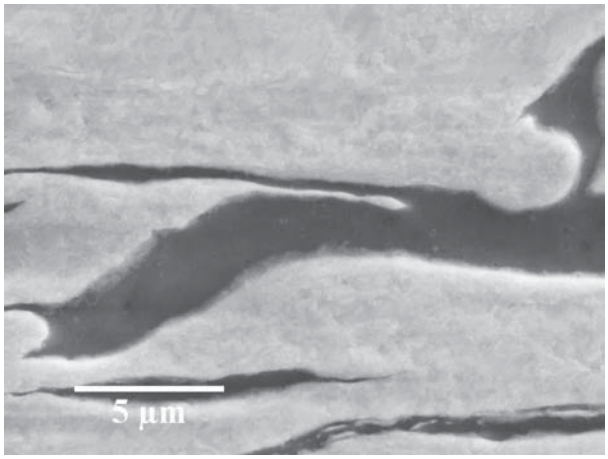

(c) tangential view near the center: 1 min at 900 °C

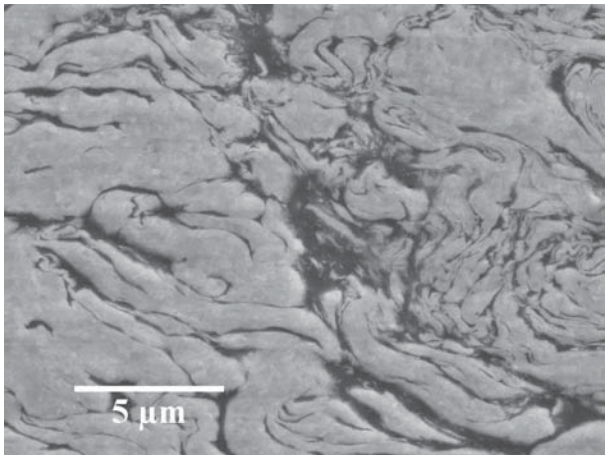

(d) tangential view near the edge: 1 min at 900 °C

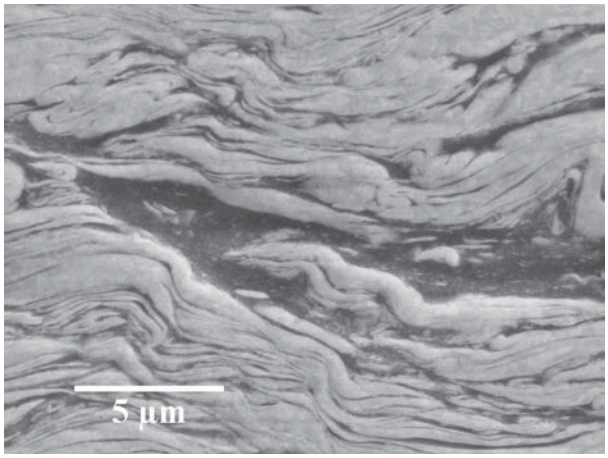

(e) tangential view near the center: 1 min at 1000 °C

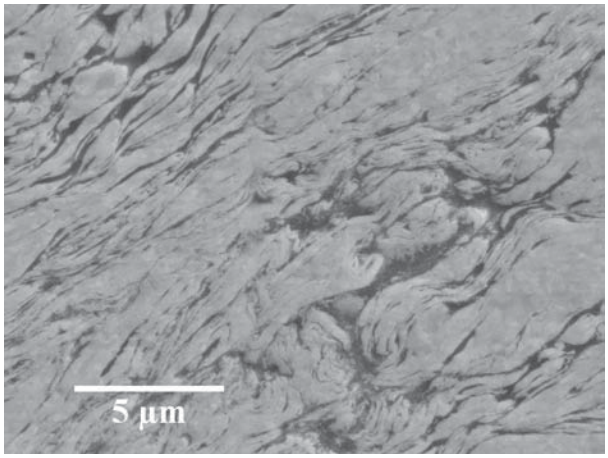

(f) tangential view near the edge: 1 min at 1000 °C

Figure 53: SEM-micrograph (SE) of annealed W – 10 wt% Cu samples. The heat treatment hardly changes the structure and compared to the sample which is not annealed (Figure 20) the W-lamellas become more roundly.

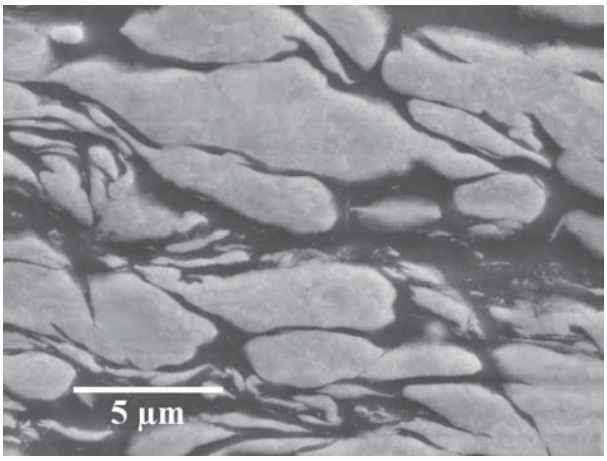

(a) tangential view near the center: 5 h at 800 °C

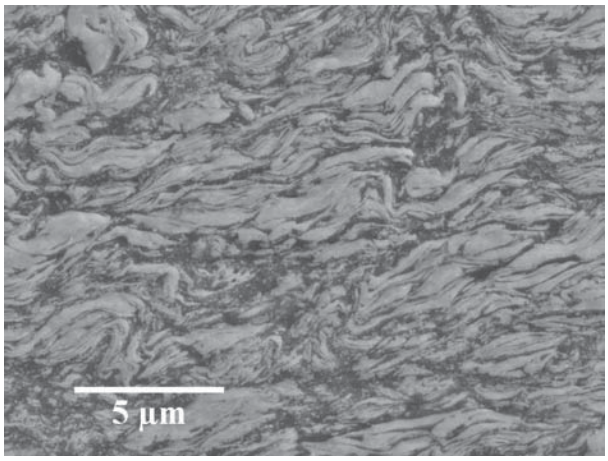

(b) tangential view near the edge: 5 h at 800 °C

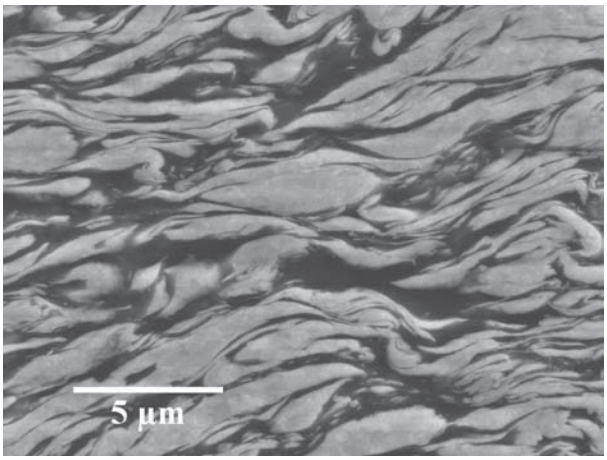

(c) tangential view near the center: 1 min at 900 °C

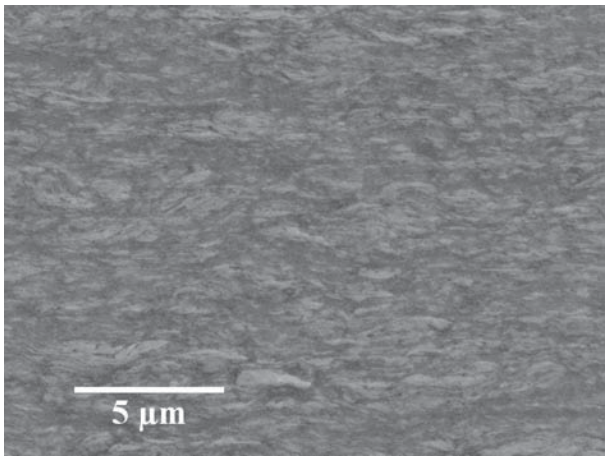

(d) tangential view near the edge: 1 min at 900 °C

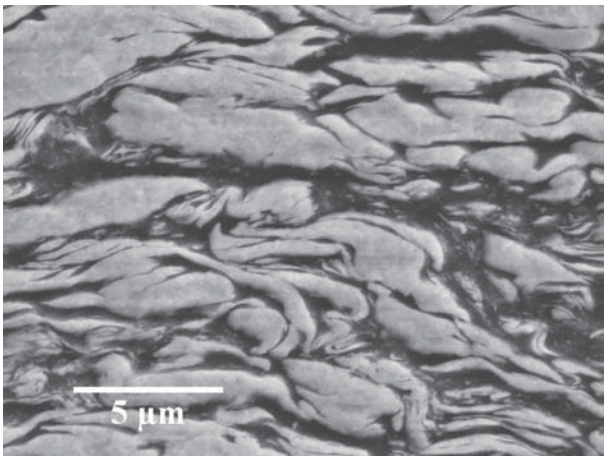

(e) tangential view near the center: 1 min at 1000 °C

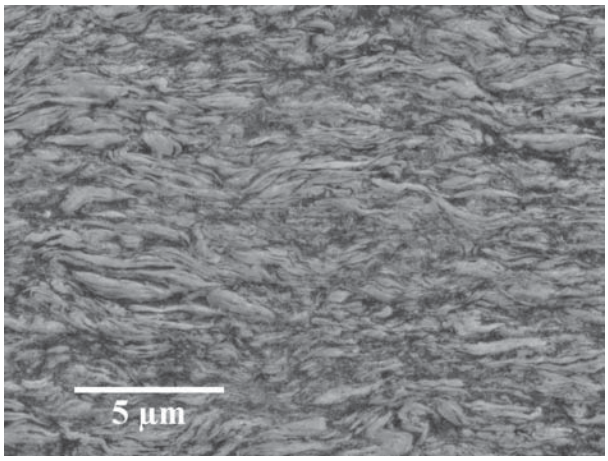

(f) tangential view near the edge: 1 min at 1000 °C

Figure 54: SEM-micrographs (SE) of W – 20 wt% Cu samples show the influence of different heat treatments on the microstructure.

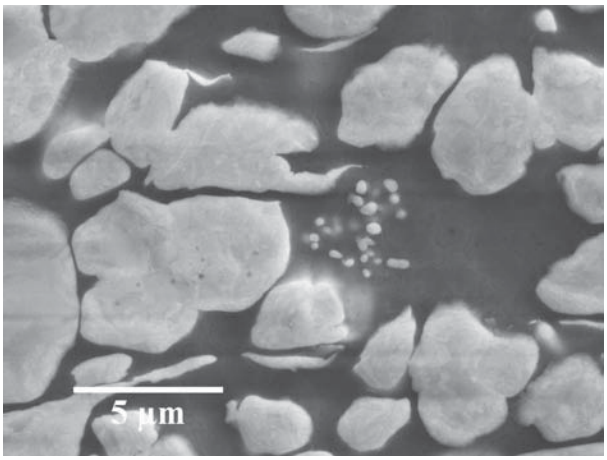

(a) tangential view near the center: 5 h at 800 °C

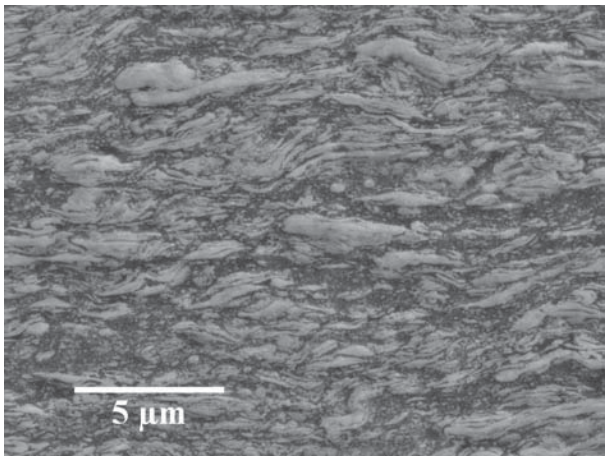

(b) tangential view near the edge: 5 h at 800 °C

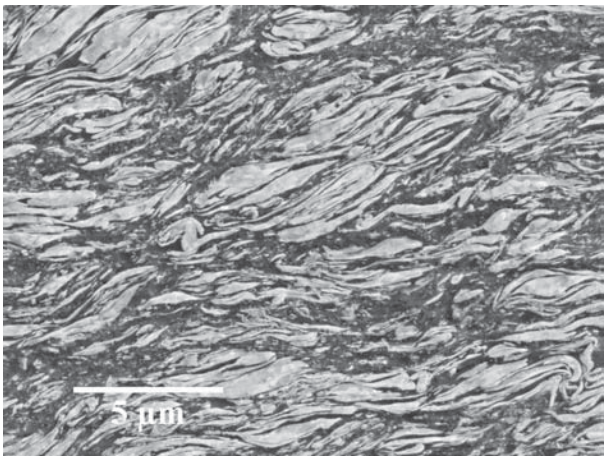

(c) tangential view near the center: 1 min at 900 °C

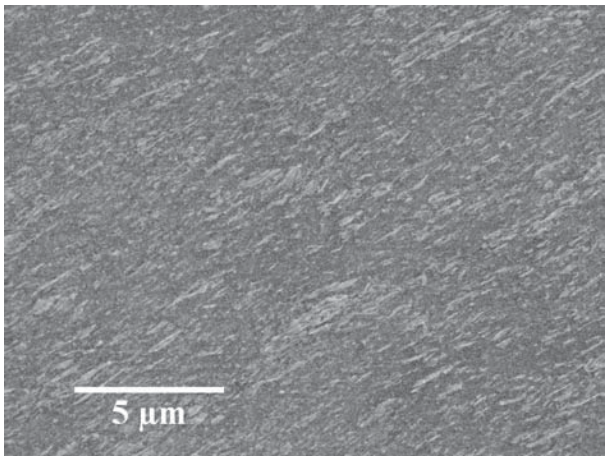

(d) tangential view near the edge: 1 min at 900 °C

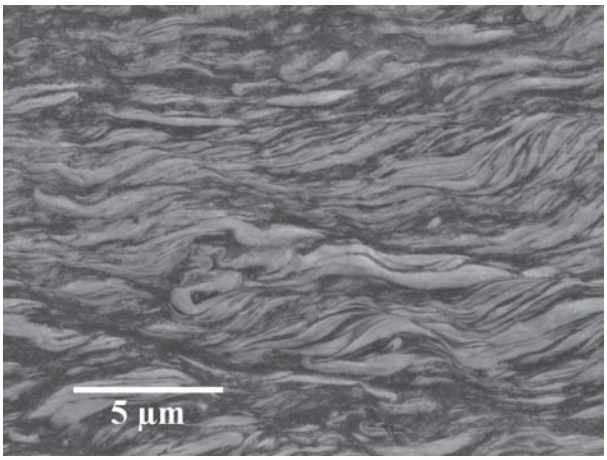

(e) tangential view near the center: 1 min at 1000 °C

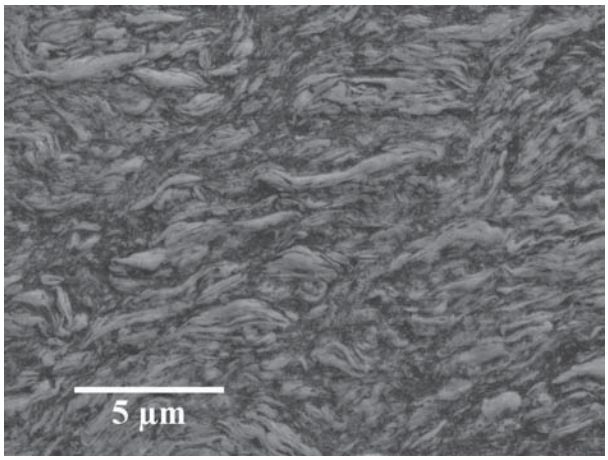

(f) tangential view near the edge: 1 min at 1000 °C

Figure 55: SEM-images (SE) of three W – 25 wt% Cu show that a longer time and higher temperatures of the heat treatment coarsen the microstructure stronger.

5 Discussion

5.1 Deformation at room temperature

The goal of this master thesis is to develop a Cu-based material, which grains are in the nanometer range and is also stabilized for applications at higher temperatures. To achieve this goal, fine particles are placed at the grain boundaries to hinder their movement and prevent grain growth. The HPT-process has so three functions: compact the mixed powder, create a nanostructured Cu-matrix, break up the harder particles and create so fine particles, which are homogeneously distributed in the matrix. After the second HPT-step, first of all the hardness was measured. It does not only show how homogeneously the powders were mixed, but the shrinking grain size can be estimated. In Figure 56, the hardness of all materials used for this thesis is presented. In this plot, all materials were deformed for 30 turns at room temperature.

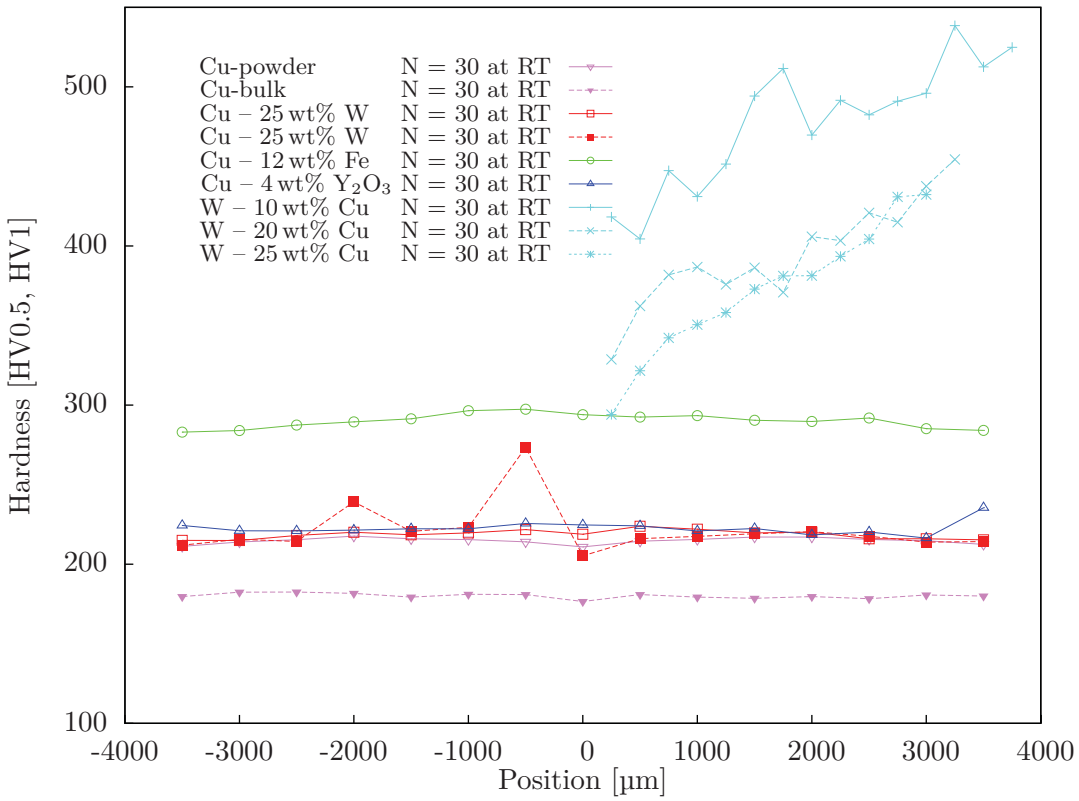

Figure 56: Vickers hardness as a function of the radius for all materials investigated in this master thesis: All samples were deformed only at room temperature for 30 turns. The hardness depends on chemical composition and the applied strain.

5.1.1 Influence of the position in the large sample after the first HPT-step

The applied strain depends strongly on the position in the HPT-disc as it increases with the radius and approaches zero in the middle. So one question is, how important the radius is at which the sample is cut out after the first HPT-step. With Equation 1 it can be calculated that the maximum strain after the first HPT-step is approximately $\epsilon_v = 70$ and after additional 30

turns with the small HPT the applied strain sums up to more than $\epsilon_v = 500$ at the edge of the specimen. While at large radii the strain of the first step can be easily neglected, it is not clear what happens in the center of the specimen since the low amount of additional strain can make a bigger difference there. But after comparing the distribution of hardness along the diameter for samples taken out at different radii it can be concluded that in the center the influence can also be neglected. In Figure 57 the distribution of hardness for two Cu – 25 wt% W samples can be seen. Both have obtained 30 turns at room temperature in the second step, but while one was cut out of the center of the large disc obtained by the first HPT-step, the other was positioned near the the edge and has experienced more deformation in the first step. In Figure 57 it can be seen that the hardness after 30 turns is about constant over the whole diameter and therefore it can be concluded that the strain obtained in the first HPT-step can also be neglected.

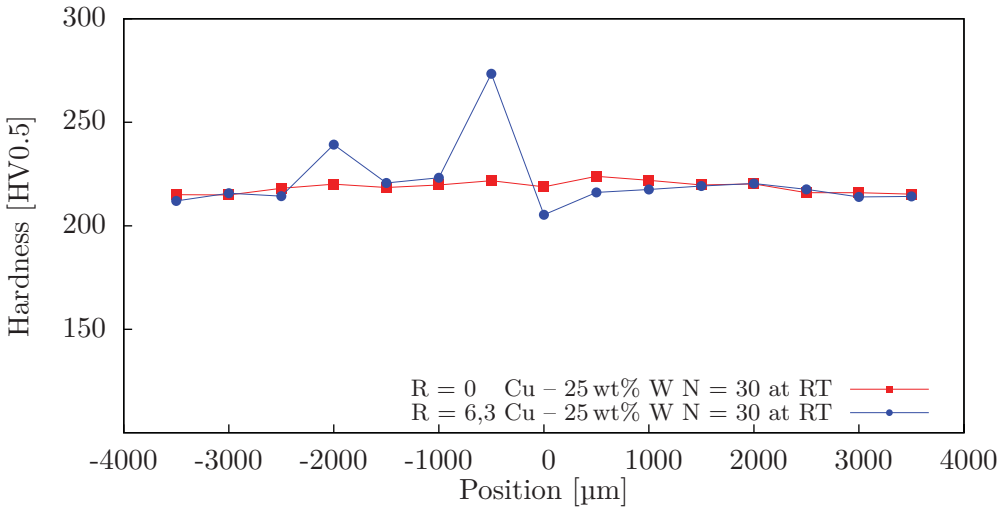

Figure 57: The hardness of two Cu – 25 wt% W samples after the second HPT-step. The hardness does not depend on the original position in the first HPT-disc, but is determined by the applied strain in the second deformation step. Sample Cu – 25 wt% W R6,3 shows two peaks, which can be easily explained because at that position where the hardness was measured there were large W-agglomerates.

5.1.2 Influence of the added elements

In Figure 56, it can be observed that Cu – 25 wt% W, Cu – 4 wt% Y_4O_3 and Cu-powder have got the same hardness after 30 turns, while the hardness of Cu – 12 wt% Fe is higher and the hardness of Cu-bulk is lower. The differences between Fe and W or Y_2O_3 are the hardness and the miscibility in Cu. So on one hand the hardness of Fe is similar to Cu and so it is easier to co-deform both phases by HPT, on the other hand, W and Y_2O_3 are nearly immiscible. These lead to a finer microstructure and therefore to the higher hardness of Cu – 12 wt% Fe. The lower hardness of Cu-bulk can be explained by knowing that it is received as bulk material which results in a higher purity than the Cu-powder. The large surface of powder and the contact with the environment leads to an increase of impurities which cannot be detected by EDX. So, the microstructure of HPT-deformed Cu-powder is finer than of HPT-deformed Cu-bulk, because impurities stabilize the grains and slow down grain growth.
Finally, it can be concluded that after 30 turns, hard materials as yttria and W do not contribute strongly to the hardness, but impurities in the Cu matrix sustain a major part. Only at higher

strains (Figure 12) W and Y_2O_3 increase the hardness further up to nearly 300 HV and a saturation could not be found even at an equivalent strain $\epsilon_v = 10000$. The decrease and later increase of hardness of Cu – 12 wt% Fe samples deformed for 200 and 400 turns (Figure 12) cannot be explained. One idea is that the material becomes a supersaturated solid solution (subsection 2.1) and due to the heat of deformation and friction of additional turns the HPT-disc is heated up and so coarsening or segregation takes place. This might explain the decrease of hardness after 200 turns and the increase of hardness after 400 turns due to the formed very fine nanoscaled structure ($\approx$ 70 nm) is obtained. The fact that in the center, the grains are slightly larger than at the edge (Table 2) contradict this theory because it is a sign that grains are refined due to the applied strain and no supersaturated solid solution was generated, because then the grain size should be the same over the whole radius.

5.1.3 Deformation and refinement of particles

It is difficult to deform a small amount of hard particles in a softer matrix because the majority of the strain is only realized by Cu. Although the plastic deformation in Cu is high, a majority of the harder particles just flow in the matrix without changing their form or breaking up. In Figure 18e the Cu-matrix flows around a circular Fe-particle and Figure 15b shows the deformation and flowing behavior of the matrix and small W-particles near a large W-agglomerate: The small dispersoids in the range of 50 nm to 100 nm become more elongated and align in direction of the flow. Near the large agglomerate the particles are parallel to the shear direction. To obtain such a distribution, the strain along the large particle must be higher than in the remaining matrix. This is very similar to phenomenon in fluid mechanics where the velocity of a fluid that flows around an obstacle is higher. This effect can also be seen on larger scale as also W-particles with a diameter larger than 1 µm are circular in the center of the specimen, but change their forms at the edge to a more lenticular form (Figure 14 and Figure 15) and their size decreases. The distribution of the particle size shifts at higher applied strains to smaller values as the number of large particles strongly decreases (Figure 16).
Yttria is more brittle than W and cannot be deformed in Cu even at high strains. So, in Figure 19 the form of the Y_2O_3-particles does not change and only the size becomes smaller as the breaking down of particles increases with the applied strains (compare center and edge).
In contrary, Fe and Cu are similarly deformable which has a big impact on the way of deformation. Not only the Cu-grains refine quickly, but also the Fe-particles break down. Compared to the center of a Cu– 12 wt% Fe sample (Figure 17a) the fraction of larger Fe-particles nearly vanishes at the edge (Figure 17d).
Not only the mechanical properties influence the behavior of deformation, but also the ratio of volume of the harder to the softer phase. If the volume of the softer phase is significantly larger, the majority of plastic deformation can take place there. But as soon as the volume of the harder phase reaches the extent of the matrix, the strain in the harder phase increases too (compare Figure 14 to Figure 22). So, a higher amount of W leads to two results: Larger areas of W are teared apart (compare Figure 22 and Figure 20) and the grain size of Cu as well as of W decreases strongly.
If samples with different percentages of W are compared (Figure 14 to 20), W – 25 wt% Cu shows the most homogenous microstructure. For obtaining uniform microstructure after a strain as small as possible, the volumes of soft and hard phase should be equal (25 wt% equals approximately 60 vol%). On the other hand, if enough strain is applied the out-coming microstructure does not depend on the starting microstructure. Sabirov et al. [22] also deformed W – 25 wt% Cu

produced by Plansee SE, Austria but the initial particle size of W was 2 µm and in this master thesis it was between 5 µm to 10 µm. The coarser initial material showed after 100 turns the same fine homogenous microstructure as it was achieved by Sabirov et al. after 30 turns. Hence, if the applied strain is high enough the ratio between soft and hard phase does not matter and the particles break up, but with a finer initial material homogeneity will be reached sooner.

5.1.4 Energy dispersive X-ray analysis

In Figure 16 it can be seen that the number of particles in a specific range of size depends on the applied strain and so on the radius. Another question is, if the concentration of the elements also depends on the radius. Scanning a large particle in the Cu-matrix (Figure 24) shows that in the particle, the Fe-content is nearly 100% and nearly no Fe is soluted in the matrix. EDX line-scans were performed which can be seen in subsubsection 4.1.3, where three different materials - Cu – 25 wt% W, Cu – 12 wt% Fe and Cu – 4 wt% Y_2O_3 - after 30 and 400 turns were investigated. The scans show no correlation between the number of turns and the distribution of concentration along the radius. Whereas the concentration of Fe and W slightly increases with smaller radius for the samples with 30 turns, it is reversed for the other specimen containing W with 400 turns and for the Fe-sample with 400 turns the slope is only less steep. The independence of chemical composition on the radius is even more pronounced in the Cu – 4 wt% Y_2O_3 sample with 30 and 400 turns; there is no even slope but two separate plateaus which can only be explained with an inhomogeneous distribution of the elements in the bigger HPT-sample. On the other side there are no plateaus in a Cu – 4 wt% yttria sample with 30 turns, but the distribution of Y varies strongly with the radius, so that the green trend line in Figure 26 only shows that the distribution does not depend on the radius.
Hence, the distribution of the concentration depends only on the initial distribution in the large disc after the first HPT-step. To obtain a homogeneous distribution, the mixing of the powder before HPT-deformation is of great importance as inequalities can be hardly compensated by HPT-deformation.

5.2 Deformation at higher temperatures

One idea was to increase the ductility in the materials with added particles for stabilization by increasing the process temperature of the second HPT-step. The applied temperature was 500 °C, which is above the ductile to brittle transition temperature of W. Additionally, the high pressure prevents the oxidation of the specimen, because only little material at the edge has direct contact with air. The SEM-pictures (see Figure 28 to 31) do not support the hypotheses that the particles are more ductile at higher deformation temperatures. The main effect is that grain growth of the Cu-matrix takes place. Also after additional turns at room temperature (see Figure 27: green line - 30 turns at 500 °C and 5 turns at room temperature) the hardness approaches again the hardness of the reference sample which was only deformed at room temperature. This shows only the independence of the results from the initial structure, as the hardness approaches again the same saturation level as before.
As the grain growth is strongly influenced by deformation induced defects, there is an important coincident with the applied strain and the deformation temperature. If the strain increases and so does the density of defects, the needed time for the recrystallization decreases. Fine W-particles would hinder the grain boundaries to move freely and slow down the recrystallization. Therefore, only a sample with refined particles to stabilize the microstructure due to a sufficient high applied strain will obtain the same hardness as the reference specimen: In Figure 27, the green line (30

turns at room temperature and 5 turns at 500 °C) decreases in the center stronger than at the edge. So at the edge the applied strain was high enough to influence the recovery and recrystallization. SEM-images of this sample (Figure 29) support this theory as fine W-particles are homogeneously distributed in the Cu-matrix.
In the center, the hardness approaches the same value for samples with 5 and 30 turns at 500 °C. The significant peaks in the hardness are caused by large W-particles at the measured positions. Due to the increased process temperature, the saturation in hardness is reached after smaller strains and the saturation hardness is lower. This is a typical phenomenon in warm SPD of single phase materials ([11]) or hot deformation. A saturation is reached at smaller strains and the evolving structure is coarser.
An interesting fact is that if no additional strain is applied (the blue lines in Figure 27: no second HPT-step is applied, but the samples are annealed at 500 °C for the same time as it was needed for applying 5 turns) the recovery and recrystallization is not as fast as if the samples are deformed in addition at 500 °C. The density of defects did not increase in this second HPT-step and so recovery and recrystallization processes are less pronounced.

5.3 Tensile testing

Tensile testing shows one of the most important drawbacks of using powder as initial material. Because of impurities, the tensile strength and fracture strain is lower compared to material with the same composition (compare Figure 58, Cu-powder and Cu-bulk). Fe strongly improves the properties of powder-processed samples as it increases not only strength but also encourages strain hardening. By comparing SEM-micrographs in subsection 4.3, it can be concluded that this is obtained not only because of the ductile behavior of Fe-dispersoids but also due to their fine distribution. Additional turns at higher temperatures further increase the ductility and the sample deformed for 30 turns at room temperature and 5 turns at 500 °C (see orange line in Figure 37 and Figure 38b) obtains nearly the same fracture strain as Cu-bulk material and even strong necking can be seen. For other materials this behavior could not be confirmed as the corresponding specimens fractured during preparation or show poor results in tensile testing due to large agglomerates (see orange line in Figure 34 and Figure 36).
Y_2O_3- and W-agglomerates are larger than Fe-particles and some agglomerates can always be found on the fracture surface. This explains also why W-reinforced Cu shows inferior results in tensile testing compared to yttria-reinforced Cu: In the tested samples the volume of W is higher than that of yttria and so is the proportion of large W-particles and agglomerates. Thus it is more likely to find one large, defect-containing agglomerate within the gauge length. This will promote fracture. The importance of the fraction of the brittle phase can be also observed in the three samples produced from the Plansee materials: The sample with the highest amount of Cu not only shows the highest tensile strength, but also the highest fracture strain. Additional SEM-micrographs show that the microstructure refines with higher amount of Cu (subsubsection 4.1.2) and also the fracture surface becomes more smooth (subsection 4.3). But this also show the importance of the quality of sample surface for testing, as W – 20 wt% Cu as well as W – 25 wt% Cu have got the fracture origin at the edge and so the additional polishing step after grinding should improve the behavior in tensile testing.

5.4 Stabilization of the microstructure at higher temperatures

The stability of the microstructure during annealing depends strongly on the applied strain and the composition of the annealed material. The influence of strain can be seen for Cu – 25 wt%

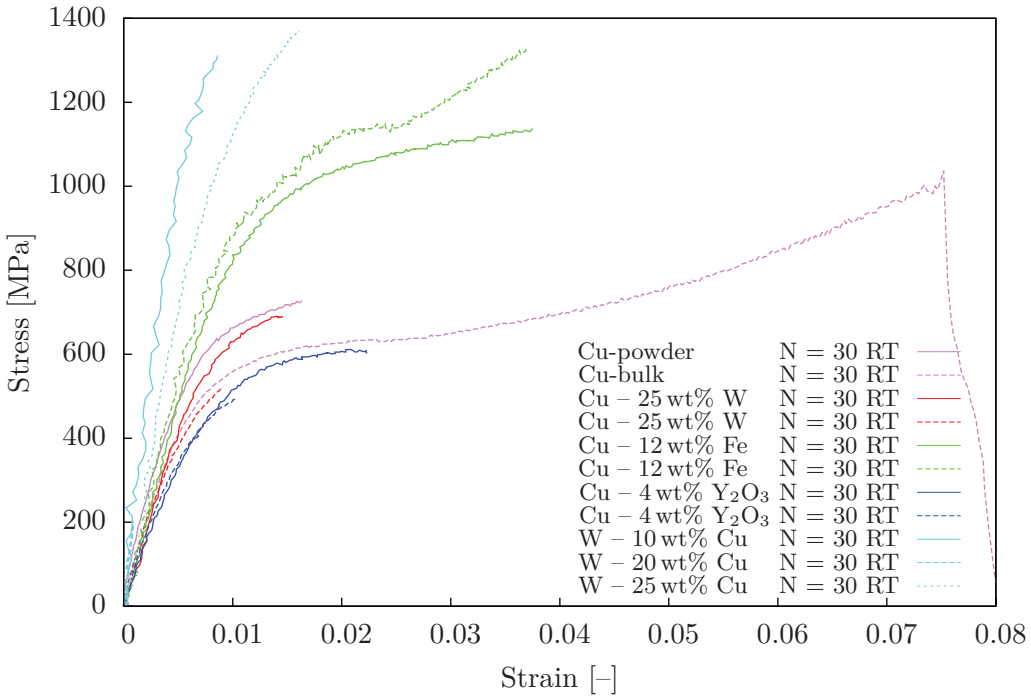

Figure 58: Comparison of tensile test data of all investigated materials after a HPT-deformation for 30 turns at room temperature. Interesting is that reinforcing with W and yttria hardly influences the behavior of Cu-powder, but Fe does.

W in Figure 45: The green lines represents the hardness of specimens which were not annealed. On the right side (at higher strains), there are full lines which show samples with 400 turns and which show no softening during annealing. The sample with 200 turns experiences a decrease of hardness after 1 h at 900 °C. In contrary, the hardness is strongly reduced for samples with only 30 turns (same color, but dashed lines at the left side of the diagram). By looking at the corresponding SEM-images, it can be seen that the decrease of hardness and a change in the microstructure are connected. The blue lines corresponds to an annealing temperature of 720 °C and the SEM pictures (Figure 46a and Figure 47a) show that the Cu-grains grow stronger in samples with less applied strain. Cu – 25 wt% W with 200 turns at room temperature does not show a strong grain growth of the Cu-matrix, but the W-particles are coarser which is expressed in a decrease in hardness. With lesser applied strain, not only the hardness decreases due to the coarser Cu-matrix, but also pores appear (see Figure 47).
In contrary to W, Y_2O_3 could not be refined strongly enough to stabilize the microstructure at higher temperatures. In Figure 48, the green line represents a sample which was not annealed. It can be seen that even the hardness of the specimen with 400 turns at room temperature decreases strongly after being annealed for 1 h at 810 °C. The hardness of the Cu – 4 wt% Y_2O_3 samples with 30 turns which were annealed inductively (1 min at 650 °C or 1 min at 1000 °C) were always below 50 HV and the one annealed at 850 °C for 1 min was too porous for hardness measurement (see Figure 50b).
Fe reinforces the Cu-matrix better and hardly any pores emerge. However, as it can be seen in Figure 49, the recrystallization of Cu and Fe becomes stronger if annealing time and temperature are increased as this process is controlled by diffusion. Hence, the sample annealed for 1 h at 900 °C shows a lower hardness due to larger Cu-grains and Fe-particle size than the specimen

annealed for 1 min at 850 °C (see Figure 48).
Also in pure Cu, produced from powder, deformed for 30 turns at room temperature and annealed for 1 h at 720 °C, pores emerge (see Figure 51). It was tried to reduce the porosity in Cu – 4 wt% Y_2O_3 by compacting the powder under vacuum (the sample which was annealed for 1 min at 580 °C), but again only a hardness of 50 HV was obtained. In Figure 50a it can be seen that the Cu-matrix is strongly coarsened and again pores weaken the material.
Even though, W-samples produced from industrial starting material were annealed at even higher temperatures than the samples produced of powder, no pores appeared and the hardness did not change that strongly. This can be attributed to the fact that the purity of this sample is higher and additional, the percentage of Cu is lower. Figure 52 shows that the hardness for W – 10 wt% Cu and W – 25 wt% Cu does not depend on the annealing temperature, but is always in the same range as for the sample which was not annealed. On the other hand, for W – 20 wt% Cu the hardness even increases during annealing. For W – 10 wt% Cu the hardness does not change because the microstructure does not change: If the pictures of all samples are compared for this material, the distance of the W-lamellas stays the same, which is true for the region near the center and the edge (Figure 53). The SEM images of W – 20 wt% Cu (see Figure 54) show that the W-lamellas are more rounded, but the distance between the W-particles stays the same. The increase of hardness is a consequence of the recovery because only few defects remain and so new dislocations must be generated for plastic deformation. In contrary to W – 20 wt% Cu, the part of Cu in W – 25 wt% Cu is so high that the growth of the grains is not fully disabled by the W, but also strongly hindered. The hardness is influenced by the growth of Cu-grains and the decreased density of dislocations and vacancies has not a big influence.

6 Conclusion

In this thesis eight different Cu-based materials were investigated for applications at higher temperatures. Not only the composition influences mechanical properties, but also the amount of applied strain and deformation temperature. Two pure Cu materials - one starting with powder and one with bulk material - were investigated for the purpose of gaining reference results. To study the influence of adding a hard bcc material suitable for fusion purposes, four Cu-W materials were taken in account. One was made of a powder mixture and three were made out of industrially produced bulk materials. Cu - Fe and Cu - Y_2O_3 were investigated to study the influence of a soft fcc phase and a hard and brittle ceramic phase on the mechanical properties and the microstructural stability.
Out off the seven used materials, Cu - Fe was the easiest to deform and a homogenous structure was soon reached with improved hardness as well as the tensile strength. This could be explained by the similar hardness of Cu and Fe which enables a simultaneous deformation of both phases and promotes so the development of a very fine microstructure. The deformability is also increased by the little, but nevertheless existing, mutual solubility which enables to produce a supersaturated solid solution. For W and Y_2O_3 the deformability as well as solubility was smaller than for Fe and not the same homogeneous microstructure could be reached. This becomes present in the hardness and especially in the results of tensile experiments. Only after application of significant higher strain, the hardness approaches the same values as for Cu - Fe. Additionally, due to large agglomerates and a coarser microstructure the full potential of these two materials could not be exploited. This problem can only be solved by refining the Y_2O_3- and W-particles, which can occur if the whole process - from mixing the powder to higher HPT-deformation - is improved. One idea would be to mix the powders in a ball mill to start the HPT-process with an already fine and homogeneously powder and handling all powders under a protective atmosphere (e.g. a glove box) to minimize the contamination. Another way is to increase the portion of W to force the material to deform simultaneously as it happened for one of the industrial produced material. To improve the ductility, the specimens should experience additional strain at higher temperatures as this reduces the density of defects.
The largest advantage of Cu - W is the good temperature stability. This is the case when the samples experienced enough strain to refine the W-particles, but then temperatures even as high as 720 °C for 1 h do not change the hardness and consequently the grain size. This is not the case for annealing Cu - Fe, for which coarsening of the Cu-matrix and the Fe-particles occurs, and for Cu - Y_2O_3. Yttria-reinforced materials show two problems: Yttria-particles cannot be refined sufficient to stabilize grain boundaries, so grain growth takes place and additional pores appear. These pores are likely caused by using powders as initial start material, as Cu-samples produced from powders show also pores after annealing, while industrial produced materials show no appearance of pores even after annealing at 1000 °C. To retain full density even during application at higher temperatures, the powder route must be improved, as pores are a sign of encased gases or water.
The three industrial materials show, due to the low percentage of Cu in the W, a high hardness and a good temperature stability. But tensile tests exhibit a low ductility, which could be improved by adding a polishing step to the grinding of the tensile samples. Without this step, for two out of three tensile tests the initiation of fracture was near or at the surface of the specimen. All in all, Cu - W materials show a good potential for application at higher temperatures, but the production route has to be optimized. In case the temperature of application is lower, Cu - Fe, due to the improved mechanical properties, is preferable.

List of abbreviations

ϵ_v	equivalent v. Mises strain
κ_y	Hall-Petch constant
σ	flow stress
σ_0	lattice fraction stress in a single crystal
ARB	accumulative roll bonding
bcc	body centered cubic
BSE	backscattered electrons
CCDF	cyclic closed die forging process
CEC	cyclic extrusion compression process
Cu	copper
CVD	chemical vapor deposition
D, d	grain size
ECAP	equal channel angular press
EDX	energy dispersive X-ray analysis
fcc	face centered cubic
FWHM	full width at half maximum
HPT	high pressure torsion process
HV	Vickers hardness
n	number of turns
NsM	nanostructured materials
OPS	oxide polishing suspension
PVD	physical vapor deposition
R, r	radius
RCS	repetitive corrugated straightening
RT	room temperature
SE	secondary electrons
SEM	scanning electron microscope
SPD	severe plastic deformation

t	thickness
T_m	melting temperature
XRD	X-ray diffraction

References

[1] G. Pintsuk, S. E. Brünings, J. E. Döring, J. Linke, I. Smid, and L. Xue. Development of W/Cu-functionally graded materials. *Fusion Engineering and Design*, 66:237–240, 2003.

[2] H. Gleiter. Nanostructured materials: state of the art and perspectives. *Nanostrucutred Materials*, 6:3–14, 1995.

[3] Reinhard Pippan, Anton Hohenwarter, Stephan Scheriau, and Andrea Bachmaier. Nanokristalline Metalle. *Physik in unserer Zeit*, 41:23–29, 2010.

[4] R. Z. Valiev. Properties and processing of nanocrystalline materials. Quarterly report. Technical report, Ufa State Aviation Technical University, Institute for Physics of Advanced Materials, 2009.

[5] A. Azushima, R. Kopp, A. Korhonen, D. Y. Yang, F. Micari, G. D. Lahoti, P. Groche, J. Yanagimoto, N. Tsuji, A. Rosochowski, and A. Yanagida. Severe plastic deformation (SPD) processes for metals. *CIRP Annals - Manufacturing Technology*, 57:716–735, 2008.

[6] Reinhard Pippan, Stephan Scheriau, Aidan Taylor, Anton Hohenwarter, and Andrea Bachmaier. Saturation of fragmentation during severe plastic deformation. *The Annual Review of Materials Research*, 40:19–43, April 2010.

[7] A. R. Kilmametov, G. Vaughan, A. R. Yavari, A. LeMoulec, W. J. Botta, and R. Z. Valiev. Microstructure evolution in copper under severe plastic deformation detected by in situ X-ray diffraction using monochromatic synchrotron light. *Materials Science & Engineering A*, 503:10–13, 2009.

[8] A. Hohenwarter, A. Bachmaier, B. Gludovatz, S. Scheriau, and R. Pippan. Technical parameters affecting grain refinement by high pressure torsion. *International Journal of Materials Research*, 100(12):1653–1661, 2009.

[9] T. Hebesberger, H. P. Stuewe, A. Vorhauer, F. Wetscher, and R. Pippan. Structure of Cu deformed by high pressure torsion. *Acta Materialia*, 53(2):393–402, 2005.

[10] Andrea Bachmaier. *Generation of bulk nanocomposites by severe plastic deformation*. PhD thesis, University of Leoben, 2011.

[11] A. Vorhauer and R. Pippan. On the homogeneity of deformation by high pressure torsion. *Scripta Materialia*, 51(9):921–925, 2004.

[12] R. Lapovok, A. Pougis, V. Lemiale, D. Orlov, L. S. Toth, and Y. Estrin. Severe plastic deformation processes for thin samples. *Journal of Materials Science*, 45(17):4554–4560, 2010.

[13] G. Gottstein. *Physikalische Grundlagen der Materialkunde*. Springer, 2007.

[14] Hans Conrad. Grain size dependence of the plastic deformation kinetics in Cu. *Materials Science & Engineering A*, 341(1):216–228, 2003.

[15] J. Chen, K. Lu, and L. Lu. Hardness and strain rate sensitivity of nanocrystalline Cu. *Scripta Materialia*, 54(11):1913–1918, 2006.

[16] R. Z. Valiev, R. K. Islamgaliev, and I. V. Alexandrov. Bulk nanostructured materials from severe plastic deformation. *Progress in Materials Science*, 2:103–189, 2000.

[17] A. Mishra, B. K. Kad, F. Gregori, and M. A. Meyers. Microstructural evolution in copper subjected to severe plastic deformation: Experiments and analysis. *Acta Materialia*, 55:13–28, 2007.

[18] E. Schafler and MB Kerber. Microstructural investigation of the annealing behaviour of high-pressure torsion (HPT) deformed copper. *Materials Science and Engineering A: Structural Materials: Properties, Microstructures and Processing*, 462(1-2):139–143, 2007.

[19] D. Edwards, I. Sabirov, W. Sigle, and R. Pippan. Microstructure and thermostability of a W-Cu nanocomposite produced via high-pressure torsion. *Philosophical Magazine*, 92(33):4151–4166, 2012.

[20] I. Sabirov. Characterization of tungsten fragmentation in a W25%Cu composite after high-pressure torsion. *Materials Characterization*, 58(10):848–853, 2007.

[21] T. Schöberl, I. Sabirov, and R. Pippan. Nanoindentation applied on a tungsten-copper composite before and after high-pressure torsion. *Z. Metallkd.*, 96:1056–1062, 2005.

[22] I. Sabirov and R. Pippan. Formation of a W25%Cu nanocomposite during high pressure torsion. *Scripta Materialia*, 52(12):1293–1298, 2005.

[23] X. Sauvage, F. Wetscher, and P. Pareige. Mechanical alloying of Cu and Fe induced by severe plastic deformation of a Cu-Fe composite. *Acta Materialia*, 53:2127–2135, 2005.

[24] P.R. Subramanian and D.E. Laughlin. Cu-W. http://www.himikatus.ru/art/phase-diagr1/Cu-W.php. Last visited on 18/12/2013.

[25] L.J. Swartzendruber. Cu-Fe. http://www.himikatus.ru/art/phase-diagr1/Cu-Fe.php. Last visited on 18.12.2013.

[26] J.P. Stobrawa, Z.M. Rdzawski, and W.J. Gluchowski. Microstructure and properties of nanocrystalline copper - yttria microcomposites. *Journal of Achievements in Materials and Manufacturing Engineering*, 24(2):83–86, 2007.

[27] J.P. Stobrawa and Z.M. Rdzawski. Deformation behaviour of dispersion hardened nanocrystalline copper. *Journal of Achievements in Materials and Manufacturing Engineering*, 17(1-2):153–156, 2006.

[28] J.P. Stobrawa and Z.M. Rdzawski. Dispersion - strengthened nanocrystalline copper. *Journal of Achievements in Materials and Manufacturing Engineering*, 24(2):35–42, 2007.

[29] J.P. Stobrawa and Z.M. Rdzawski. Thermal stability of functional properties in dispersion and precipitation hardened selected copper alloys. *Archives of Materials Science and Engineering*, 30(1):17–20, 2008.

[30] J.P. Stobrawa and Z.M. Rdzawski. Characterisation of nanostructured copper - wc materials. *Journal of Achievements in Materials and Manufacturing Engineering*, 32(2):171–178, 2009.

[31] A. Bachmaier, M. Kerber, D. Setman, and R. Pippan. The formation of supersaturated solid solutions in fe-cu alloys deformed by high-pressure torsion. *Acta Materialia*, 60(3):860–871, 2012.

[32] Georg.B. Rathmayr, Andrea Bachmaier, and Reinhard Pippan. Development of a new testing procedure for performing tensile tests on specimens with sub-millimetre dimensions. *Journal of Testing and Evaluation*, 41(4):635–646, 2013.